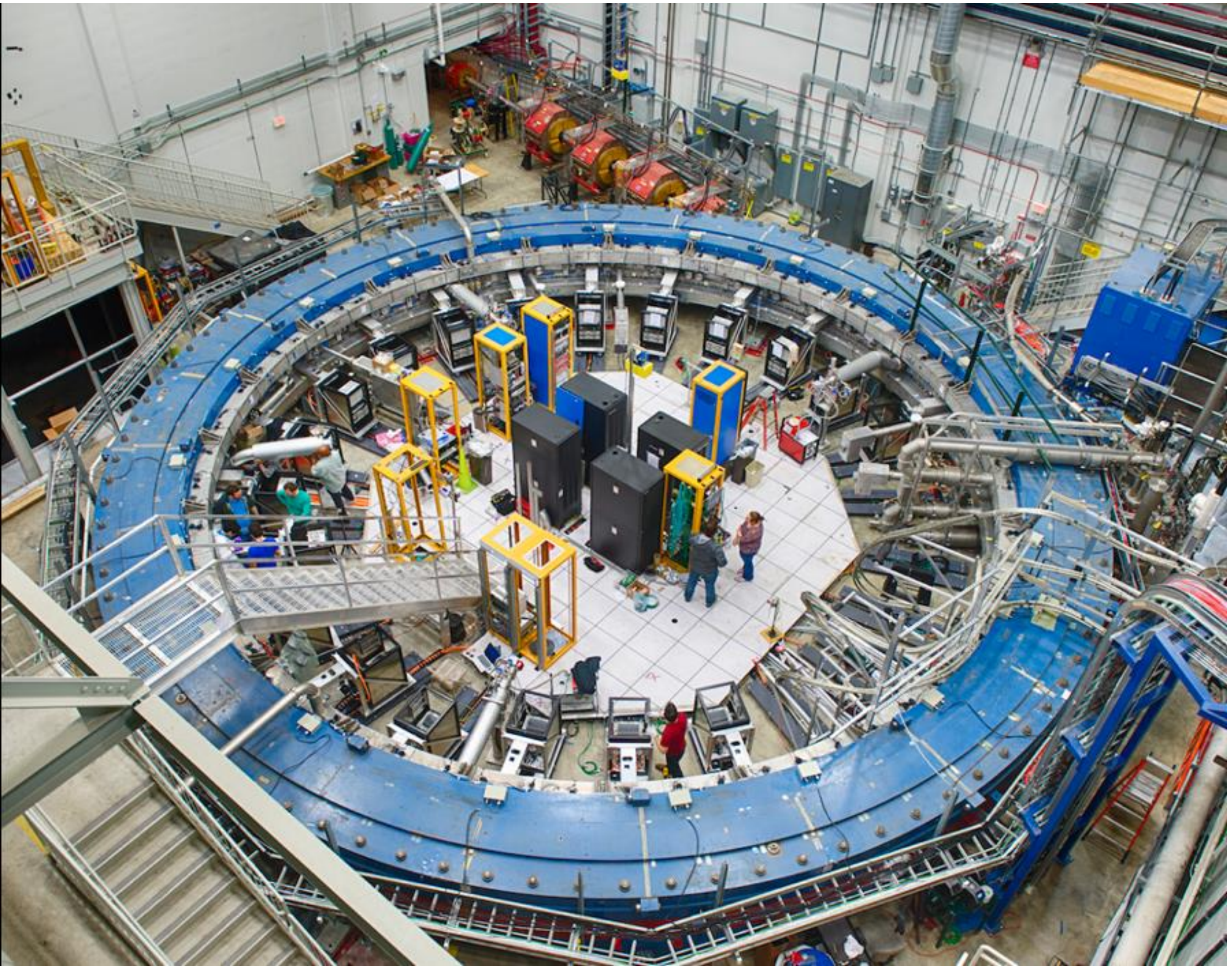

CLFV 2023

Muon g-2 at Fermilab

René Reimann
on behalf of Muon g-2 Collaboration

CLFV 2023, Heidelberg

June 21st, 2022

PRiSMA+ Cluster of Excellence
Precision Physics, Fundamental Interactions and Structure of Matter

μ g-2

JOHANNES GUTENBERG UNIVERSITÄT MAINZ

JG|U

Approaches to new physics

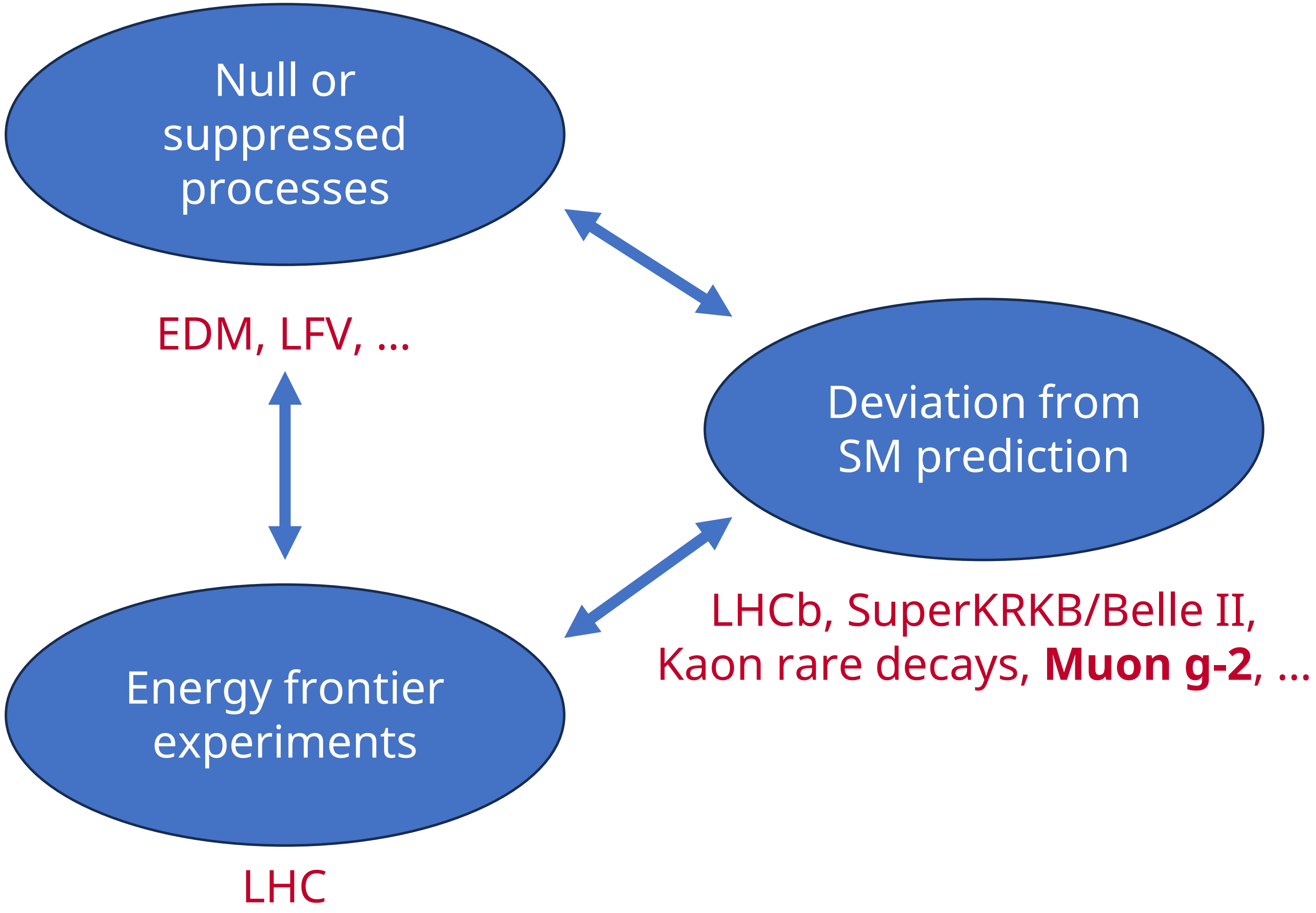

Approaches to new physics

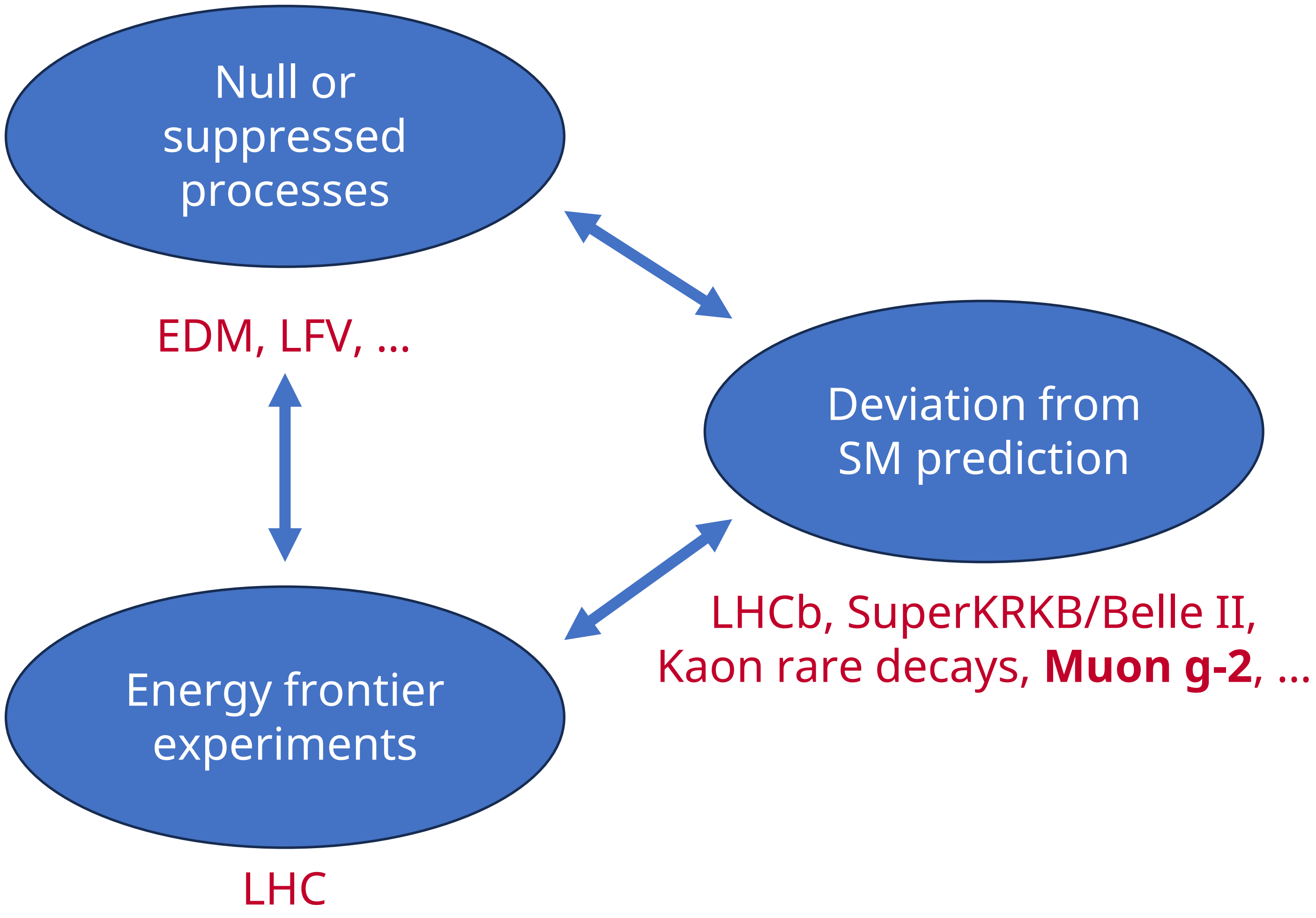

Most precise SM measurements

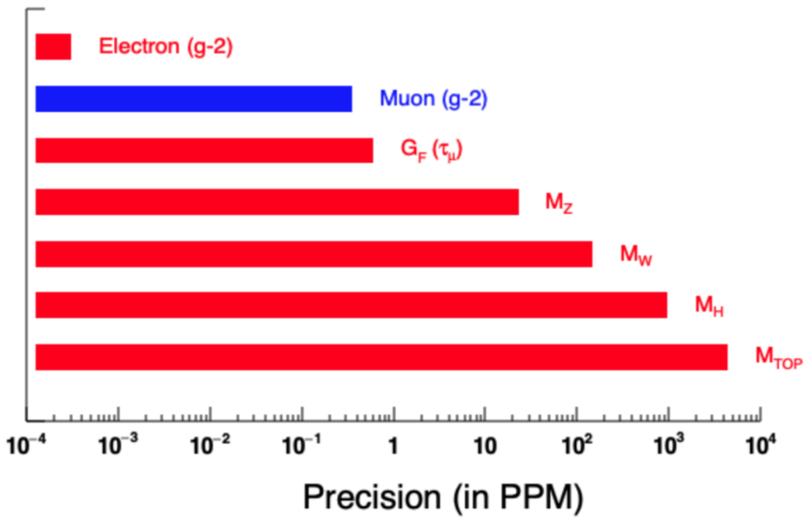

high precision measurement
+
high precision theory calculation
=
stringent SM test

Muon magnetic moment

$$\vec{\mu}_\mu = -g_\mu \frac{e}{2m_\mu} \vec{S}$$

magnetic moment

proportionality constant

spin

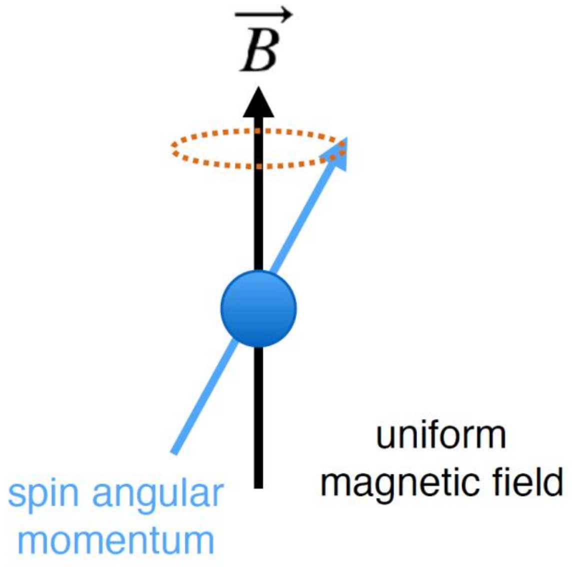

Muon magnetic moment

$$\vec{\mu}_\mu = -g_\mu \frac{e}{2m_\mu} \vec{S}$$

magnetic moment

proportionality constant

spin

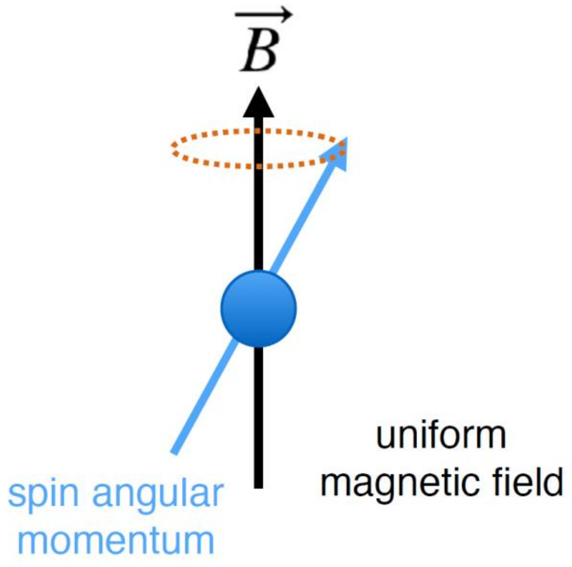

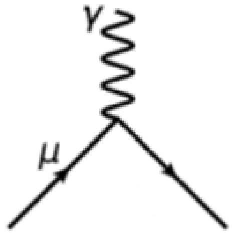

Dirac
(bare lepton)
g=2

Muon magnetic moment

$$\vec{\mu}_\mu = -g_\mu \frac{e}{2m_\mu} \vec{S}$$

magnetic moment

proportionality constant

spin

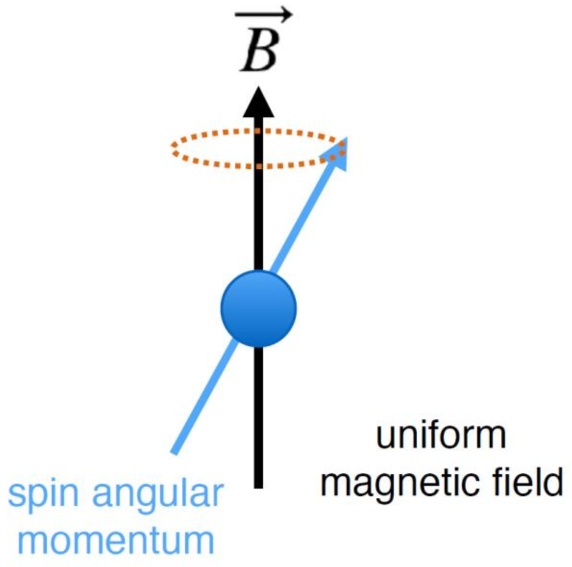

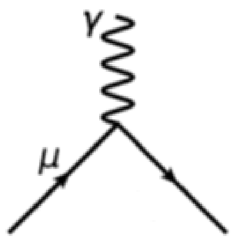

Dirac
(bare lepton)
g=2

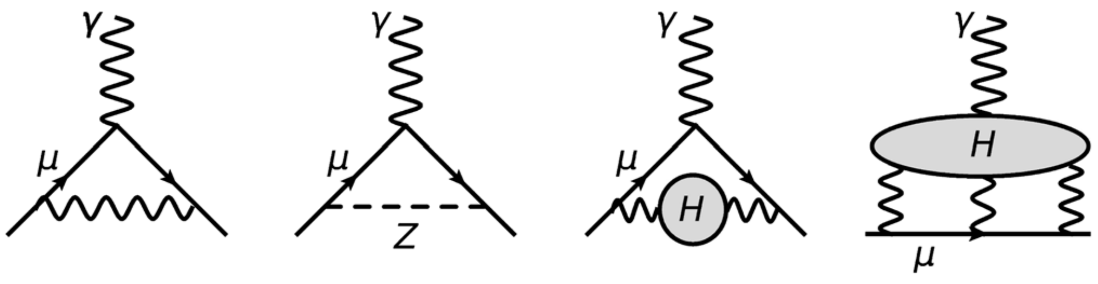

anomalous magnetic moment

Muon magnetic moment

$$\vec{\mu}_\mu = -g_\mu \frac{e}{2m_\mu}\vec{S}$$

magnetic moment

proportionality constant

spin

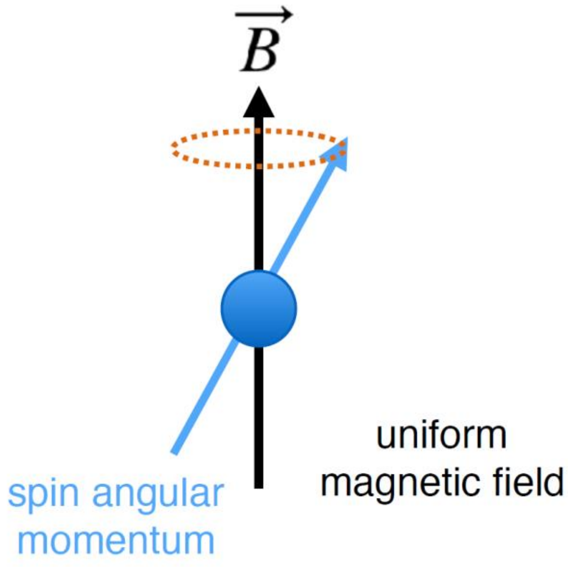

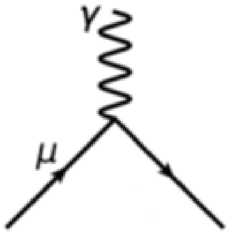

Dirac
(bare lepton)
g=2

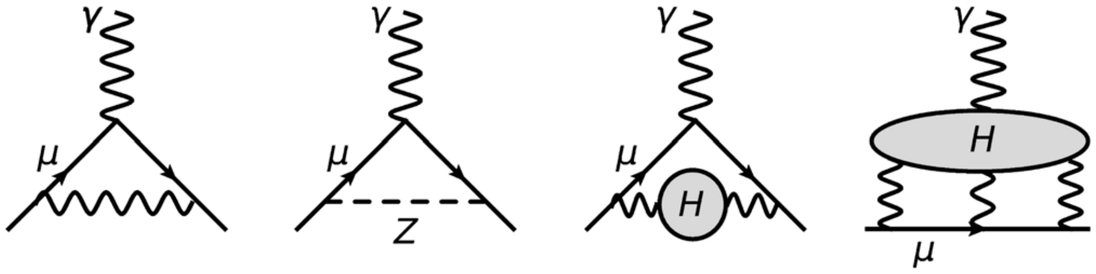

anomalous magnetic moment

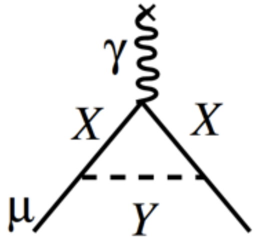

BSM physics

Muon magnetic moment

$$\vec{\mu}_\mu = -g_\mu \frac{e}{2m_\mu} \vec{S}$$

magnetic moment

proportionality constant

spin

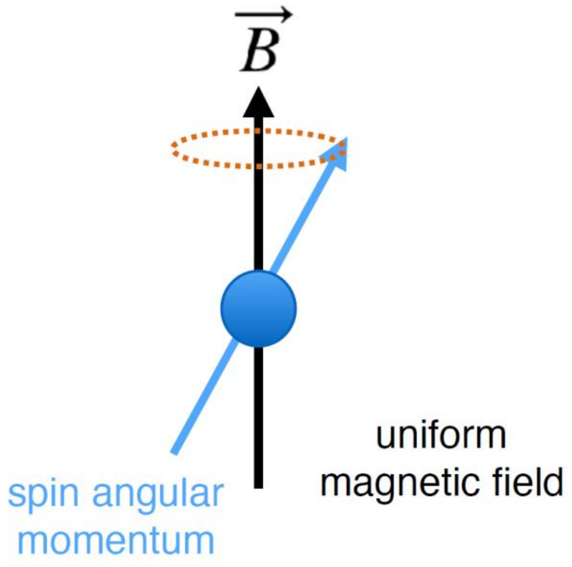

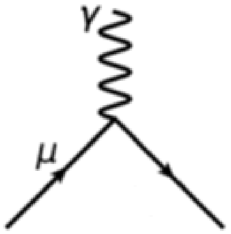

Dirac
(bare lepton)
g=2

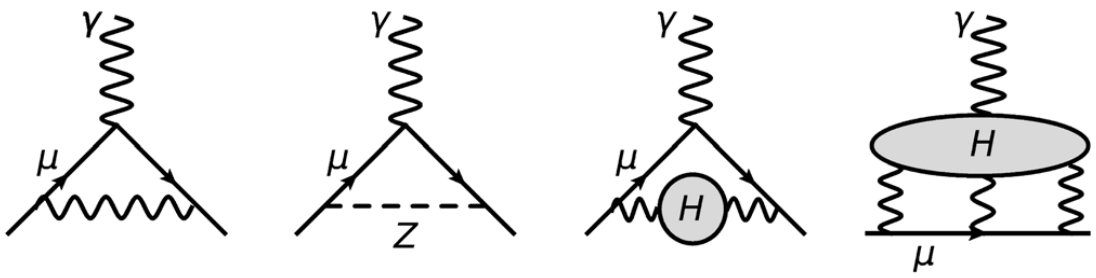

anomalous magnetic moment

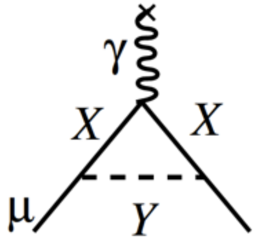

BSM physics

$$\Delta a_l^{\mathrm{BSM}} \propto \frac{g_{\mathrm{BSM}}}{16\pi^2} \frac{(\text{lepton mass})^2}{(\text{new particle mass})^2}$$

Current status

- Long standing discrepancy between theory calculation and experimental result
- Muon g-2 collaboration published Run 1 result
  B. Abi *et al.* (Muon g−2 Collaboration) Phys. Rev. Lett. **126**, 141801, 2021
  - In agreement with BNL measurement
- Uncertainty in theory calculation dominated by calculation of hadronic vacuum polarization (HVP)

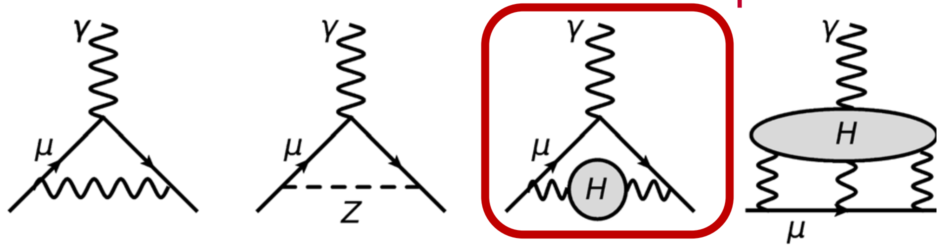

  - Dispersive approach, 4.2σ tension
    T. Aoyama *et al.*, Phys. Rept. **887** (2020) 1-166
  - Lattice QCD approach , 1.5σ tension
    Borsányi *et al.*, Nature **593**, 51–55, 2021 and arXiv:2002.12347

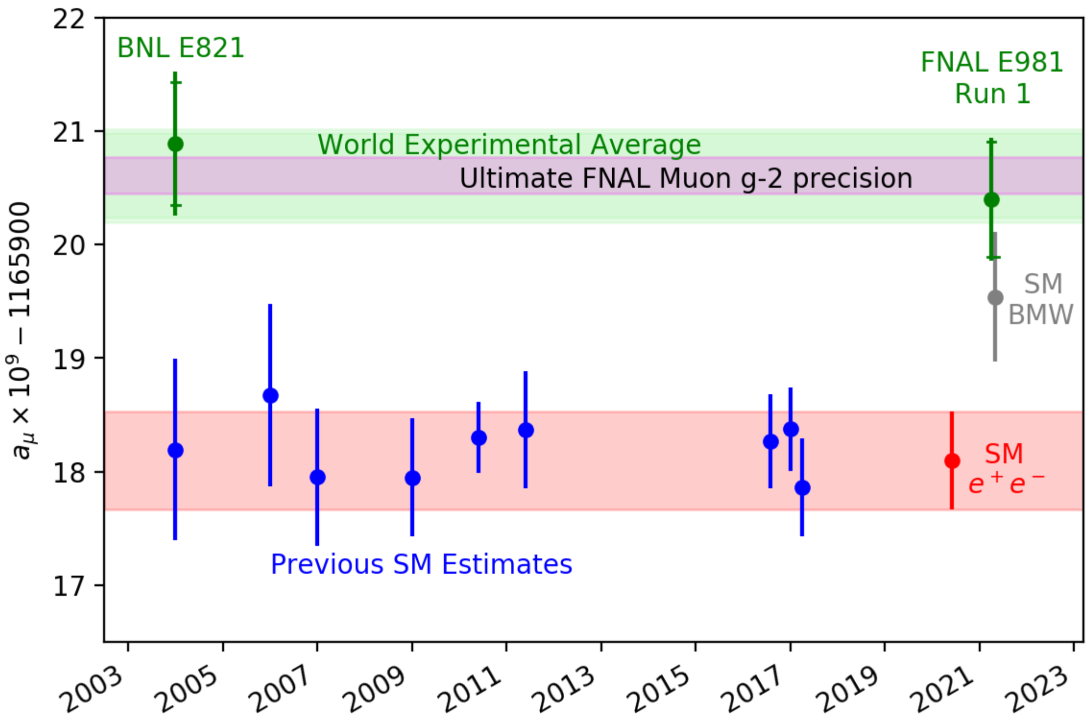

Current status

- Long standing discrepancy between theory calculation and experimental result
- Muon g-2 collaboration published Run 1 result
  B. Abi *et al.* (Muon g−2 Collaboration) Phys. Rev. Lett. **126**, 141801, 2021
  - In agreement with BNL measurement
- Uncertainty in theory calculation dominated by calculation of hadronic vacuum polarization (HVP)

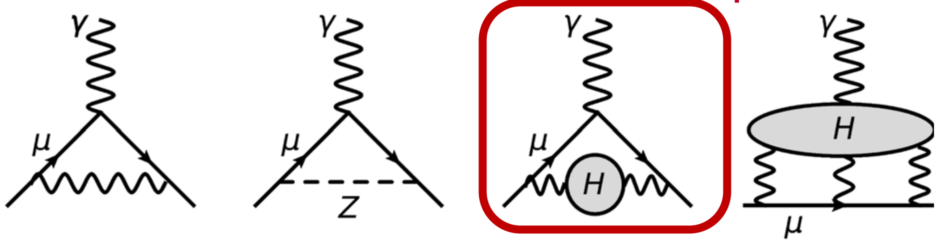

  - Dispersive approach, 4.2σ tension
    T. Aoyama *et al.*, Phys. Rept. **887** (2020) 1-166
  - Lattice QCD approach , 1.5σ tension
    Borsányi *et al.*, Nature **593**, 51–55, 2021 and arXiv:2002.12347

See talk by Ch. Lehner

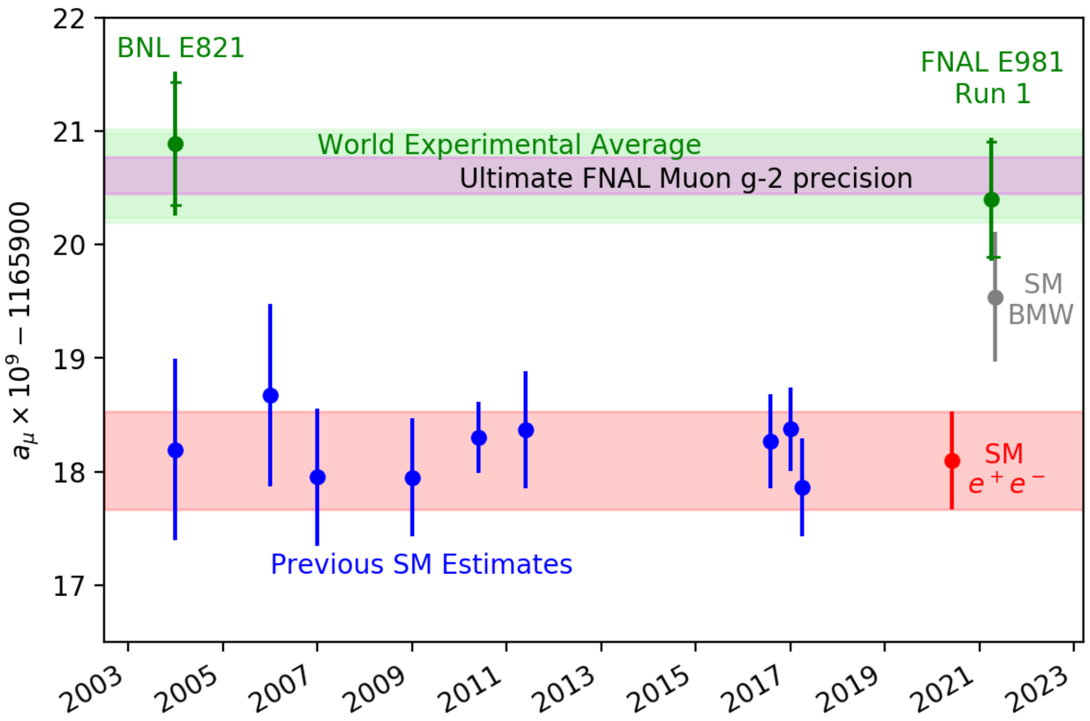

Current status

- Long standing discrepancy between theory calculation and experimental result
- Muon g-2 collaboration published Run 1 result
  B. Abi *et al.* (Muon g−2 Collaboration) Phys. Rev. Lett. **126**, 141801, 2021
  - In agreement with BNL measurement
- Uncertainty in theory calculation dominated by calculation of hadronic vacuum polarization (HVP)

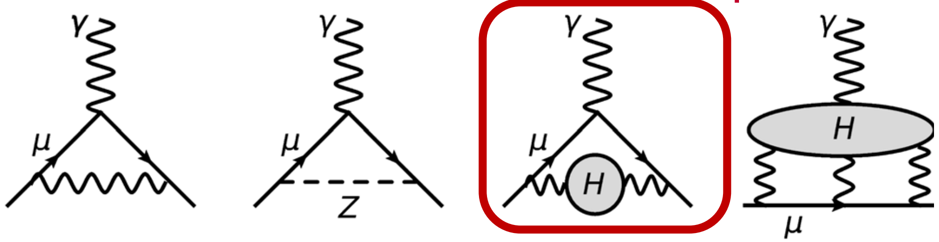

  - Dispersive approach, 4.2σ tension
    T. Aoyama *et al.*, Phys. Rept. **887** (2020) 1-166
  - Lattice QCD approach , 1.5σ tension
    Borsányi *et al.*, Nature **593**, 51–55, 2021 and arXiv:2002.12347

See talk by Ch. Lehner

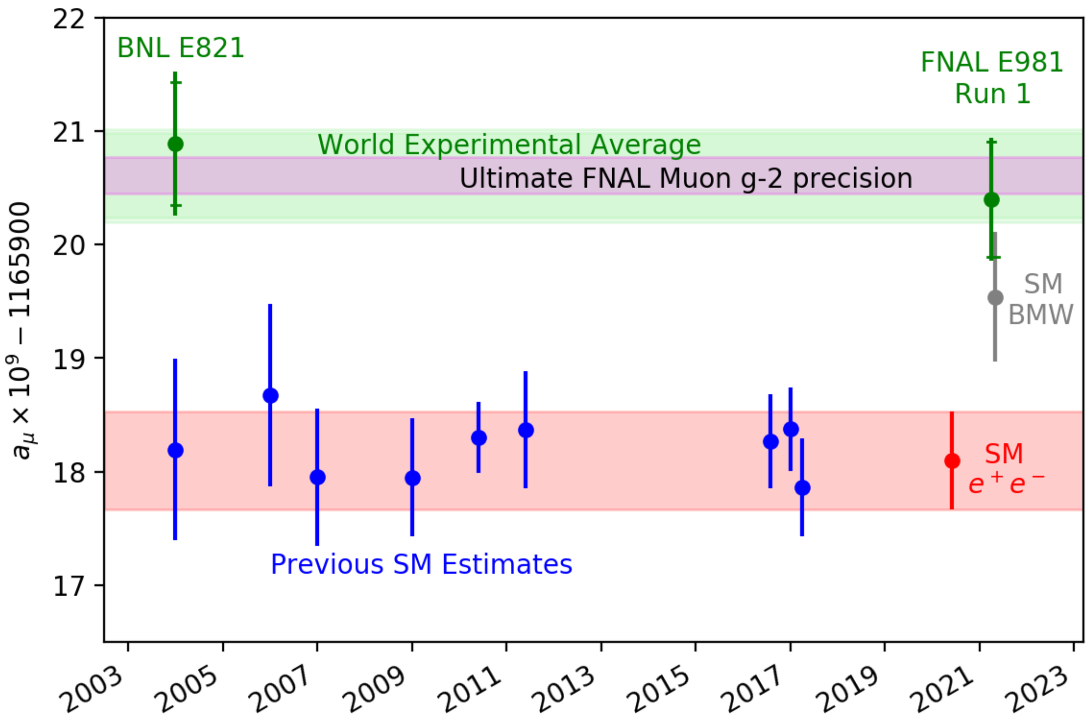

→ improve statistics & systematics of measurement

Muon in homogeneous magnetic field

Muon in homogeneous magnetic field

Cyclotron Motion

centrifugal force = Lorentz force

$$\vec{\omega}_C = -\frac{e}{m\gamma}\vec{B}$$

Muon in homogeneous magnetic field

Cyclotron Motion

centrifugal force = Lorentz force

$$\vec{\omega}_C = -\frac{e}{m\gamma}\vec{B}$$

Spin Precession

magnetic moment and field couple

$$\vec{\omega}_S = -g\frac{e}{2m}\vec{B} - (1-\gamma)\frac{e}{\gamma m}\vec{B}$$

Muon in homogeneous magnetic field

Cyclotron Motion

centrifugal force = Lorentz force

$$\vec{\omega}_C = -\frac{e}{m\gamma}\vec{B}$$

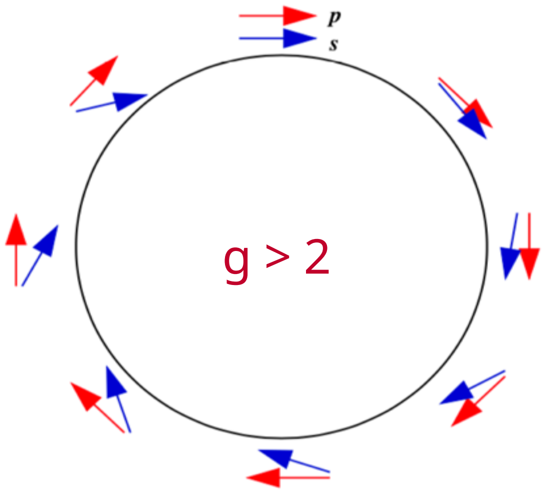

Spin Precession

magnetic moment and field couple

$$\vec{\omega}_S = -g\frac{e}{2m}\vec{B} - (1-\gamma)\frac{e}{\gamma m}\vec{B}$$

$$\underbrace{\omega_s - \omega_c}_{\omega_a} = g_\mu \frac{e}{2m_\mu}B - \frac{e}{m}B = \underbrace{\frac{g_\mu - 2}{2}}_{a_\mu}\frac{e}{m_\mu}B$$

anomalous spin-precession frequency

anomalous magnetic moment

Relativistic muon in magnetic & electric fields

$$\vec{\omega}_\mathrm{a} = \vec{\omega}_\mathrm{s} - \vec{\omega}_\mathrm{c} = \frac{e}{m}\left[a_\mu \vec{B} - a_\mu \left(\frac{\gamma}{\gamma+1}\right)\left(\vec{\beta}\cdot\vec{B}\right)\vec{\beta} - \left(a_\mu - \frac{1}{\gamma^2-1}\right)\frac{\vec{\beta}\times\vec{E}}{c}\right]$$

non-relativistic limit

Relativistic muon in magnetic & electric fields

$$\vec{\omega}_{\mathrm{a}} = \vec{\omega}_{\mathrm{s}} - \vec{\omega}_{\mathrm{c}} = \frac{e}{m}\left[a_\mu \vec{B} - a_\mu \left(\frac{\gamma}{\gamma+1}\right)\left(\vec{\beta}\cdot\vec{B}\right)\vec{\beta} - \left(a_\mu - \frac{1}{\gamma^2 - 1}\right)\frac{\vec{\beta}\times\vec{E}}{c}\right]$$

non-relativistic limit

electron motion
non-perpendicular
to magnetic field

cyclotron motion assumed motion
perpendicular to magnetic field

pitch of electron

Relativistic muon in magnetic & electric fields

$$\vec{\omega}_{\mathrm{a}} = \vec{\omega}_{\mathrm{s}} - \vec{\omega}_{\mathrm{c}} = \frac{e}{m}\left[a_\mu \vec{B} - a_\mu \left(\frac{\gamma}{\gamma+1}\right)\left(\vec{\beta}\cdot\vec{B}\right)\vec{\beta} - \left(a_\mu - \frac{1}{\gamma^2-1}\right)\frac{\vec{\beta}\times\vec{E}}{c}\right]$$

non-relativistic limit

electron motion
non-perpendicular
to magnetic field

cyclotron motion assumed motion
perpendicular to magnetic field

pitch of electron

relativistically generated
motional magnetic field

proportional to electric field

Relativistic muon in magnetic & electric fields

$$\vec{\omega}_{\mathrm{a}} = \vec{\omega}_{\mathrm{s}} - \vec{\omega}_{\mathrm{c}} = \frac{e}{m}\left[a_\mu \vec{B} - a_\mu \left(\frac{\gamma}{\gamma+1}\right)\left(\vec{\beta}\cdot\vec{B}\right)\vec{\beta} - \left(a_\mu - \frac{1}{\gamma^2-1}\right)\frac{\vec{\beta}\times\vec{E}}{c}\right]$$

non-relativistic limit

electron motion
non-perpendicular
to magnetic field

cyclotron motion assumed motion
perpendicular to magnetic field

pitch of electron

relativistically generated
motional magnetic field

proportional to electric field

$a_\mu^{SM} = 116591810(43) \times 10^{-11}$

disappears for γ≈ 29.3

Relativistic muon in magnetic & electric fields

$$\vec{\omega}_{\mathrm{a}} = \vec{\omega}_{\mathrm{s}} - \vec{\omega}_{\mathrm{c}} = \frac{e}{m}\left[a_\mu \vec{B} - a_\mu \left(\frac{\gamma}{\gamma+1}\right)\left(\vec{\beta}\cdot\vec{B}\right)\vec{\beta} - \left(a_\mu - \frac{1}{\gamma^2-1}\right)\frac{\vec{\beta}\times\vec{E}}{c}\right]$$

non-relativistic limit

electron motion
non-perpendicular
to magnetic field

cyclotron motion assumed motion
perpendicular to magnetic field

pitch of electron

relativistically generated
motional magnetic field

proportional to electric field

$a_\mu^{SM} = 116591810(43) \times 10^{-11}$

disappears for γ≈ 29.3

magic momentum
p_μ=3.094 GeV/c

Extracting a_μ

Anchor B, e and m_μ to other high-precision measurements and calculations

$$a_\mu = \frac{\omega_a}{\tilde{B}} \frac{m_\mu}{e}$$

Extracting a_μ

Anchor B, e and m_μ to other high-precision measurements and calculations

$$a_\mu = \frac{\omega_a}{\tilde{B}}\frac{m_\mu}{e} = \frac{\omega_a}{\tilde{\omega}'_p(T_r)}\frac{\mu'_p(T_r)}{\mu_e(H)}\frac{\mu_e(H)}{\mu_e}\frac{m_\mu}{m_e}\frac{g_e}{2}$$

$$\tilde{B} = \frac{\hbar\tilde{\omega}'_p}{2\mu'_p}$$

proton spin-precession

Extracting a_μ

Anchor *B*, *e* and m_μ to other high-precision measurements and calculations

$$\frac{\mu'_p(T_r)}{\mu_e(H)}$$

10.5 ppb uncertainty at T_r = 34.7°C

Metrologia 13, 179 (1977)

$$a_\mu = \frac{\omega_a}{\tilde{B}}\frac{m_\mu}{e} = \frac{\omega_a}{\tilde{\omega}'_p(T_r)}\frac{\mu'_p(T_r)}{\mu_e(H)}\frac{\mu_e(H)}{\mu_e}\frac{m_\mu}{m_e}\frac{g_e}{2}$$

$$\tilde{B} = \frac{\hbar\tilde{\omega}'_p}{2\mu'_p}$$

proton spin-precession

Extracting a_μ

Anchor *B*, *e* and m_μ to other high-precision measurements and calculations

$$\frac{\mu'_p(T_r)}{\mu_e(H)}$$

10.5 ppb uncertainty at T_r = 34.7°C

Metrologia 13, 179 (1977)

$$a_\mu = \frac{\omega_a}{\tilde{B}}\frac{m_\mu}{e} = \frac{\omega_a}{\tilde{\omega}'_p(T_r)}\frac{\mu'_p(T_r)}{\mu_e(H)}\frac{\mu_e(H)}{\mu_e}\frac{m_\mu}{m_e}\frac{g_e}{2}$$

$$\frac{\mu_e(H)}{\mu_e}$$

Bound state QED calculation exact

Rev. Mod. Phys. 88, 035009 (2016)

$$\tilde{B} = \frac{\hbar\tilde{\omega}'_p}{2\mu'_p}$$

proton spin-precession

Extracting a_μ

Anchor *B*, *e* and m_μ to other high-precision measurements and calculations

$$\frac{\mu'_p(T_r)}{\mu_e(H)}$$

10.5 ppb uncertainty at T_r = 34.7°C
Metrologia 13, 179 (1977)

$$\frac{m_\mu}{m_e}$$

Muonium hyperfine splitting
22 ppb uncertainty
Phys. Rev. Lett. 82, 11 (1999)

$$a_\mu = \frac{\omega_a}{\tilde{B}}\frac{m_\mu}{e} = \frac{\omega_a}{\tilde{\omega}'_p(T_r)}\frac{\mu'_p(T_r)}{\mu_e(H)}\frac{\mu_e(H)}{\mu_e}\frac{m_\mu}{m_e}\frac{g_e}{2}$$

$$\tilde{B} = \frac{\hbar\tilde{\omega}'_p}{2\mu'_p}$$

proton spin-precession

$$\frac{\mu_e(H)}{\mu_e}$$

Bound state QED calculation
exact
Rev. Mod. Phys. 88, 035009 (2016)

Extracting a_μ

Anchor *B*, *e* and m_μ to other high-precision measurements and calculations

$$\frac{\mu'_p(T_r)}{\mu_e(H)}$$

10.5 ppb uncertainty at T_r = 34.7°C
Metrologia 13, 179 (1977)

$$\frac{m_\mu}{m_e}$$

Muonium hyperfine splitting
22 ppb uncertainty
Phys. Rev. Lett. 82, 11 (1999)

$$a_\mu = \frac{\omega_a}{\tilde{B}} \frac{m_\mu}{e} = \frac{\omega_a}{\tilde{\omega}'_p(T_r)} \frac{\mu'_p(T_r)}{\mu_e(H)} \frac{\mu_e(H)}{\mu_e} \frac{m_\mu}{m_e} \frac{g_e}{2}$$

$$\tilde{B} = \frac{\hbar \tilde{\omega}'_p}{2\mu'_p}$$

proton spin-precession

$$\frac{\mu_e(H)}{\mu_e}$$

Bound state QED calculation
exact
Rev. Mod. Phys. 88, 035009 (2016)

$$\frac{g_e}{2}$$

Measurement
0.13 ppt uncertainty
Phys. Rev. Lett. 130, 071801 (2023)

Extracting a_μ

Anchor *B*, *e* and m_μ to other high-precision measurements and calculations

$$\frac{\mu'_p(T_r)}{\mu_e(H)}$$

10.5 ppb uncertainty at T_r = 34.7°C
Metrologia 13, 179 (1977)

$$\frac{m_\mu}{m_e}$$

Muonium hyperfine splitting
22 ppb uncertainty
Phys. Rev. Lett. 82, 11 (1999)

$$a_\mu = \frac{\omega_a}{\tilde{B}}\frac{m_\mu}{e} = \frac{\omega_a}{\tilde{\omega}'_p(T_r)}\frac{\mu'_p(T_r)}{\mu_e(H)}\frac{\mu_e(H)}{\mu_e}\frac{m_\mu}{m_e}\frac{g_e}{2}$$

$$\tilde{B} = \frac{\hbar\tilde{\omega}'_p}{2\mu'_p}$$

proton spin-precession

total uncertainty from
external quantities
25 ppb

$$\frac{\mu_e(H)}{\mu_e}$$

Bound state QED calculation
exact
Rev. Mod. Phys. 88, 035009 (2016)

$$\frac{g_e}{2}$$

Measurement
0.13 ppt uncertainty
Phys. Rev. Lett. 130, 071801 (2023)

Extracting a_μ

Anchor *B*, *e* and m_μ to other high-precision measurements and calculations

$$\frac{\mu'_p(T_r)}{\mu_e(H)}$$

10.5 ppb uncertainty at T_r = 34.7°C

Metrologia 13, 179 (1977)

$$\frac{m_\mu}{m_e}$$

Muonium hyperfine splitting
22 ppb uncertainty

Phys. Rev. Lett. 82, 11 (1999)

We measure this ratio

$$a_\mu = \frac{\omega_a}{\tilde{B}}\frac{m_\mu}{e} = \frac{\omega_a}{\tilde{\omega}'_p(T_r)}\frac{\mu'_p(T_r)}{\mu_e(H)}\frac{\mu_e(H)}{\mu_e}\frac{m_\mu}{m_e}\frac{g_e}{2}$$

$$\tilde{B} = \frac{\hbar\tilde{\omega}'_p}{2\mu'_p}$$

proton spin-precession

total uncertainty from
external quantities
25 ppb

$$\frac{\mu_e(H)}{\mu_e}$$

Bound state QED calculation
exact

Rev. Mod. Phys. 88, 035009 (2016)

$$\frac{g_e}{2}$$

Measurement
0.13 ppt uncertainty

Phys. Rev. Lett. 130, 071801 (2023)

Extracting a_μ

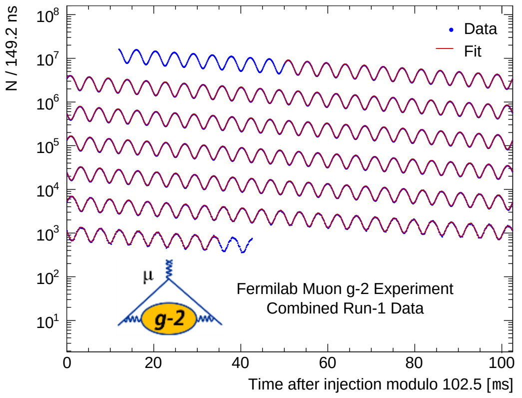

Anomalous spin precession frequency

Muon beam dynamics corrections

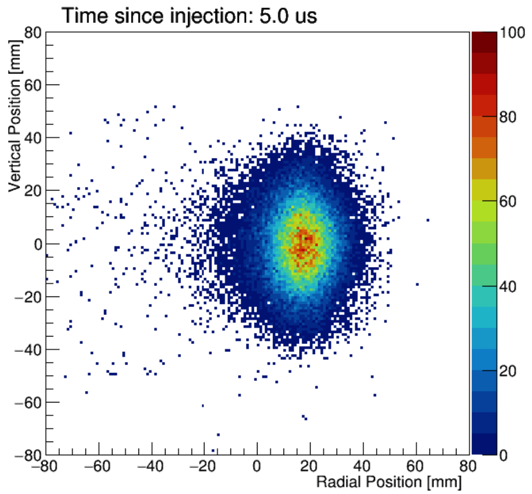

Clock blinding

$$\frac{\omega_a}{\tilde{\omega}'_p} = \frac{f_{\mathrm{clock}}\,\omega_a^{\mathrm{meas}}\left(1 + C_e + C_p + C_{ml} + C_{pa}\right)}{f_{\mathrm{calib}}\left\langle M(x,y,\phi)\,\omega'_p(x,y,\phi)\right\rangle\left(1 + B_k + B_q\right)}$$

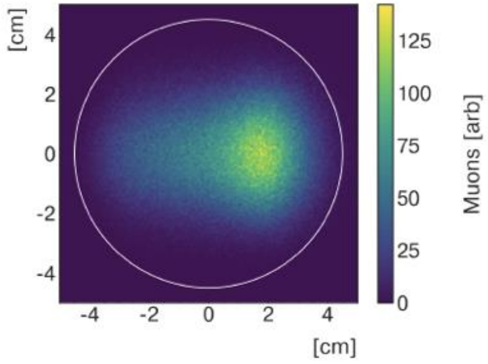

Spatial muon distribution

Magnetic field calibration

Spatial distribution of magnetic field

Transient magnetic fields

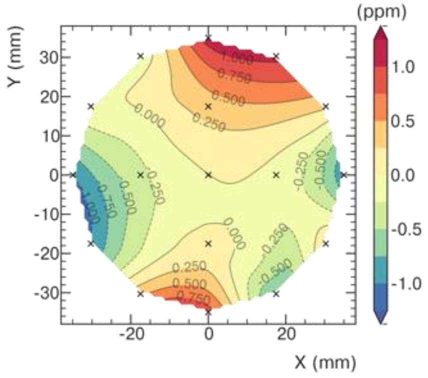

Muon Campus at Fermilab

Momentum selective beam line

$$p = 3.094\frac{GeV}{c} \pm 2\%$$

~10,000 μ^+ at 3.1 GeV
every 10 ms and 120 ns bunch length

The superconducting storage ring

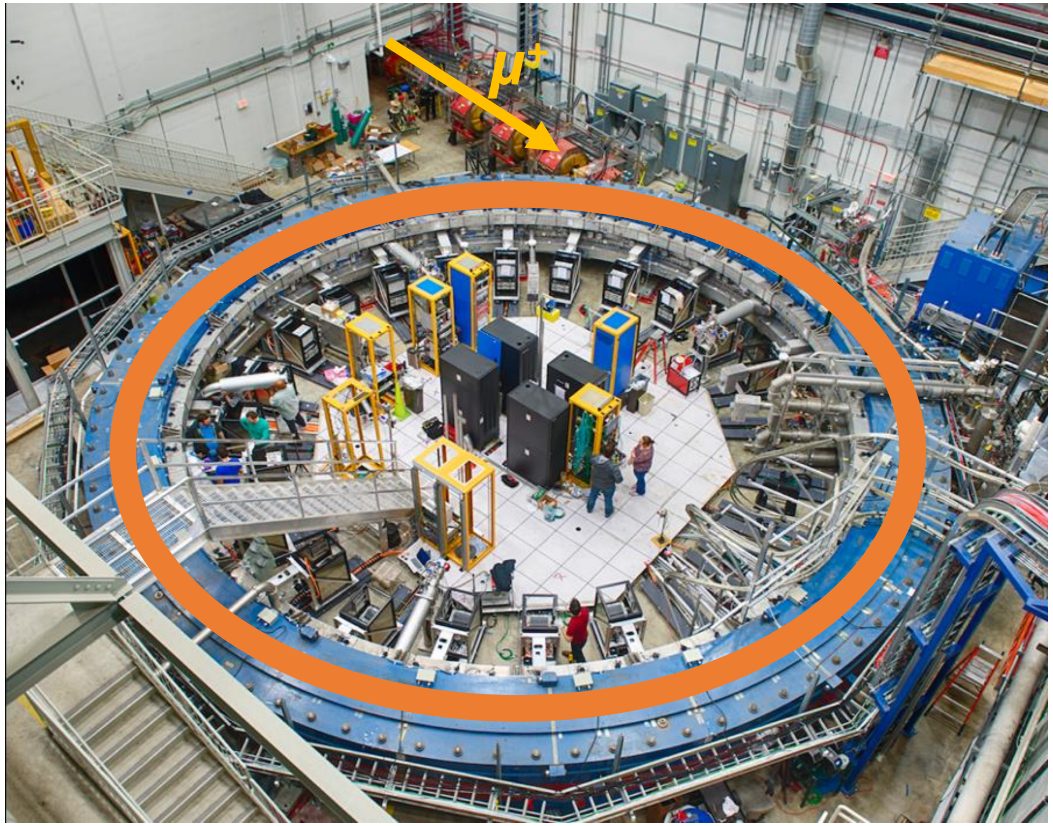

- $p_\mu^{magic} = 3.094 \frac{GeV}{c} \pm 0.5\%$
- 3 cryostats with 4 superconducting coils (5300 A)
- 1.45 T vertical magnetic field
- 90 mm muon storage region
- 180 mm gap for vacuum chambers
- muon cyclotron period 149 ns (~6.7 MHz)

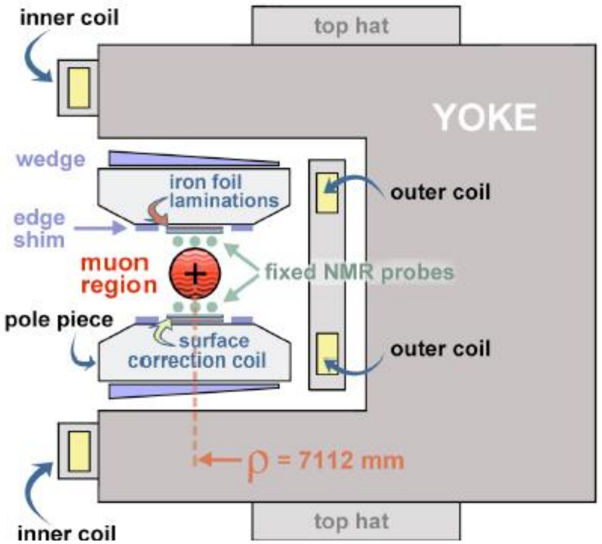

Beam Injection

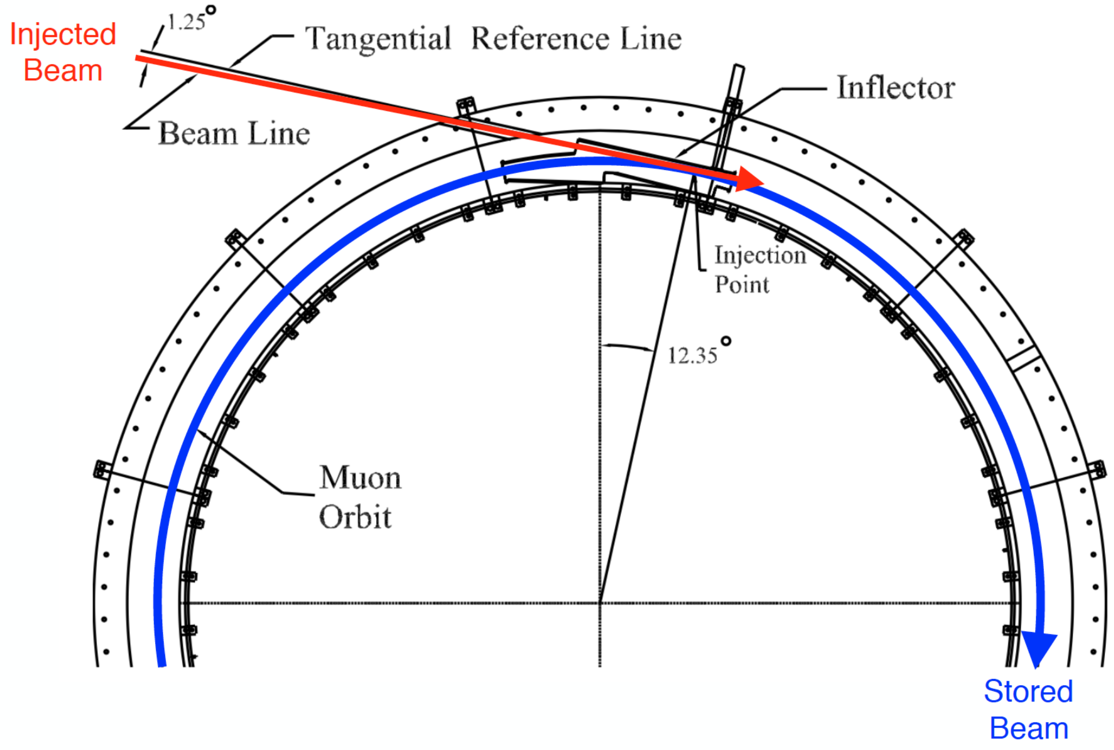

- Inflector magnet cancles B field in iron yoke
- Muon can travel straight & enter the ring

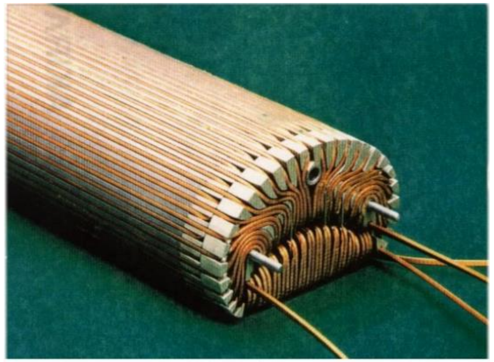

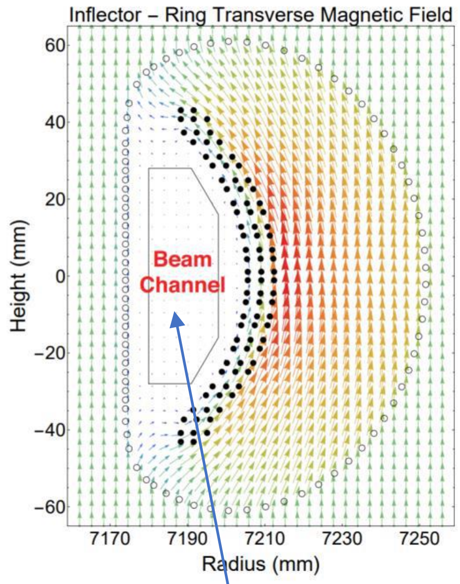

field free region

How to get the beam onto storage orbit?

How to get the beam onto storage orbit?

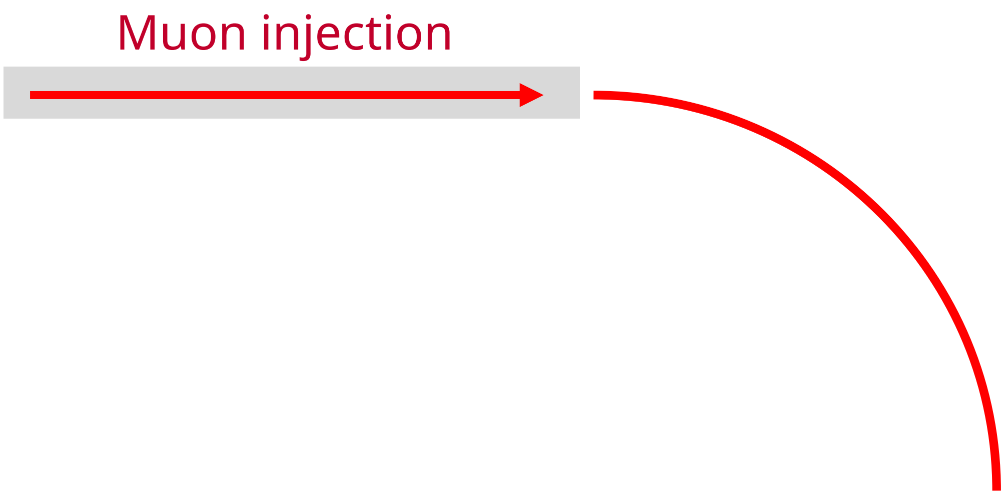

How to get the beam onto storage orbit?

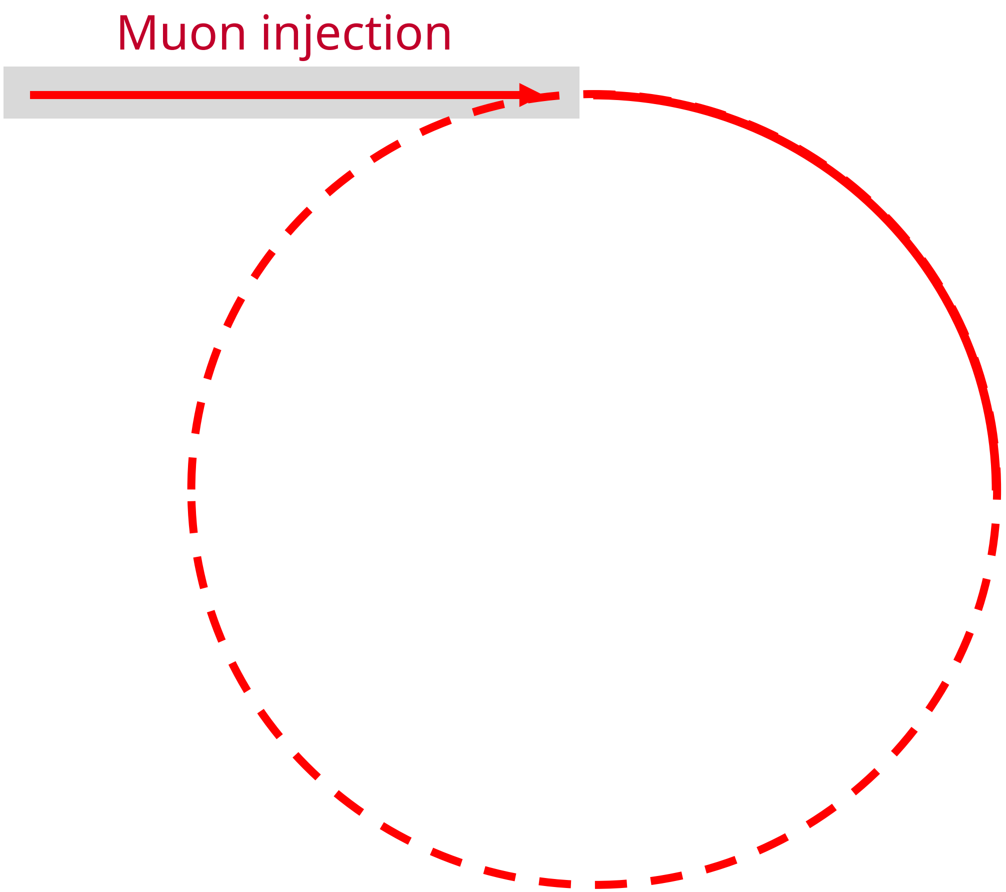

How to get the beam onto storage orbit?

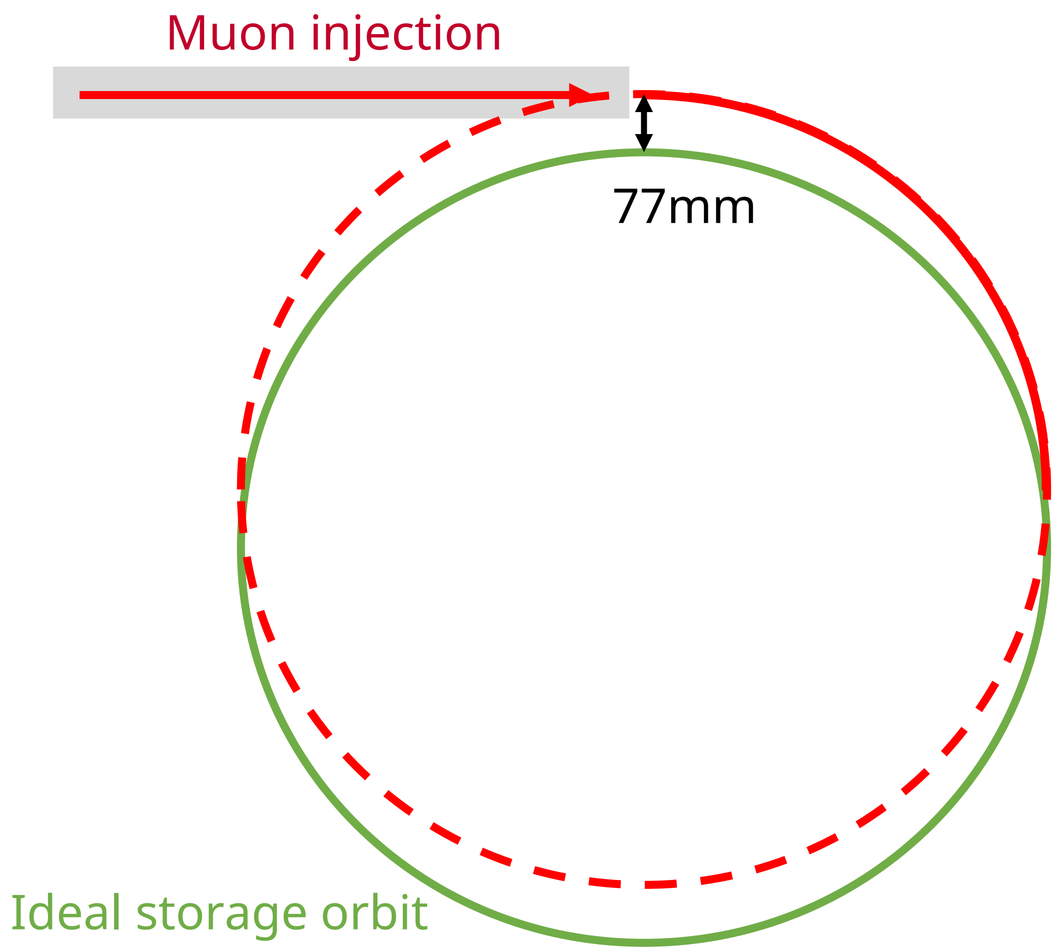

How to get the beam onto storage orbit?

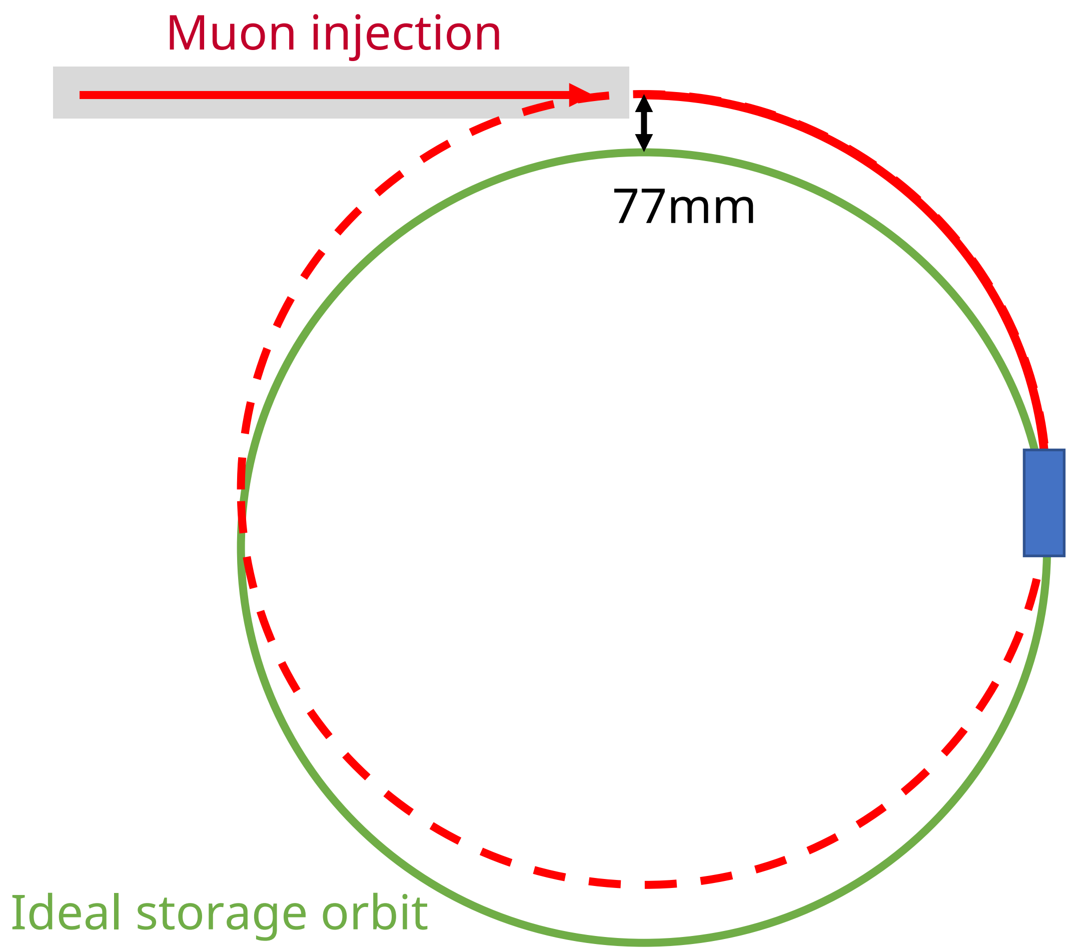

How to get the beam onto storage orbit?

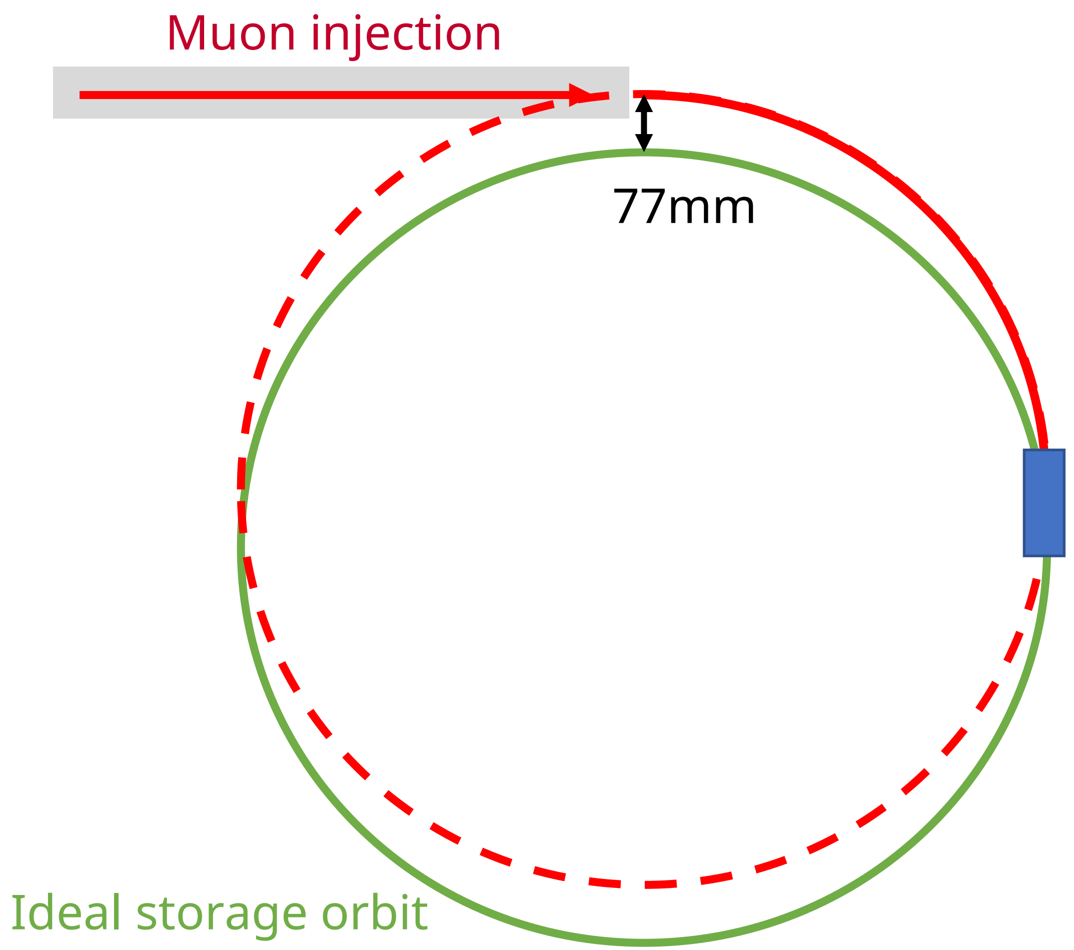

- Change field locally by 2% within ~150 ns
- 3 pairs of plates at roughly 90°
- Apply HV pulse at 4700 A into ~12.5 Ω in 150 ns

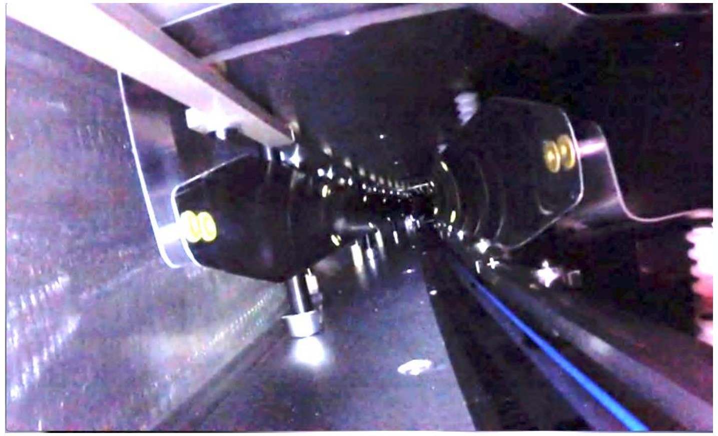

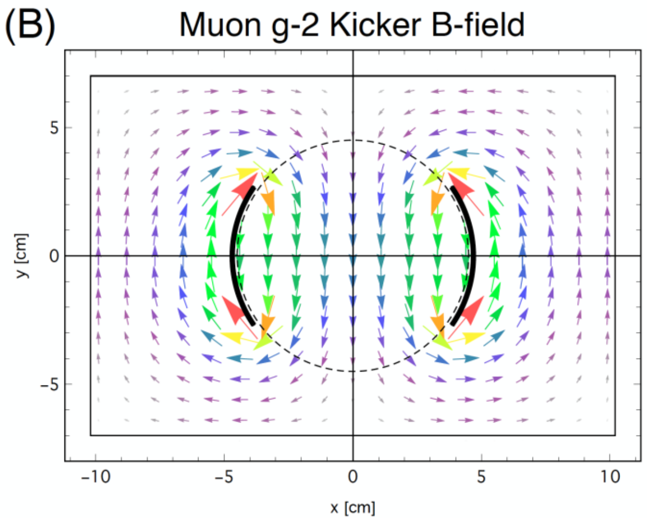

Keeping the muons stored

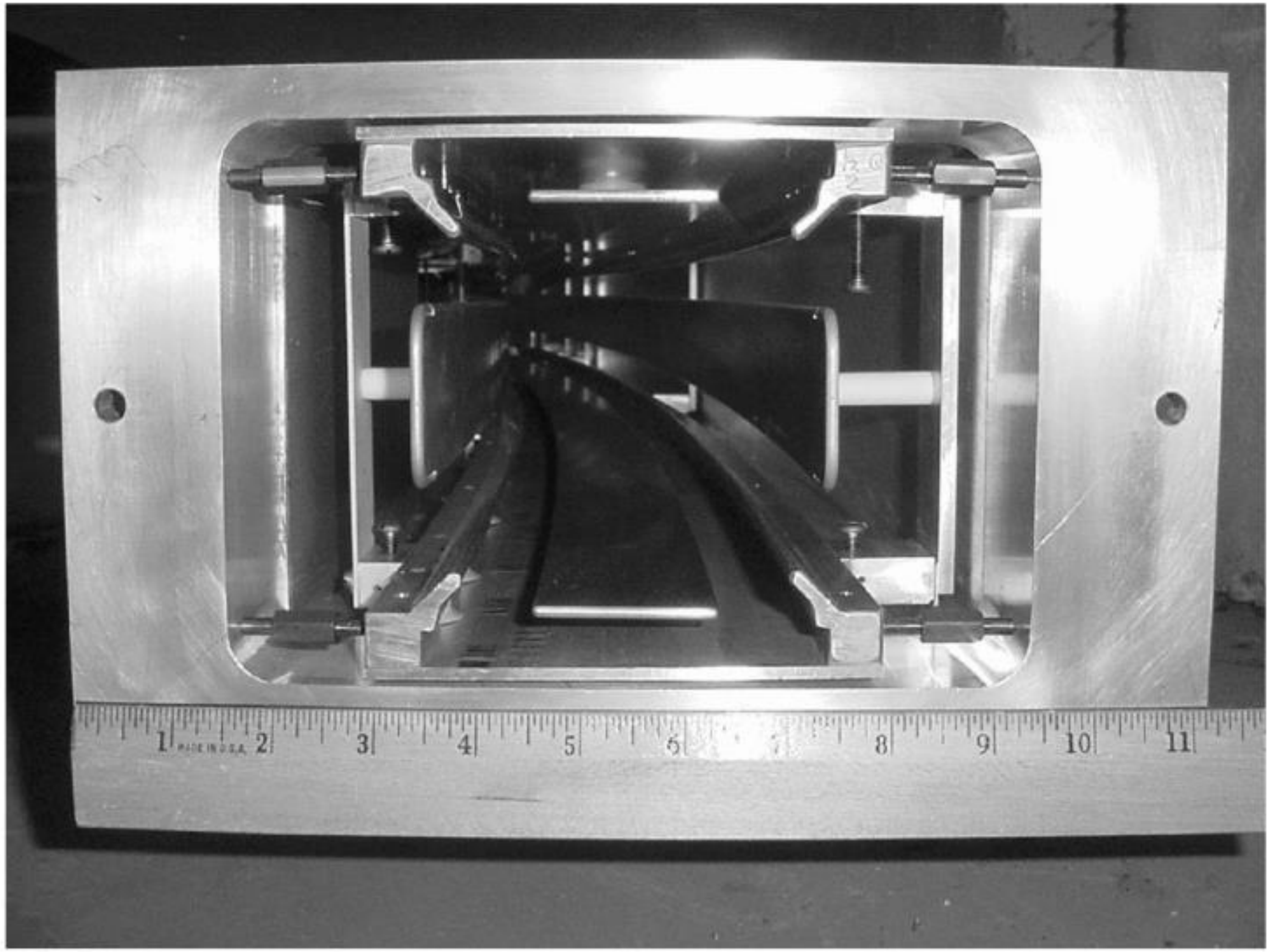

- At magic momentum electric fields have a very small impact on ω_a

Keeping the muons stored

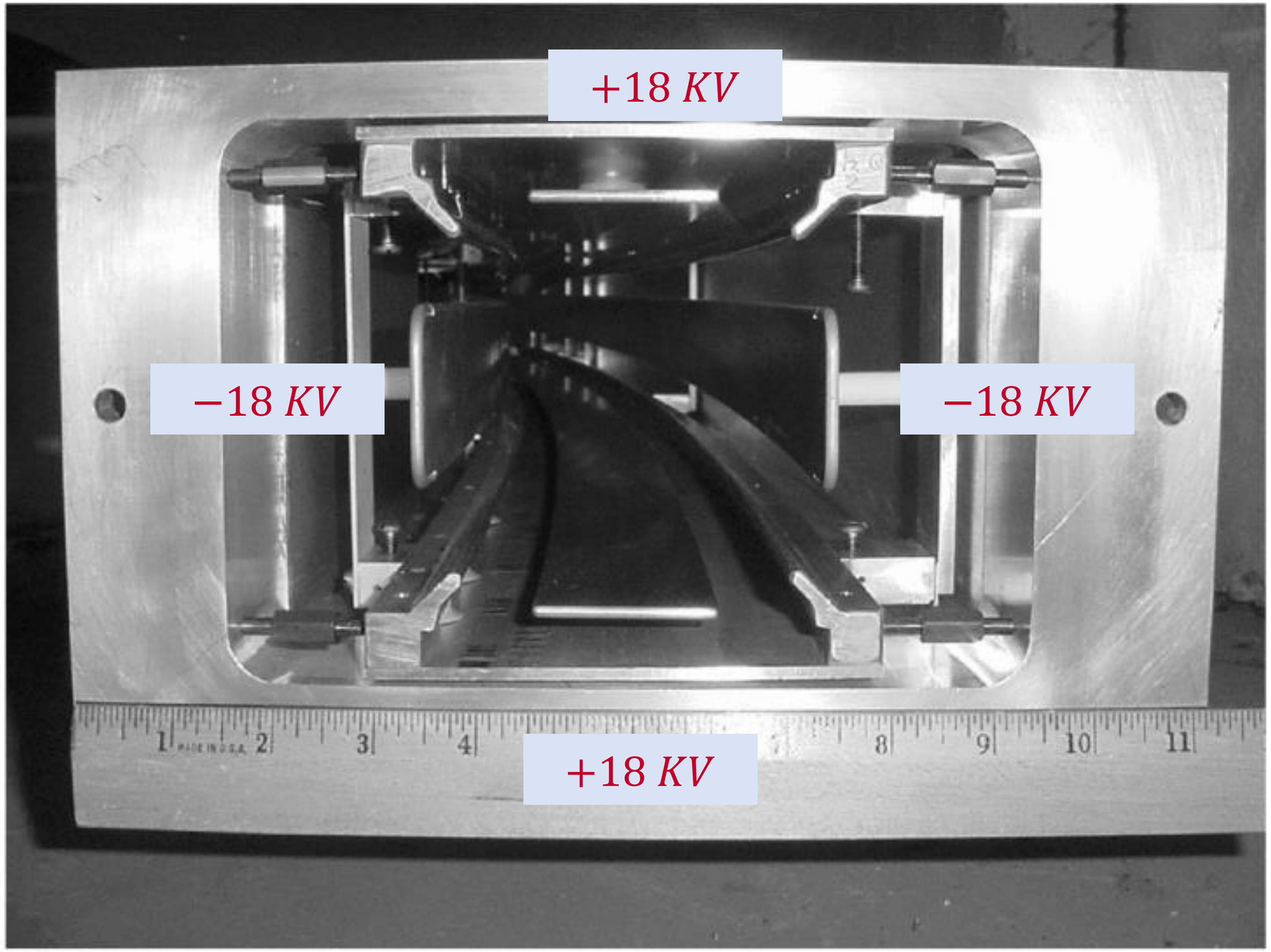

- At magic momentum electric fields have a very small impact on ω_a

Keeping the muons stored

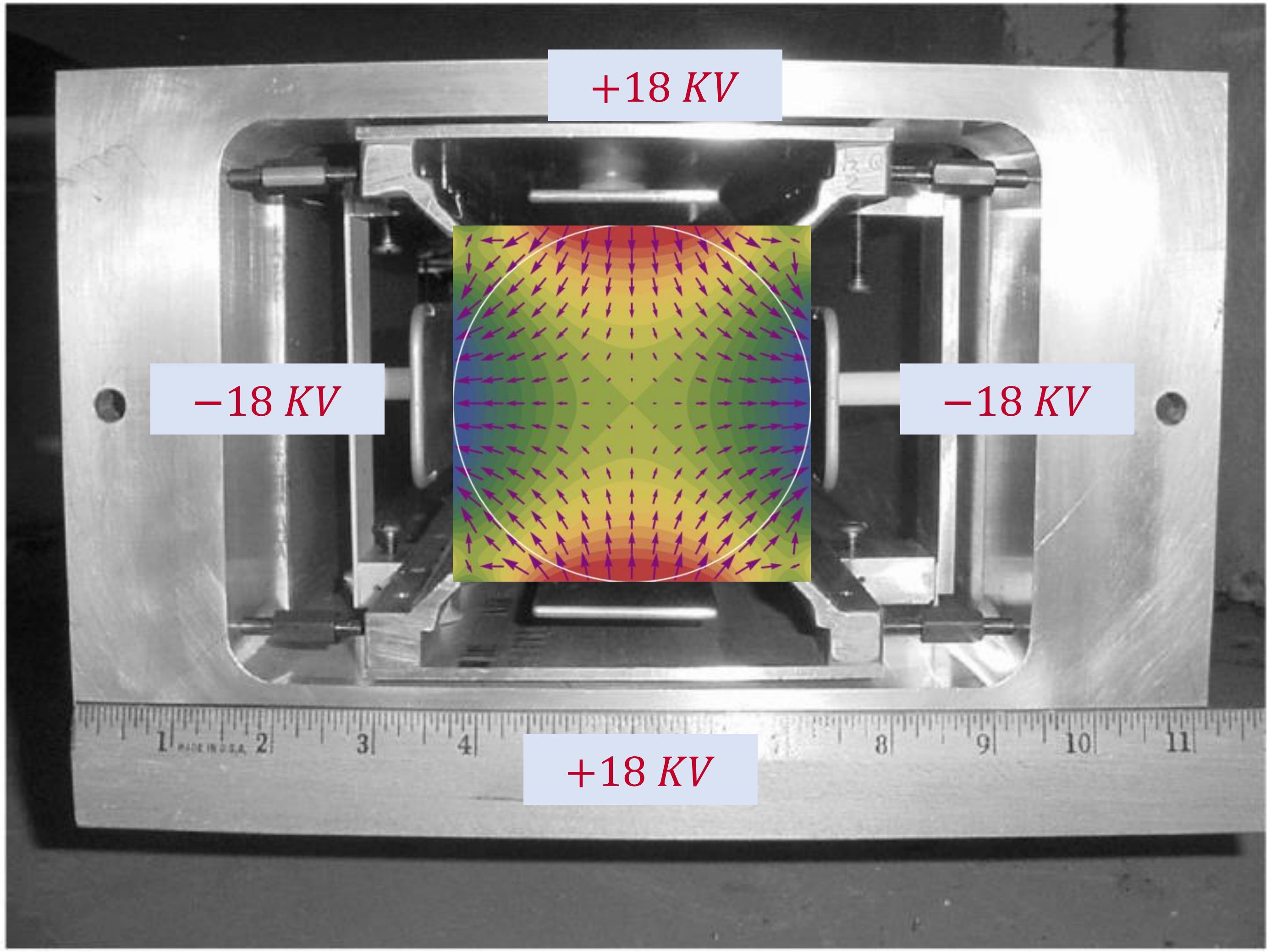

- At magic momentum electric fields have a very small impact on ω_a

Keeping the muons stored

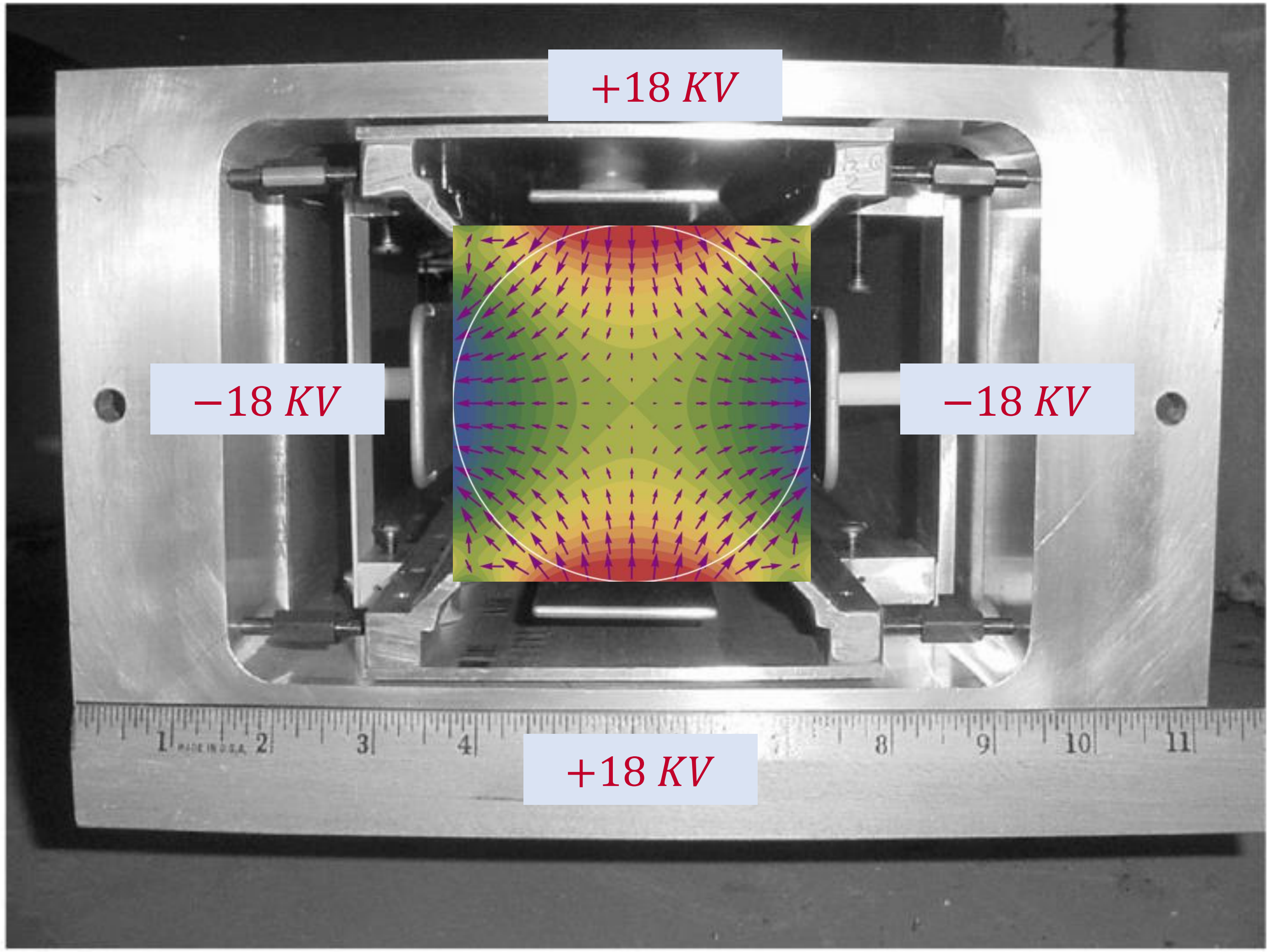

- At magic momentum electric fields have a very small impact on ω_a
- Electrostatic quadrupoles focus beam vertically
- Electrostatic quadrupoles defocus beam radially
- Magnetic field focus beam radially → Complex beam dynamics

Keeping the muons stored

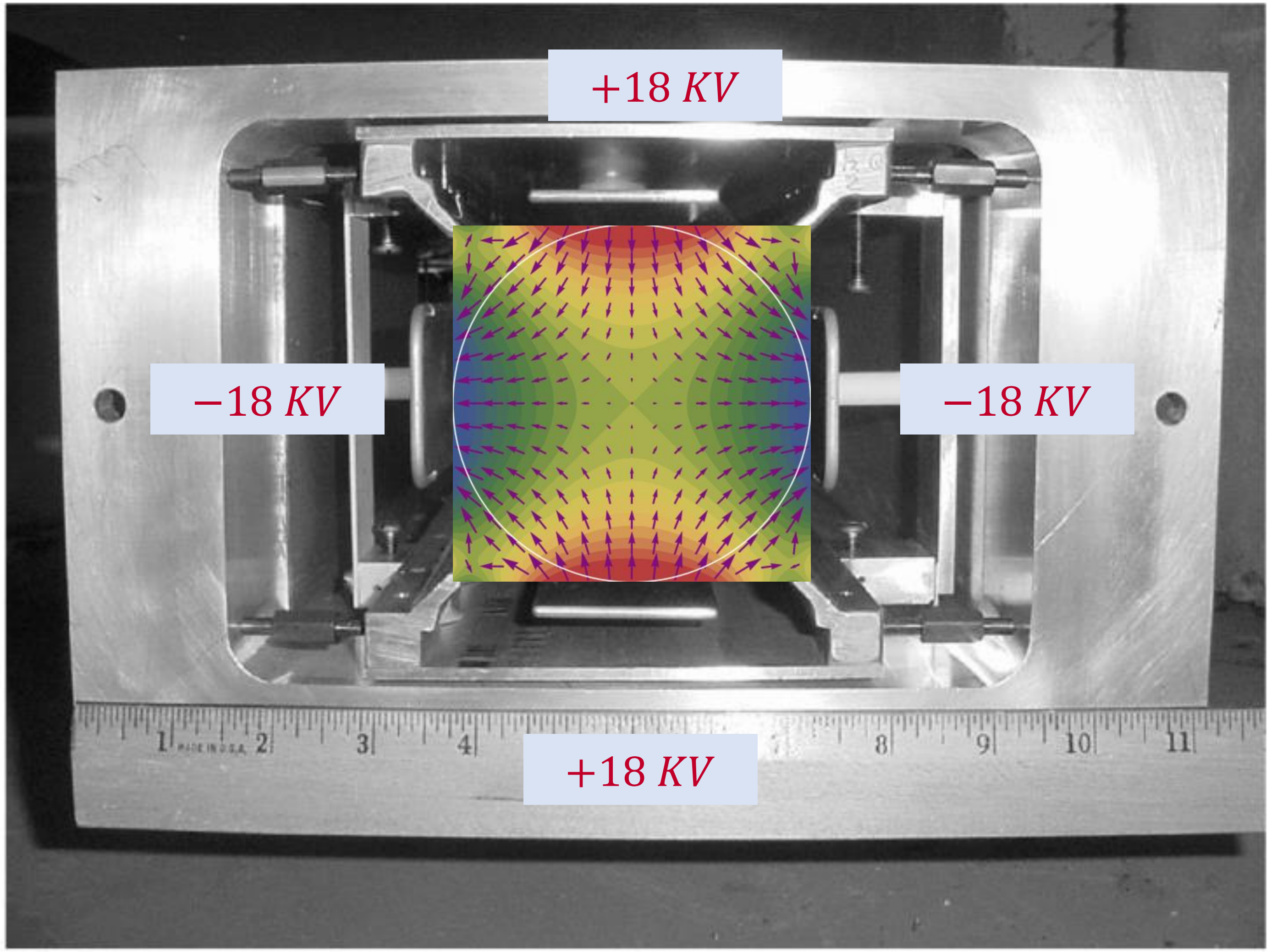

- At magic momentum electric fields have a very small impact on ω_a
- Electrostatic quadrupoles focus beam vertically
- Electrostatic quadrupoles defocus beam radially
- Magnetic field focus beam radially → Complex beam dynamics
- Quasi-penning trap cover 43% of the ring

Keeping the muons stored

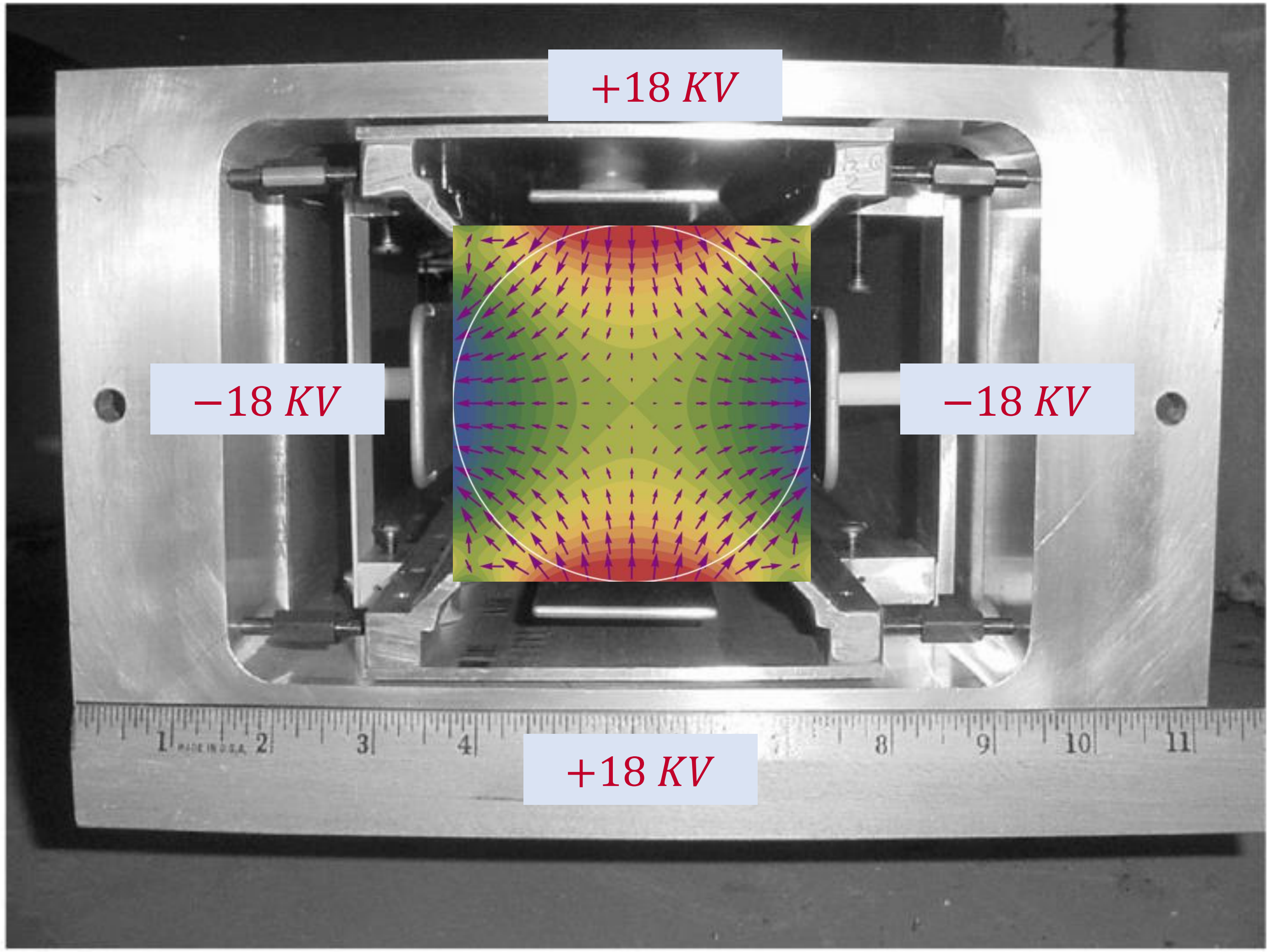

- At magic momentum electric fields have a very small impact on ω_a

- Electrostatic quadrupoles focus beam vertically
- Electrostatic quadrupoles defocus beam radially
- Magnetic field focus beam radially → Complex beam dynamics

- Quasi-penning trap cover 43% of the ring

- Pulsed “electrostatic” quadrupoles

Spin projection detection

muon rest frame

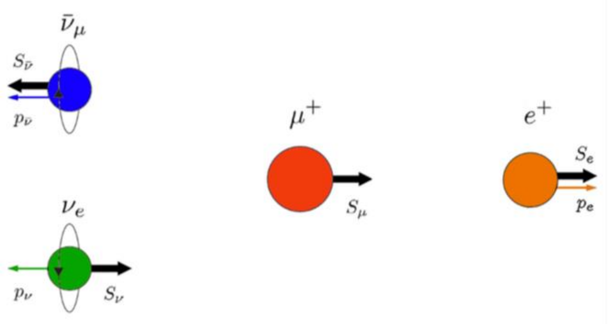

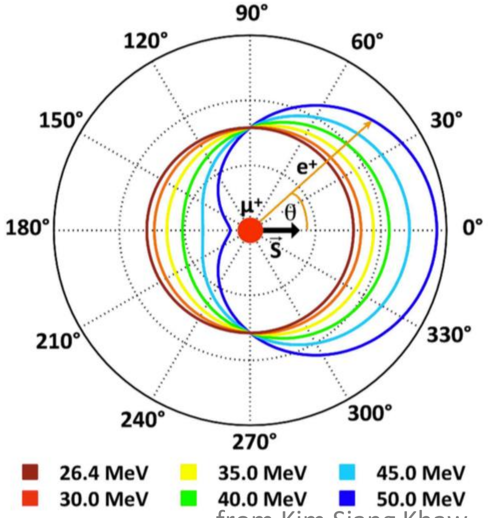

from Kim Siang Khaw

Spin projection detection

muon rest frame

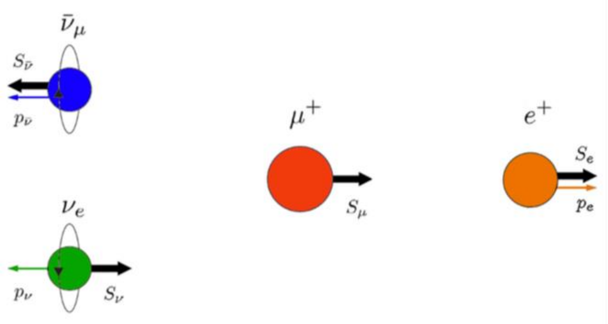

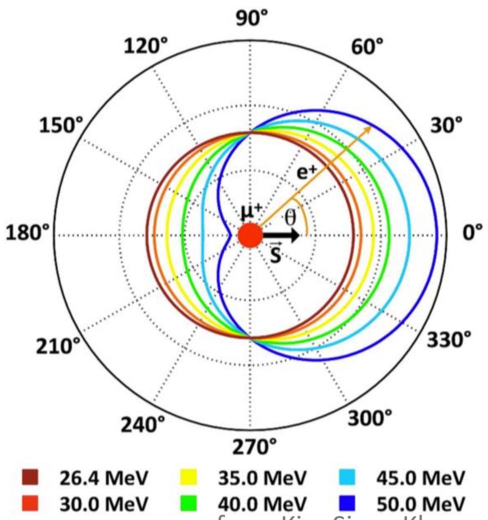

from Kim Siang Khaw

rest frame

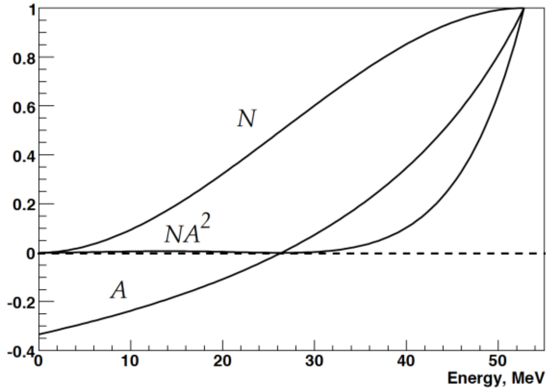

Spin projection detection

muon rest frame

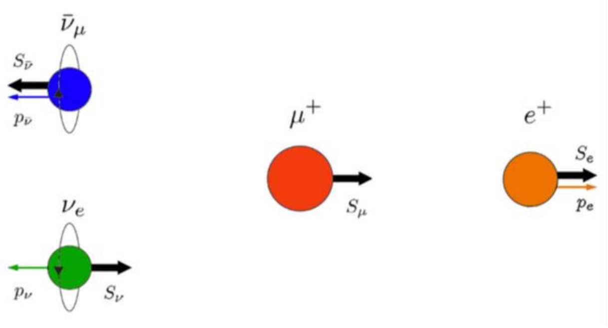

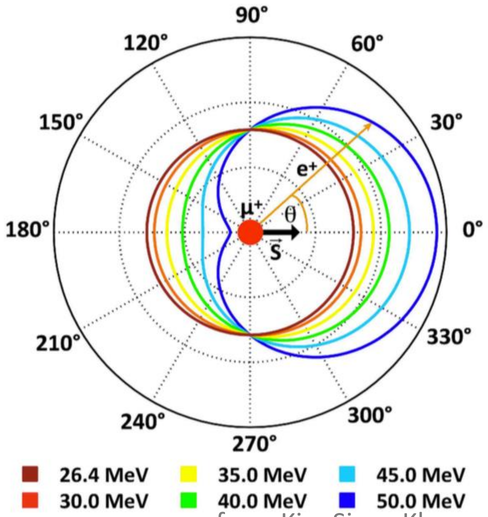

from Kim Siang Khaw

rest frame

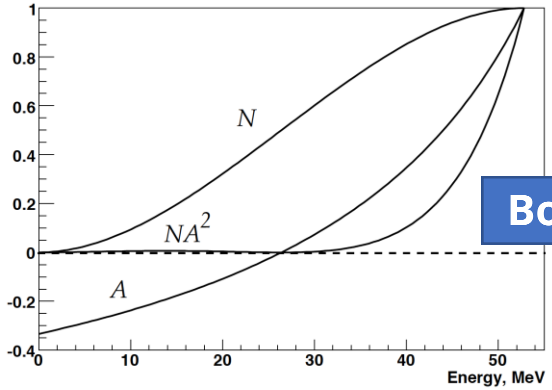

laboratory frame

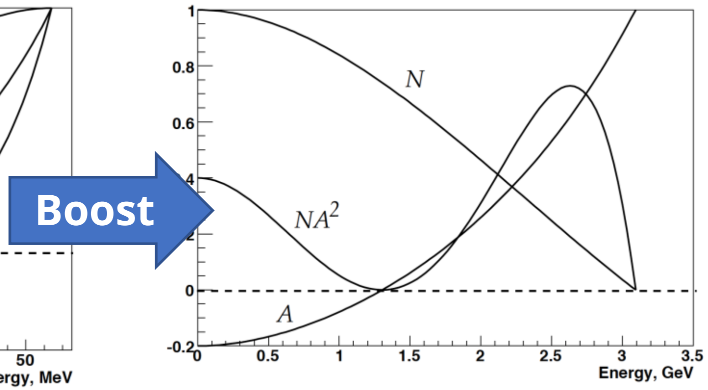

Spin projection detection

muon rest frame

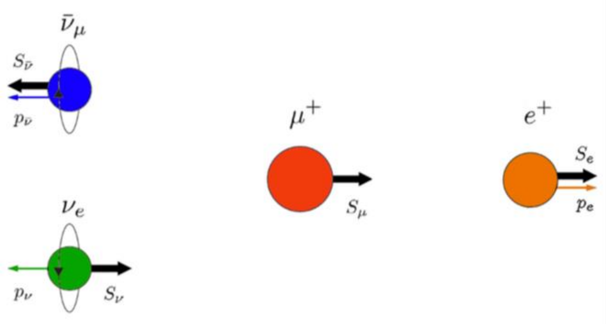

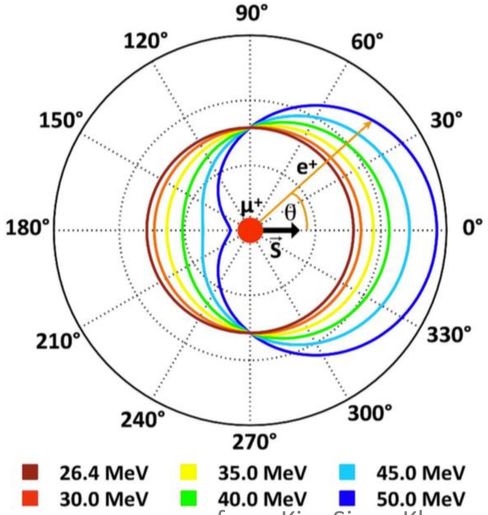

from Kim Siang Khaw

rest frame

laboratory frame

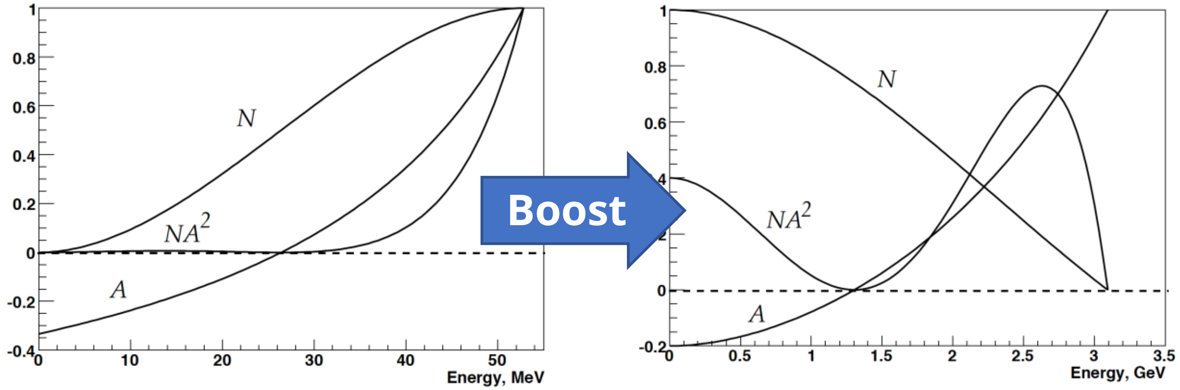

1/12 of the ring

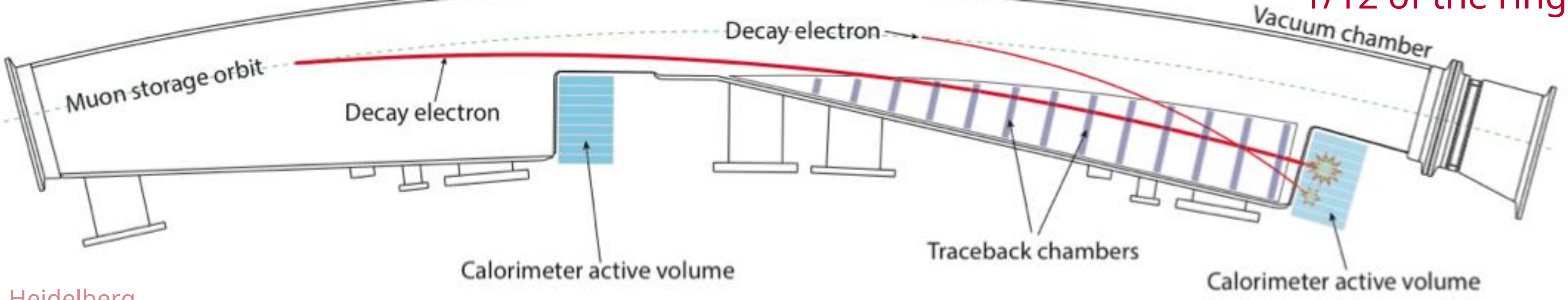

Spin projection detection

muon rest frame

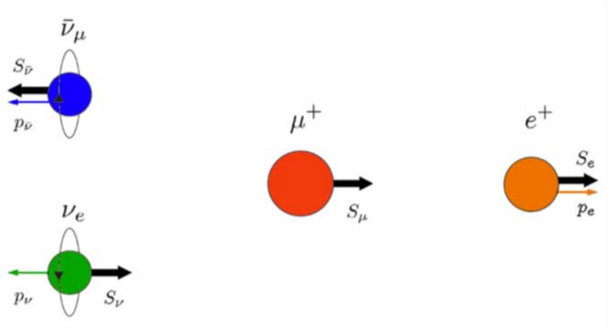

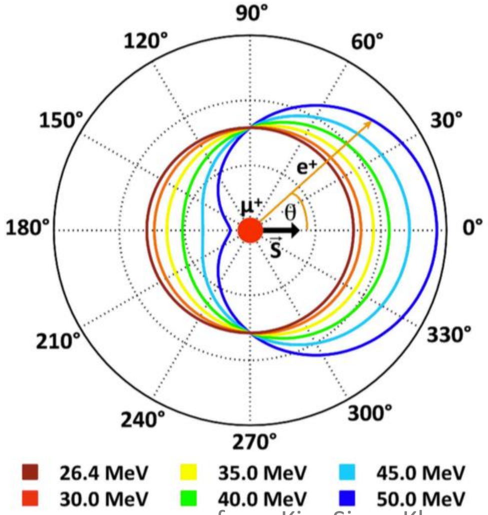

from Kim Siang Khaw

rest frame

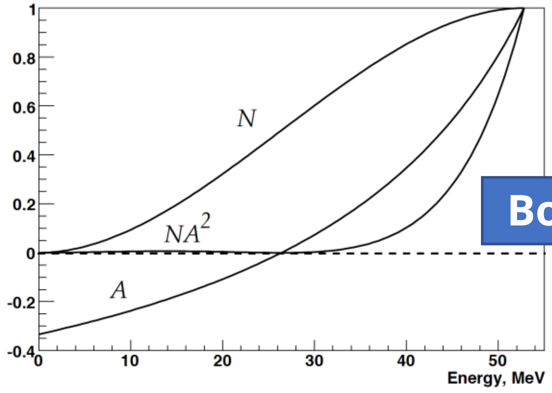

Boost

laboratory frame

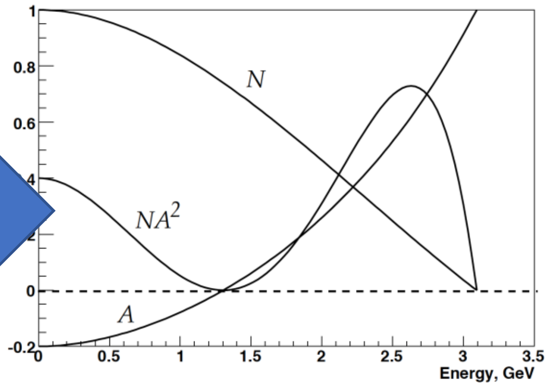

1/12 of the ring

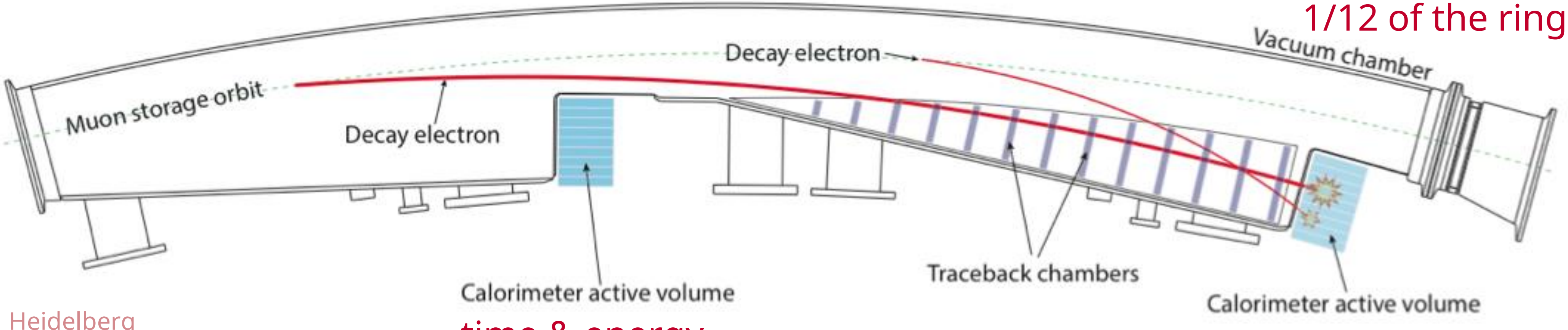

time & energy

Spin projection detection

muon rest frame

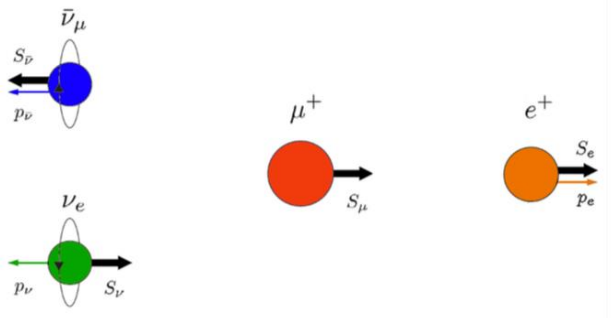

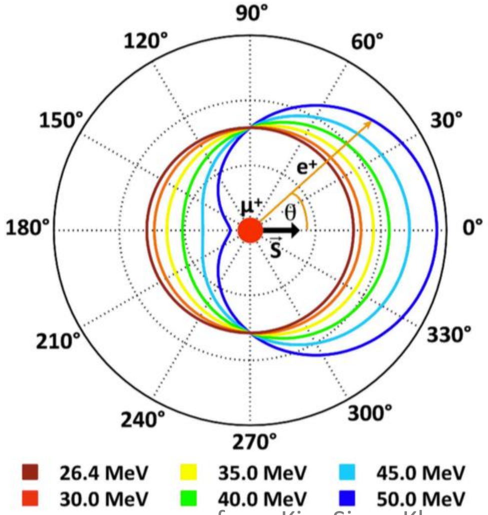

from Kim Siang Khaw

rest frame

laboratory frame

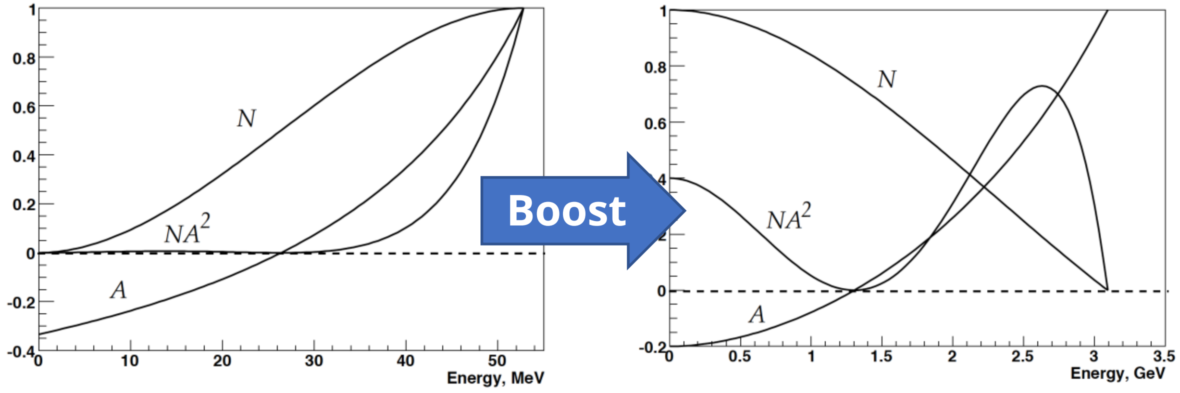

1/12 of the ring

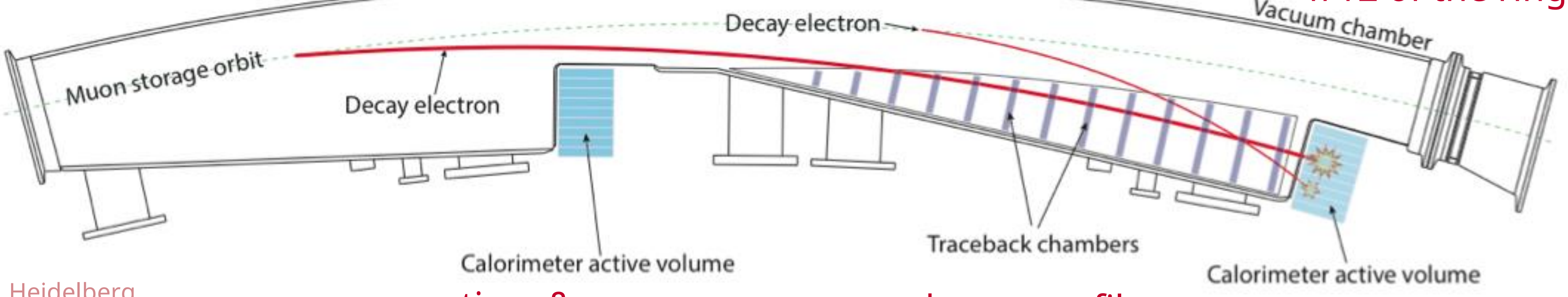

time & energy

beam profile

Tracking detectors

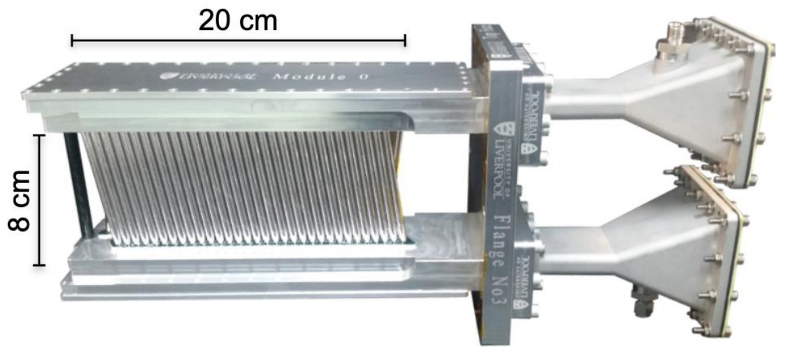

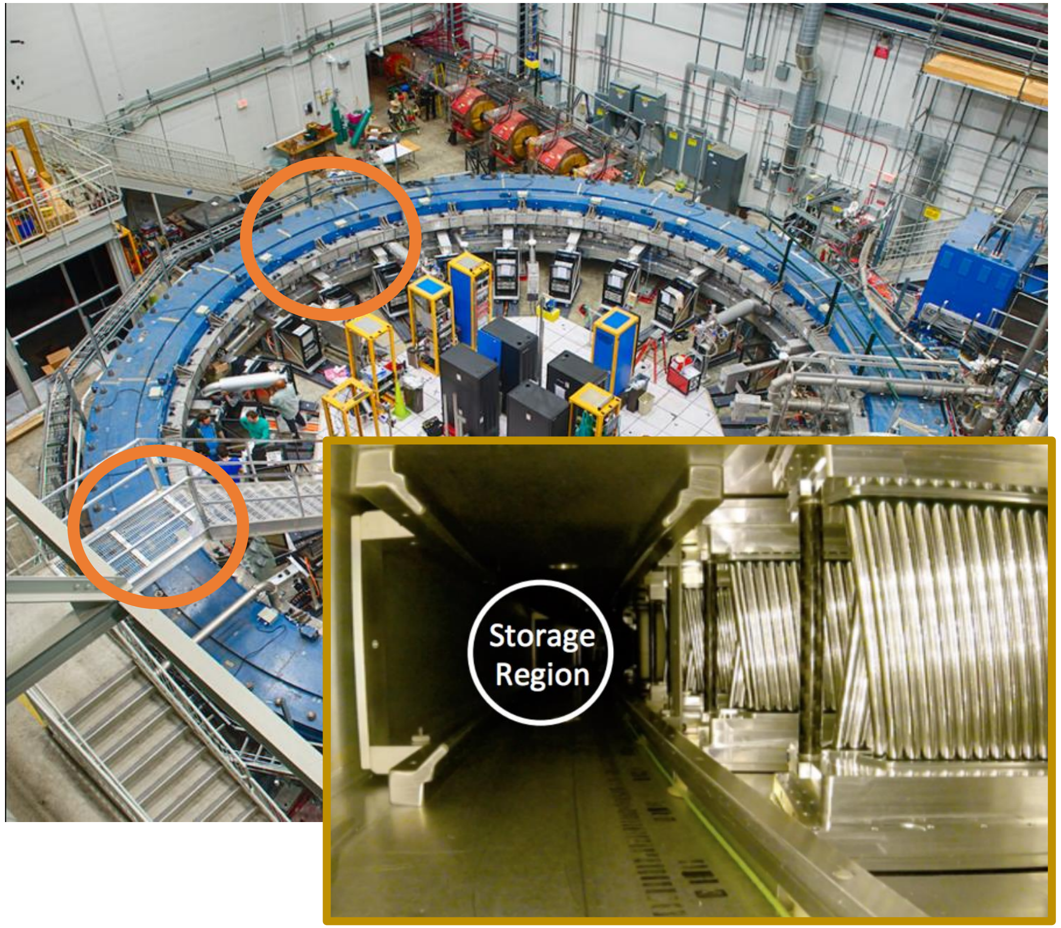

- Two tracking stations, each with 8 modules
- 128 gas-filled straws per module
- Determine e+ trajectory to decay position and extrapolate to find muon beam distribution!
- Input for beam dynamics simulations

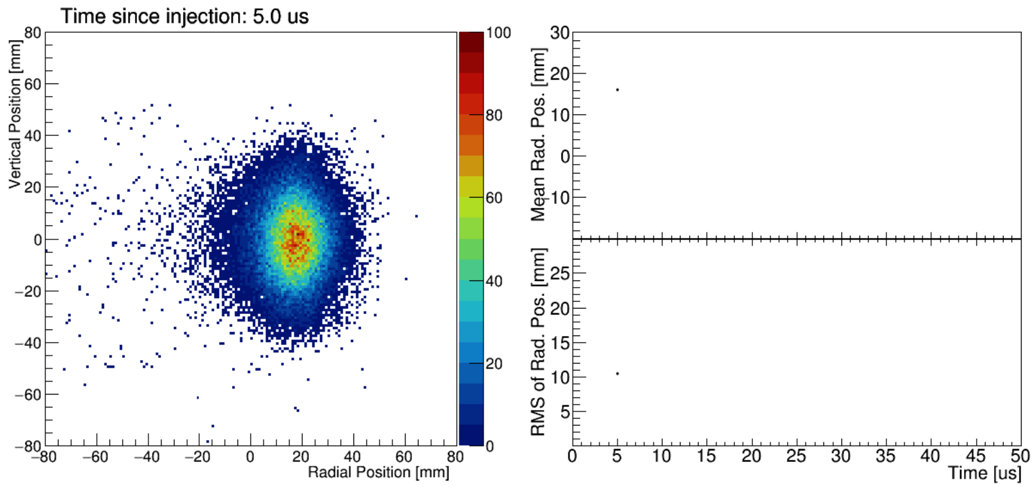

Positron detection

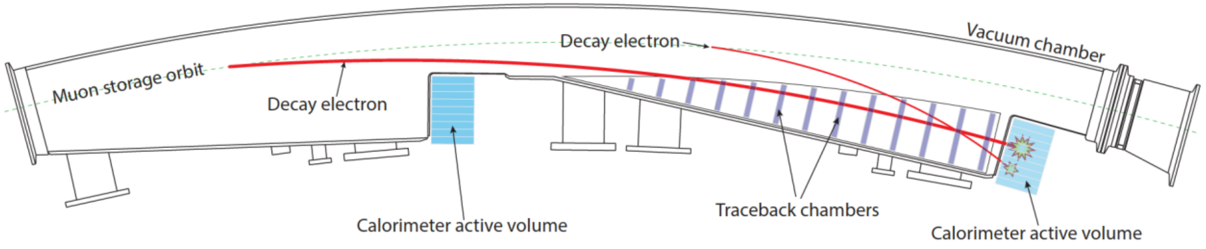

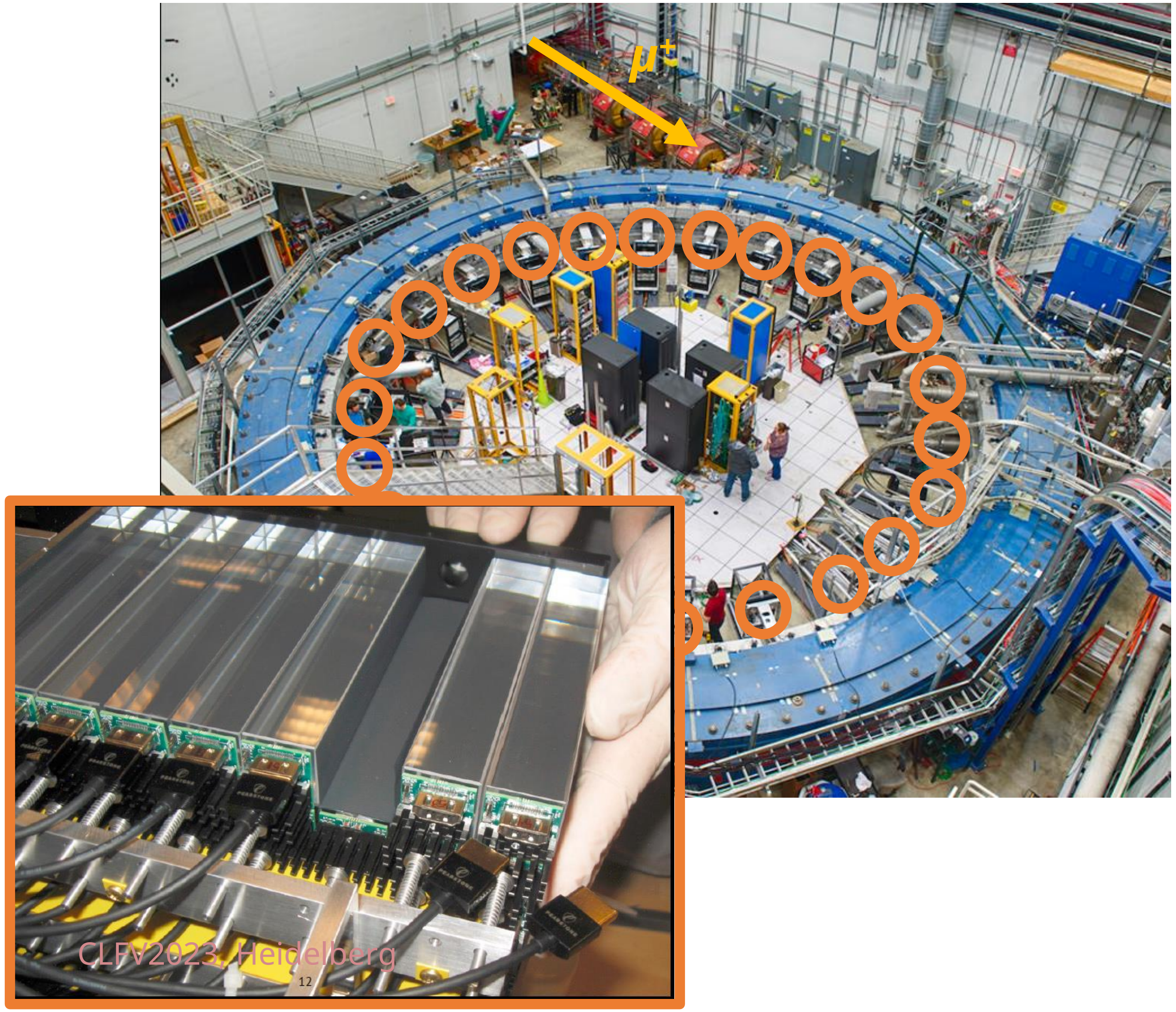

- 24 calorimeter stations
- 9 x 6 arrays of PbF_2 crystals (Cherenkov detectors!)
- Individual SiPM readout boards

Positron detection

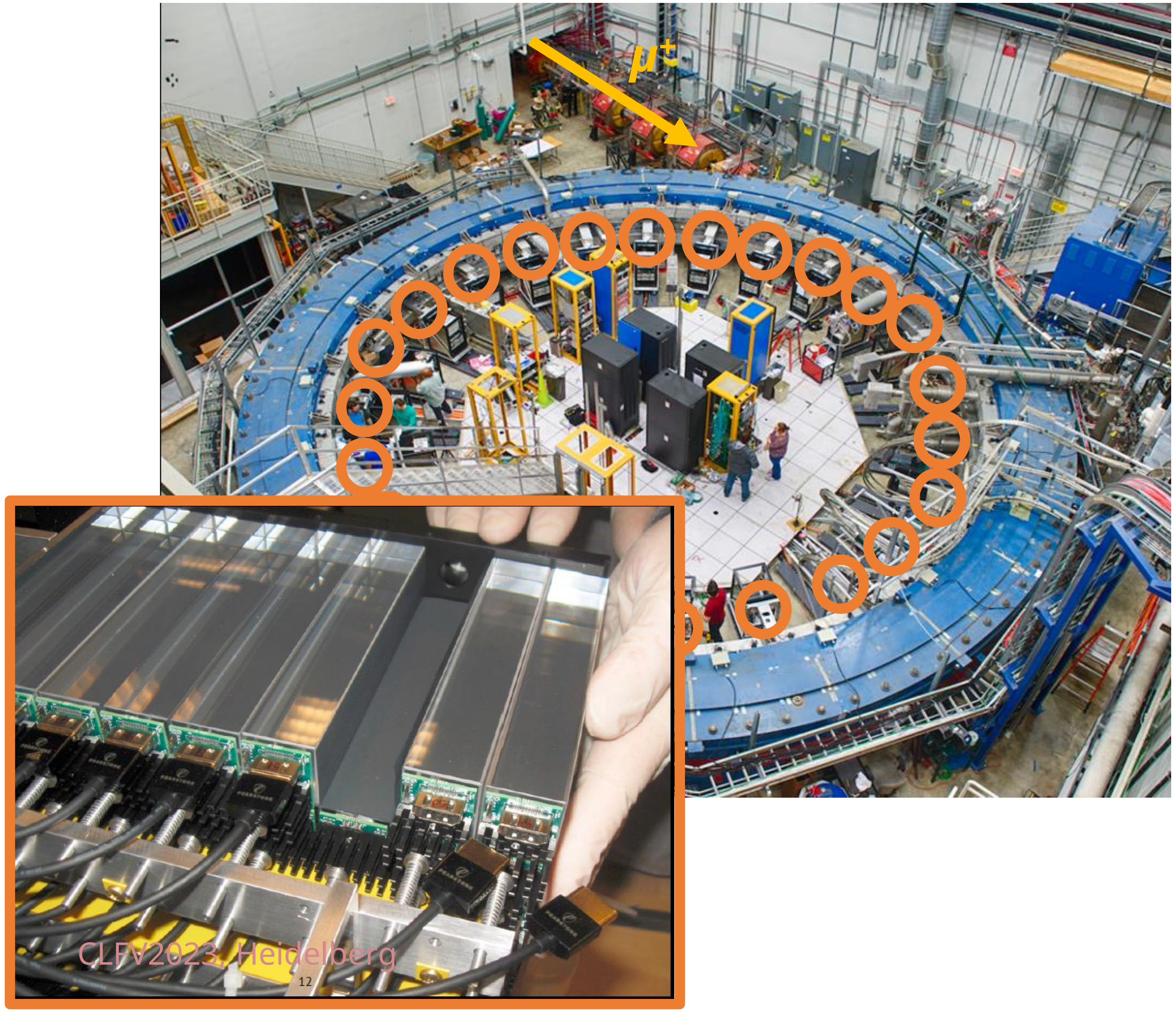

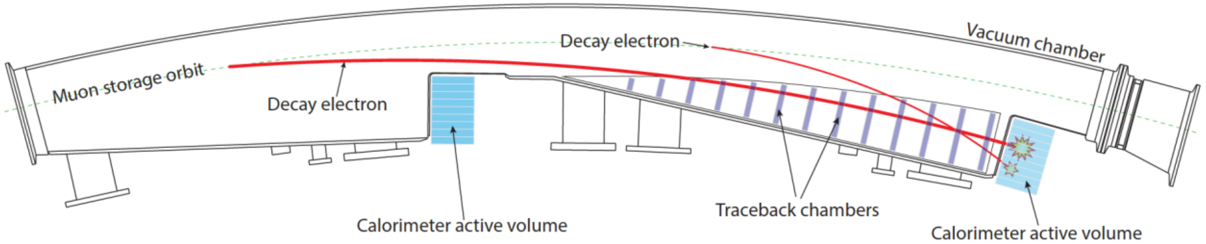

- 24 calorimeter stations
- 9 x 6 arrays of PbF2 crystals (Cherenkov detectors!)
- Individual SiPM readout boards

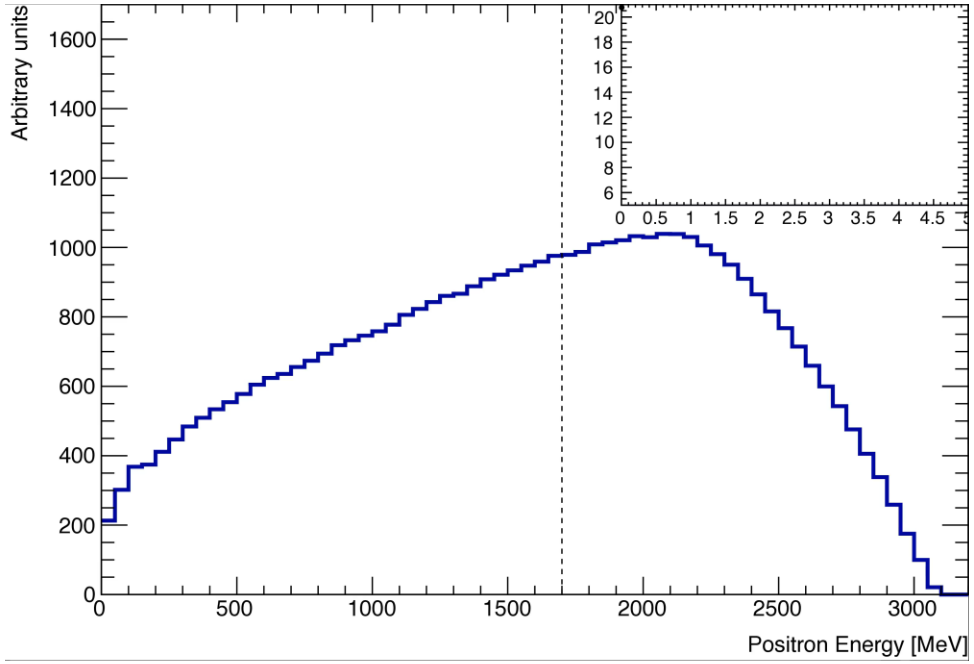

Fitting the “wiggle” plot

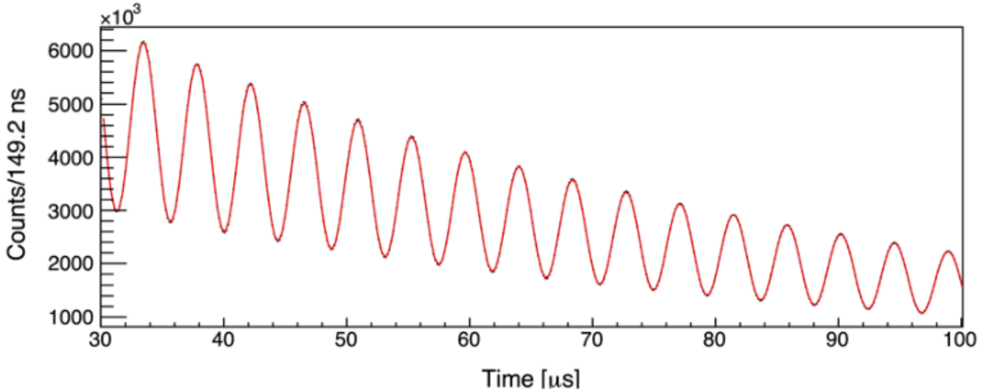

Fitting the “wiggle” plot

$$f(t) \propto N_0 e^{-\frac{t}{\gamma\tau}} \left[\langle N\rangle_{\mathrm{thresh}} + \langle A\rangle_{\mathrm{thresh}} \cos\left(\omega_{\mathrm{a}} t - \langle\phi\rangle_{\mathrm{thresh}}\right)\right]$$

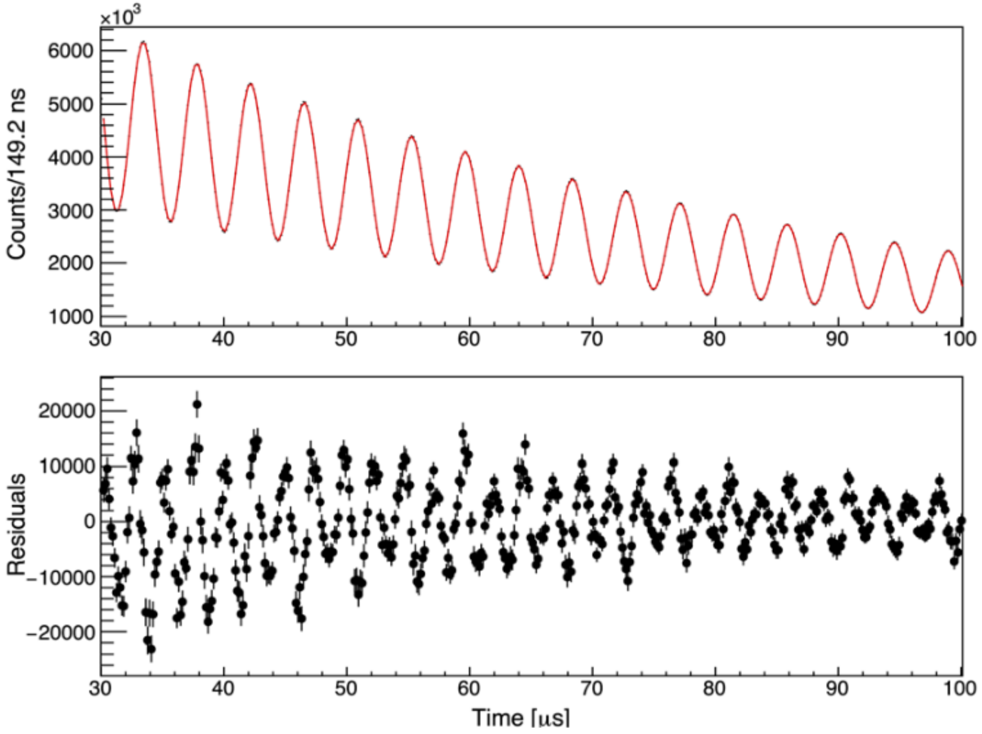

Fitting the “wiggle” plot

$$f(t) \propto N_0 e^{-\frac{t}{\gamma\tau}} \left[\langle N\rangle_{\text{thresh}} + \langle A\rangle_{\text{thresh}} \cos\left(\omega_{\text{a}} t - \langle\phi\rangle_{\text{thresh}}\right)\right]$$

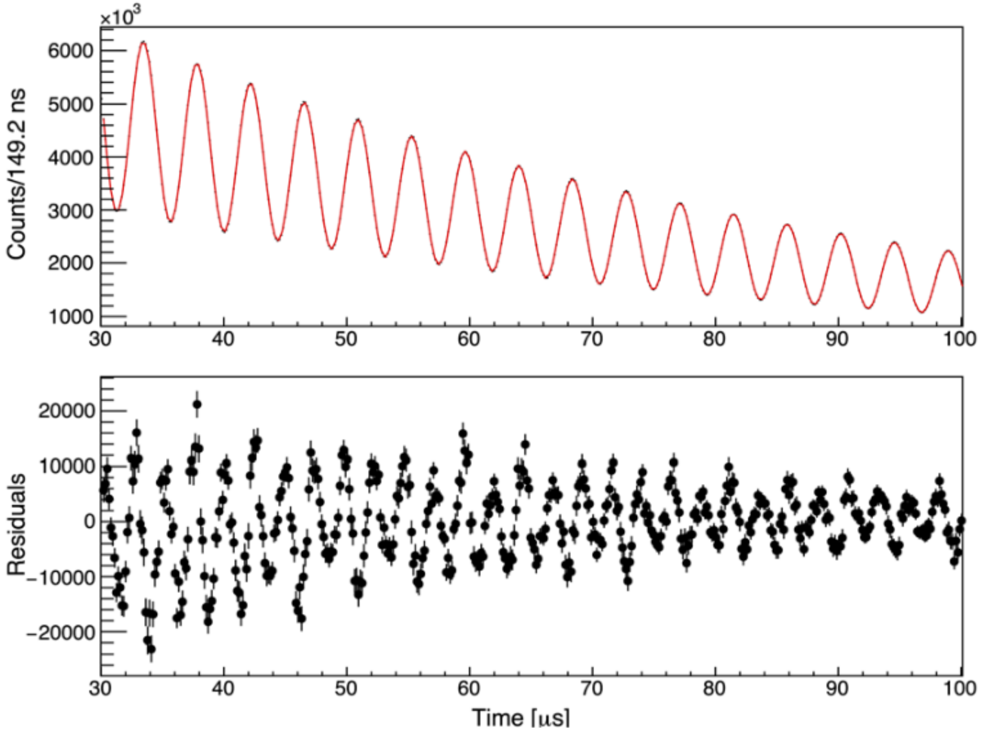

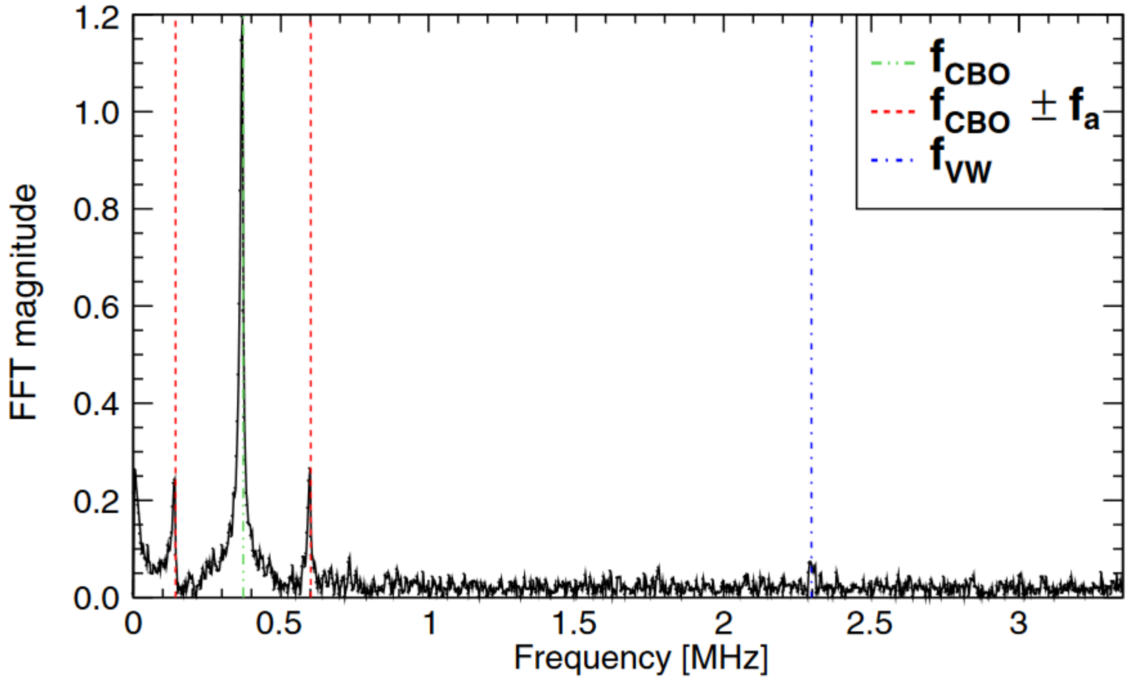

Fitting the “wiggle” plot

$$f(t) \propto N_0 e^{-\frac{t}{\gamma\tau}} \left[\langle N\rangle_{\text{thresh}} + \langle A\rangle_{\text{thresh}} \cos\left(\omega_{\text{a}} t - \langle\phi\rangle_{\text{thresh}}\right)\right]$$

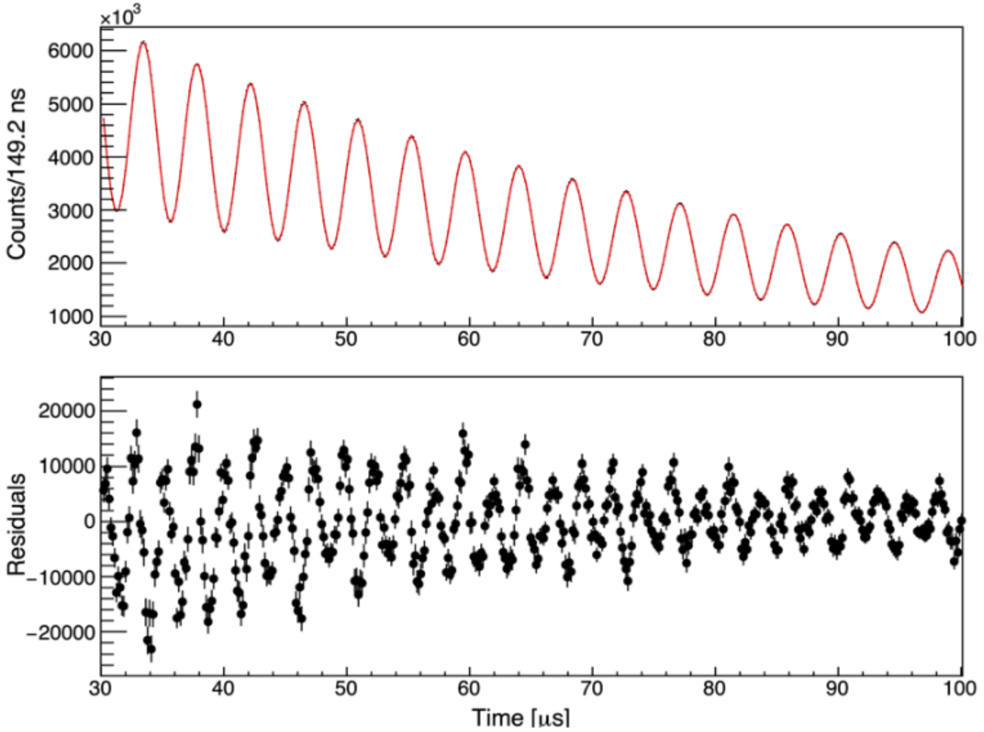

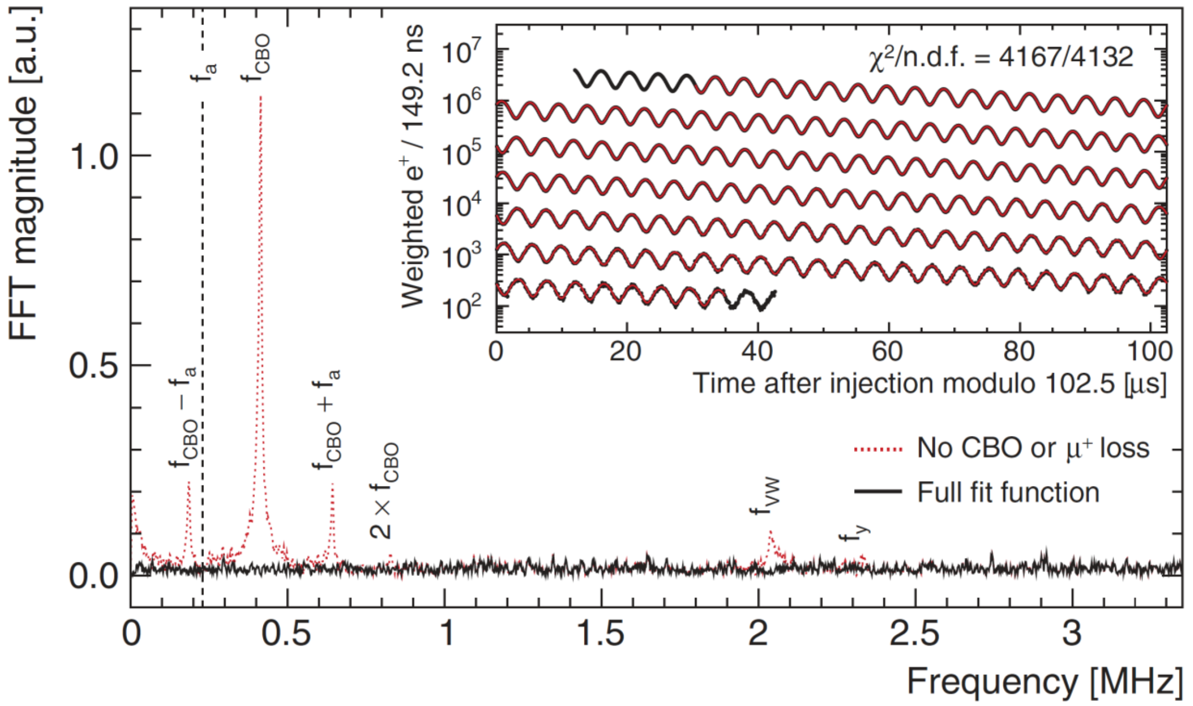

Account for complex beam dynamics
~27 free parameters in fit

Fitting the "wiggle" plot

$$f(t) \propto N_0 e^{-\frac{t}{\gamma\tau}} \left[\langle N\rangle_{\mathrm{thresh}} + \langle A\rangle_{\mathrm{thresh}} \cos\left(\omega_{\mathrm{a}} t - \langle\phi\rangle_{\mathrm{thresh}}\right)\right]$$

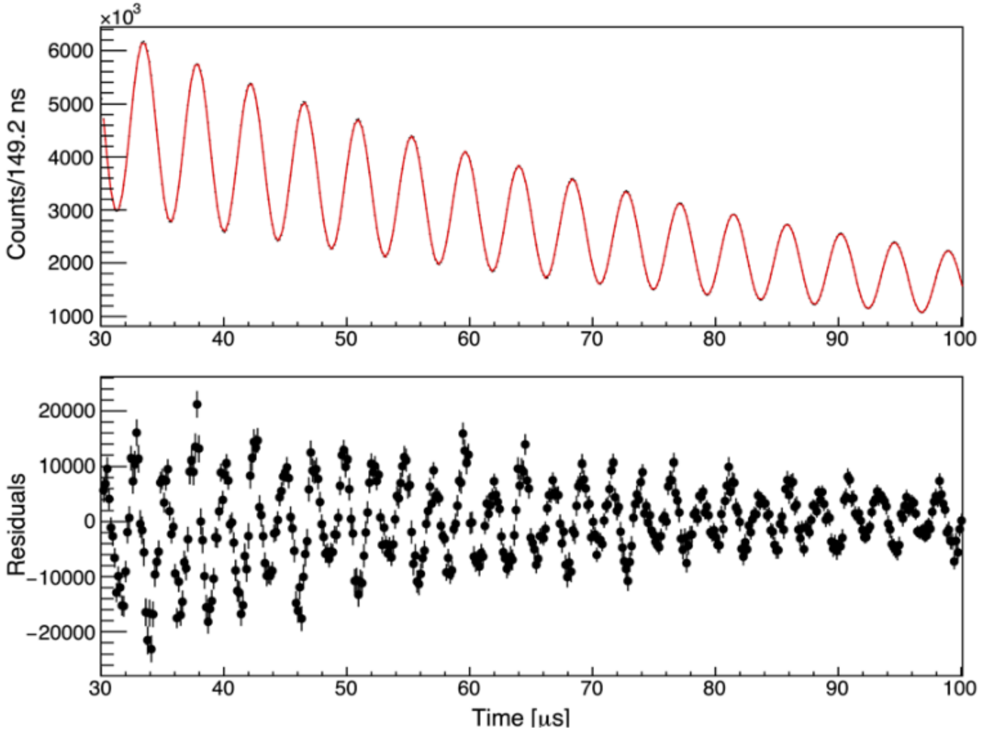

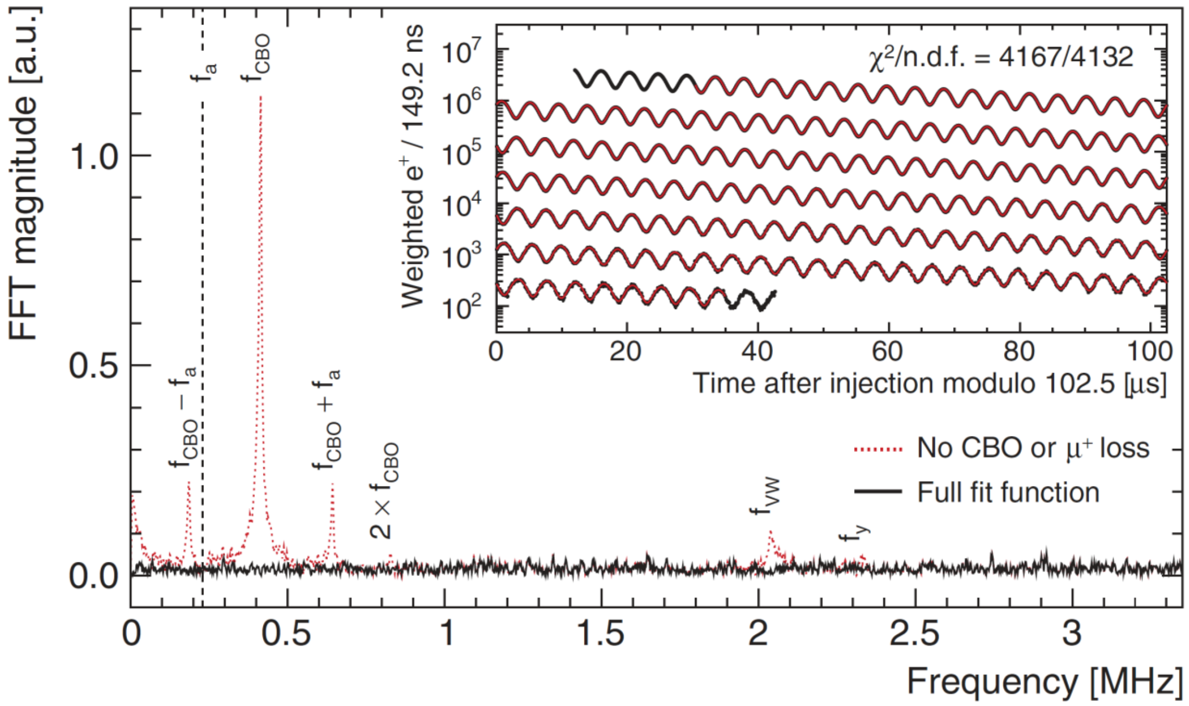

Any time dependent phase shift will bias the frequency

Account for complex beam dynamics
~27 free parameters in fit

Magnetic field tracking

Magnetic field tracking

Trolley system

17 NMR probes

pulled through ring every ~3 days

measures spatial field dist. in storage region

Magnetic field tracking

Trolley system

17 NMR probes

pulled through ring every ~3 days

measures spatial field dist. in storage region

Fixed probe system

72 azimuthal location (stations)

tracks field drift 24/7

measures field differences (drift)

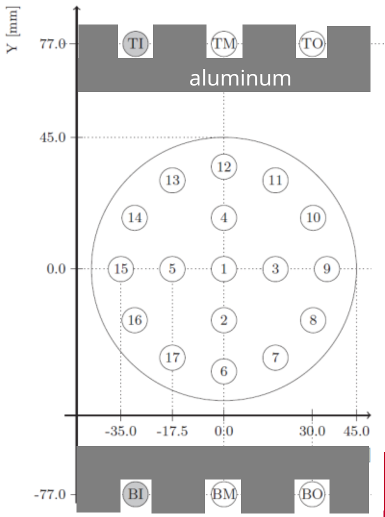

Magnetic field tracking

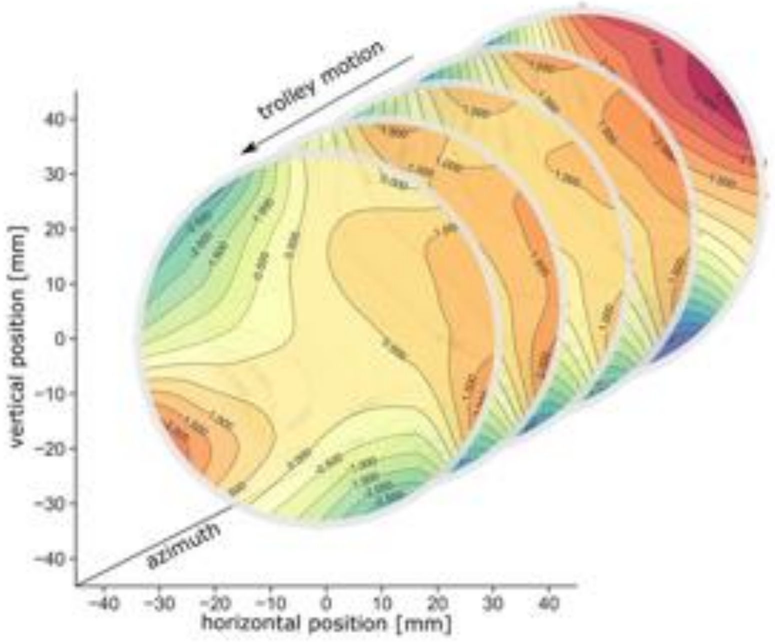

Magnetic field tracking

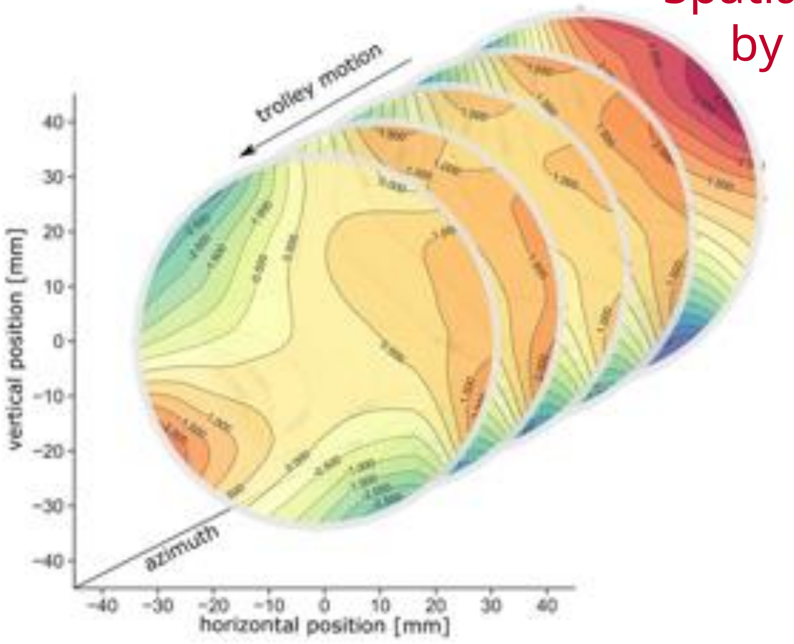

Spatial distribution described by multipole expansion

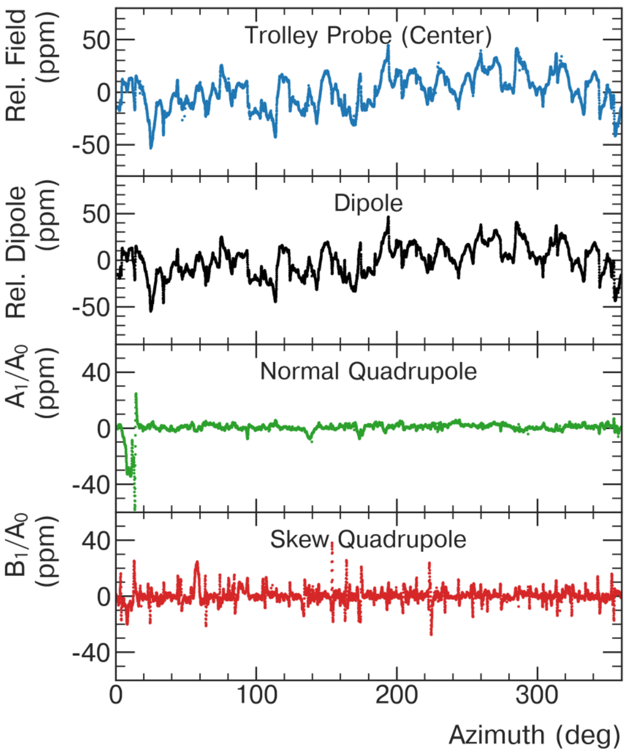

Magnetic field tracking

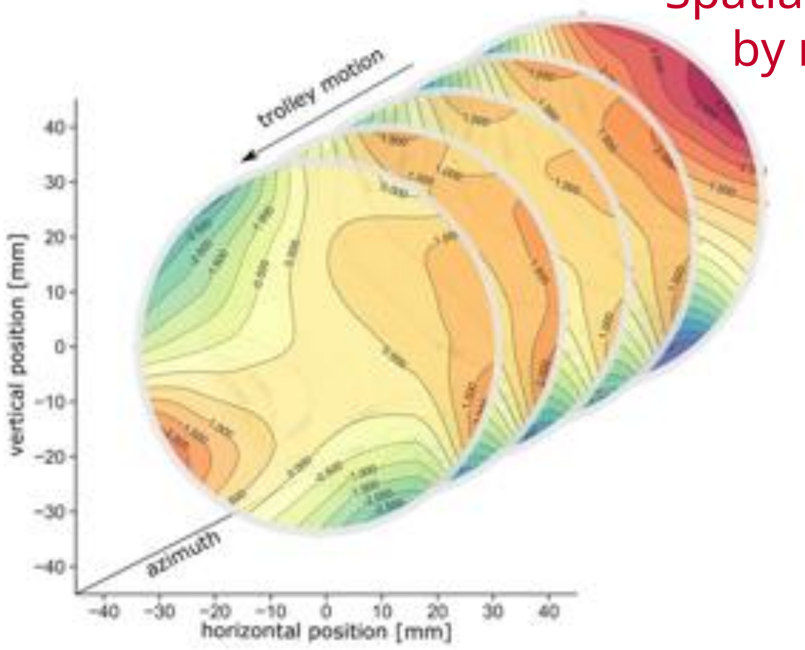

Spatial distribution described by multipole expansion

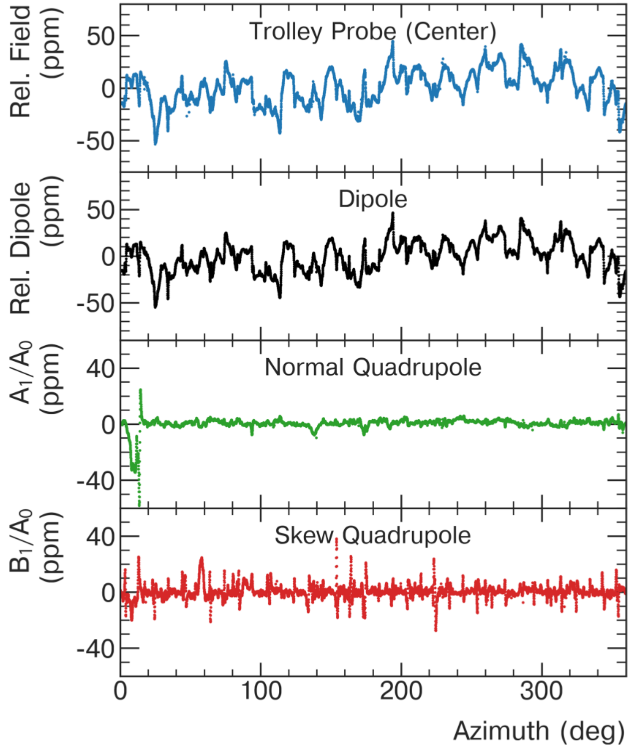

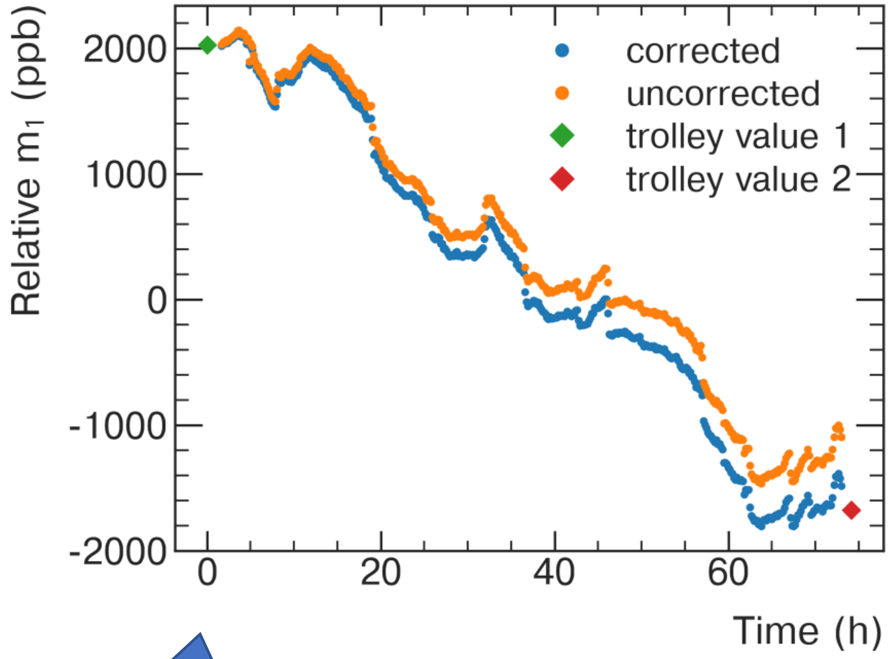

time interpolation using fixed probe data

Muon weighted magnetic field

- We need the field seen by the muons
- Tracking magnetic field multipole moments
- Muon distribution given by tracker data and beam dynamics simulation

$$\frac{\omega_a}{\tilde{\omega}'_p} = \frac{f_{\text{clock}}\,\omega_a^{\text{meas}}\,(1 + C_e + C_p + C_{ml} + C_{pa})}{f_{\text{calib}}\,\langle M(x,y,\phi)\,\omega'_p(x,y,\phi)\rangle\,(1 + B_k + B_q)}$$

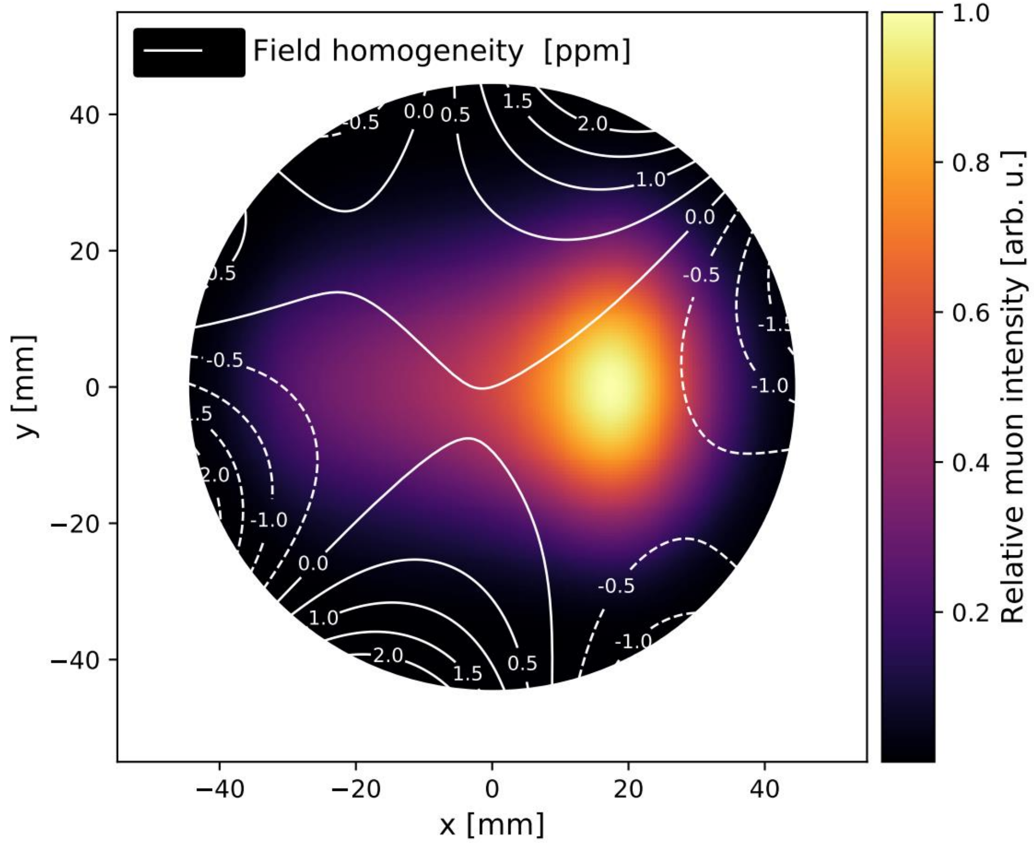

Field calibration

- Trolley is main device to measure the field
  - Trolley probes based on petroleum jelly
  - Needs calibration

Field calibration

- Trolley is main device to measure the field
  - Trolley probes based on petroleum jelly
  - Needs calibration
- Absolute calibrated water probe
- Cross-calibrated at Argonne National Lab test magnet

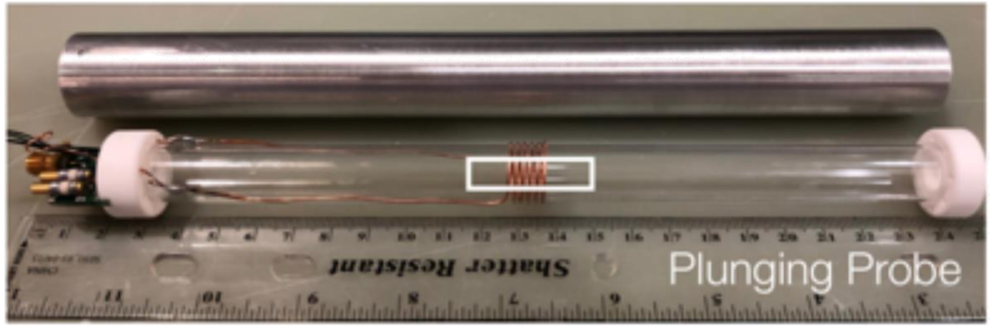

Field calibration

- Trolley is main device to measure the field
    - Trolley probes based on petroleum jelly
    - Needs calibration
- Absolute calibrated water probe
- Cross-calibrated at Argonne National Lab test magnet

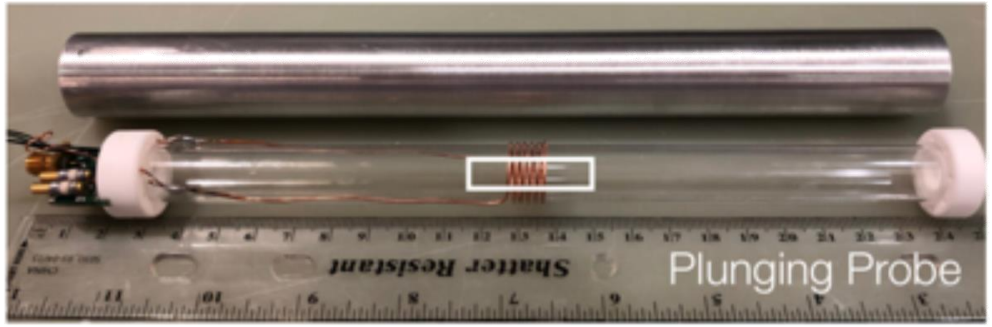

- Probe can be placed in ring by 3D translation stage
- Swap trolley and calibration probe ten times
- Derive calibration constants for each trolley probe

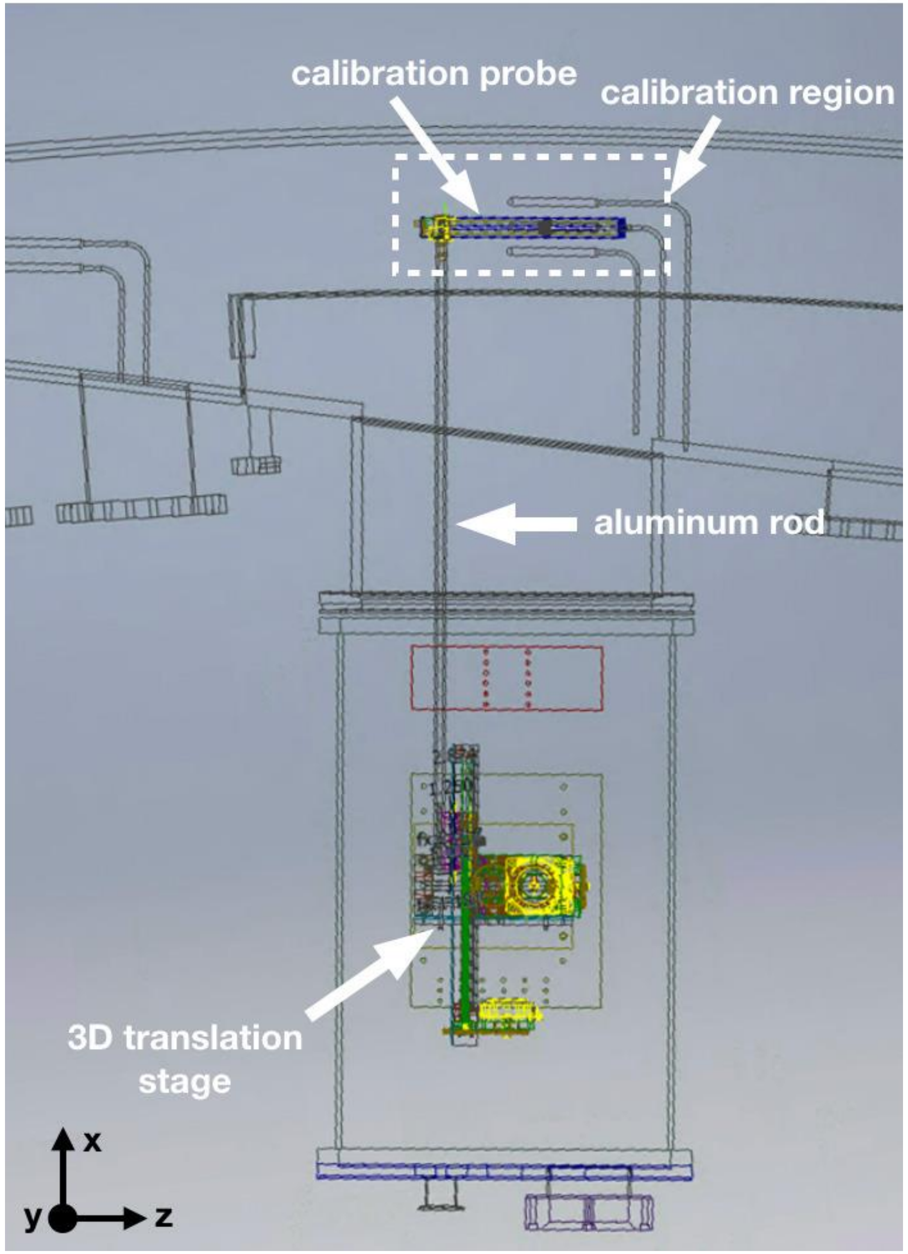

Kicker transient magnetic field

Kicker used to place beam on storage orbit

Kicker pulse induces 22mT field in radial direction

Measurement based on optical faraday rotation

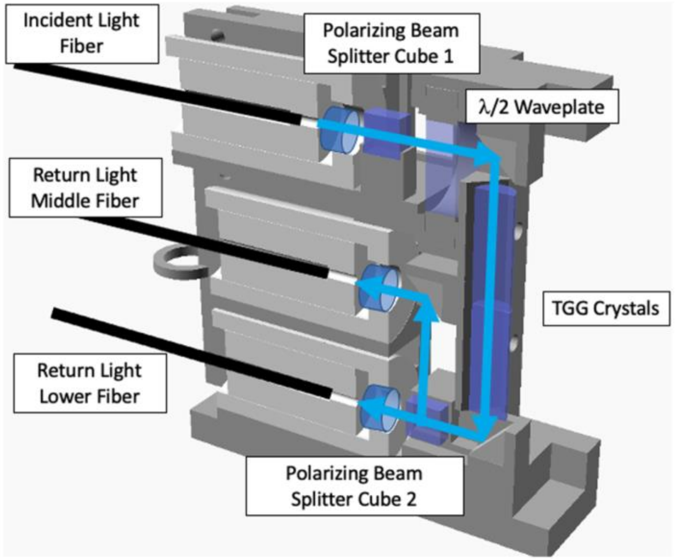

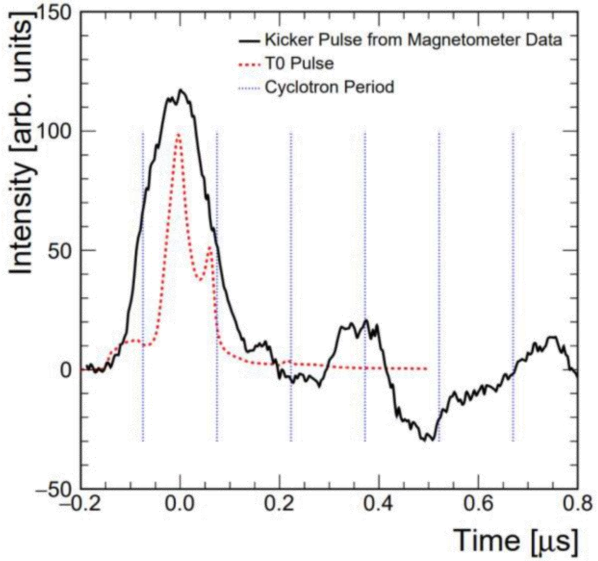

Magnetic field quadrupole transients

Pulsing electrostatic quadrupoles for beam confinement leads to magnetic field transient.

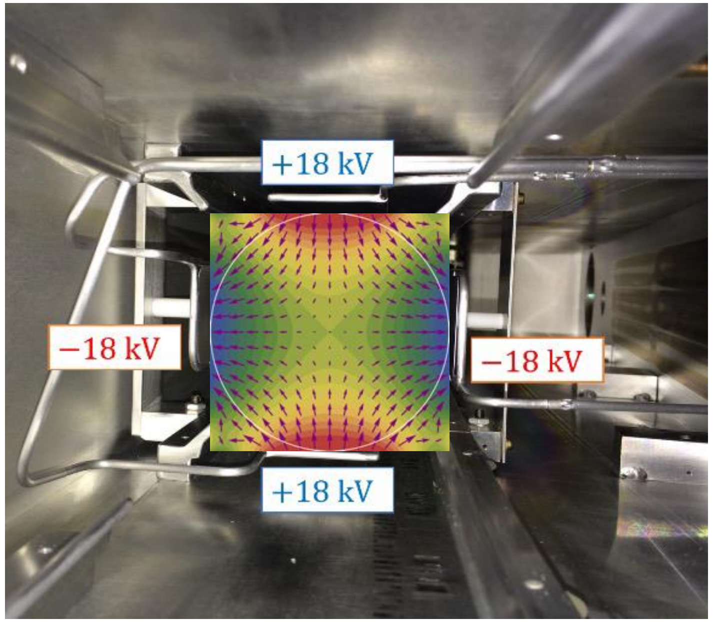

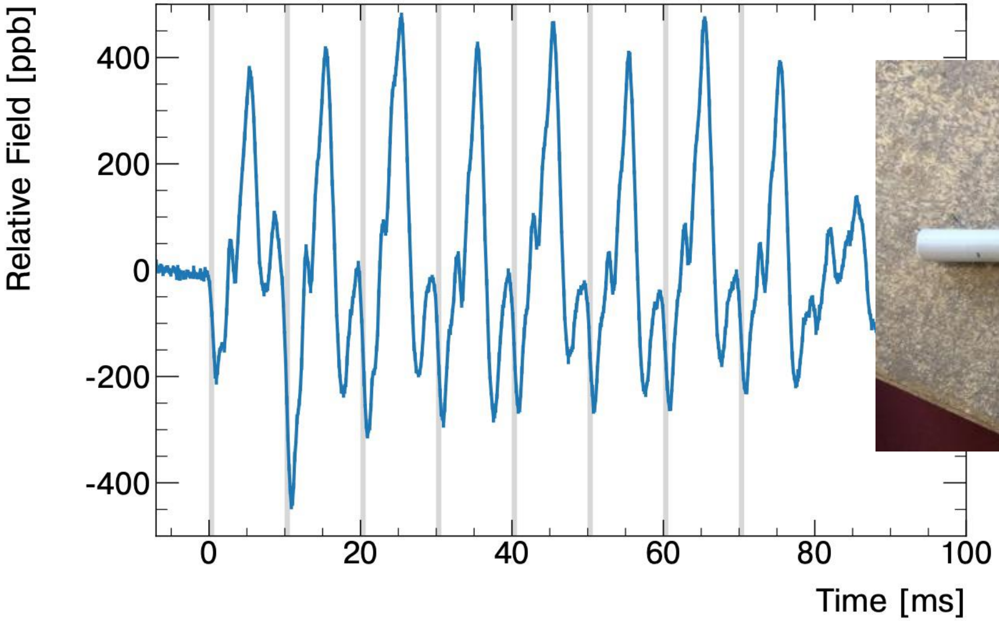

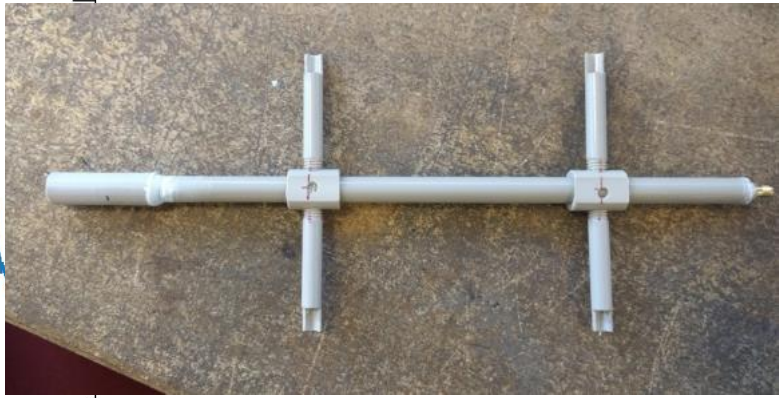

NMR probes run asynchronous with beam injection
Fast transient fields are shielded by aluminum in vacuum chambers

Magnetic field quadrupole transients

Pulsing electrostatic quadrupoles for beam confinement leads to magnetic field transient.

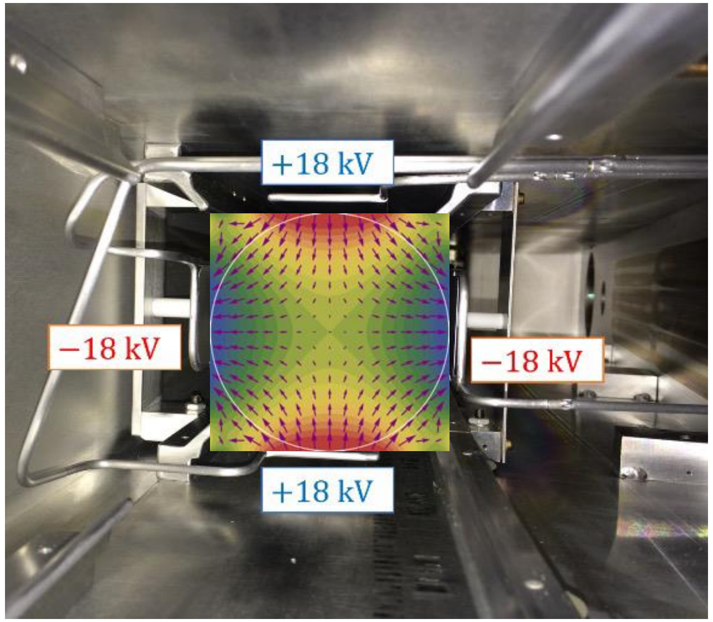

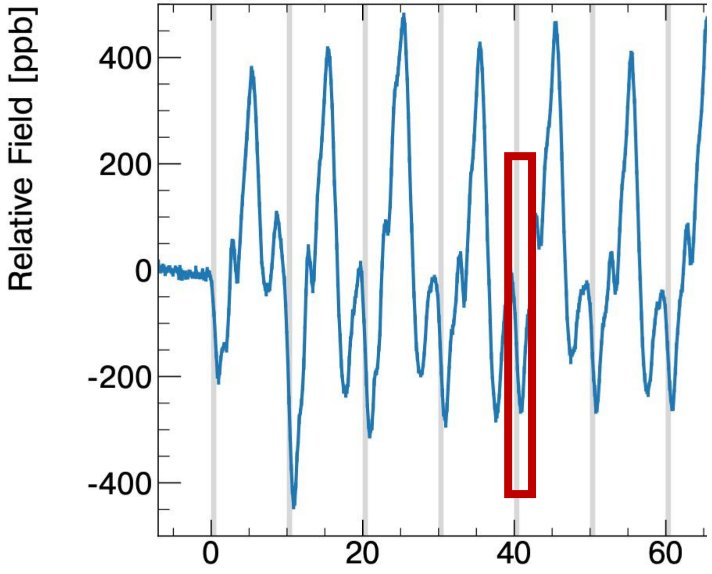

μ present

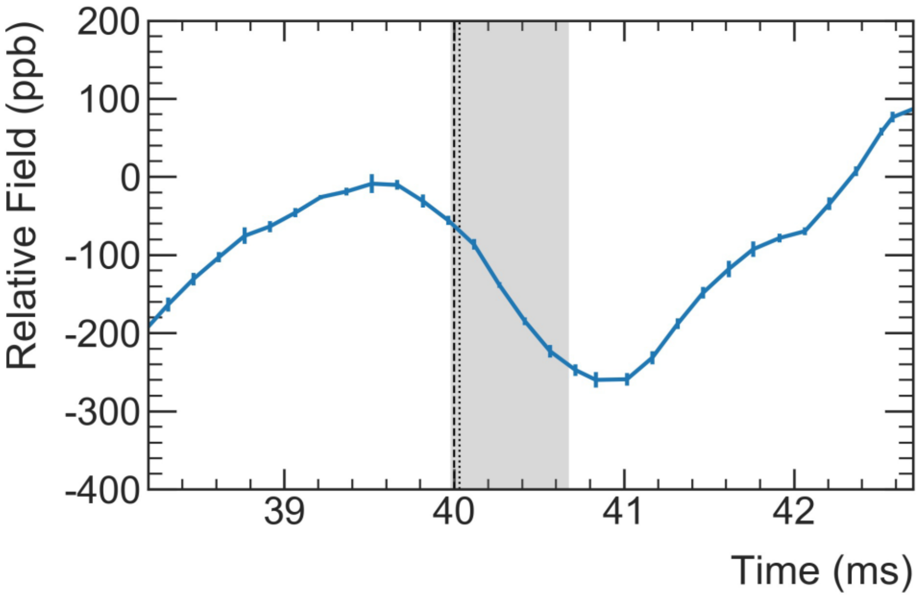

NMR probes run asynchronous with beam injection

Fast transient fields are shielded by aluminum in vacuum chambers

Uncertainties for Run 1

$$\frac{\omega_a}{\tilde{\omega}'_p} = \frac{f_{\text{clock}}\,\omega_a^{\text{meas}}\,(1 + C_e + C_p + C_{ml} + C_{pa})}{f_{\text{calib}}\,\langle M(x,y,\phi)\,\omega'_p(x,y,\phi)\rangle\,(1 + B_k + B_q)}$$

Quantity	Correction Terms (ppb)	Uncertainty (ppb)	Run 1 Design goal
ω_a^m (statistical)	–	434	100 ppb
ω_a^m (systematic)	–	56	70 ppb (bracket: ω_a^m (systematic) through C_{pa})
C_e	489	53	
C_p	180	13	
C_{ml}	-11	5	
C_{pa}	-158	75	
$f_{\text{calib}}\langle\omega_p(x,y,\phi) \times M(x,y,\phi)\rangle$	–	56	70 ppb (bracket: f_{calib} through B_q)
B_k	-27	37	
B_q	-17	92	
$\mu'_p(34.7°)/\mu_e$	–	10	
m_μ/m_e	–	22	
$g_e/2$	–	0	
Total systematic	–	157	100 ppb
Total fundamental factors	–	25	
Totals	544	462	140 ppb

- Improve statistics
  → take more data
- Systematics must be improved to achieve design goal
  → Reduce systematics in operations
  → Improve understanding of systematic effects

Data Taking

- Run 1 analysis published
  - Statistics → ~462 ppb
  - Systematic → 157 ppb
- Run2/3 analysis completed
  - Internal review, still blind
  - New result coming soon
  - Statistics → ~230 ppb
  - Systematic → ~110ppb

- No negative muons
- Past design goal of 21 BNL /27.02
- Run6 focus on systematic studies
- Run 4/5/6 analysis starting

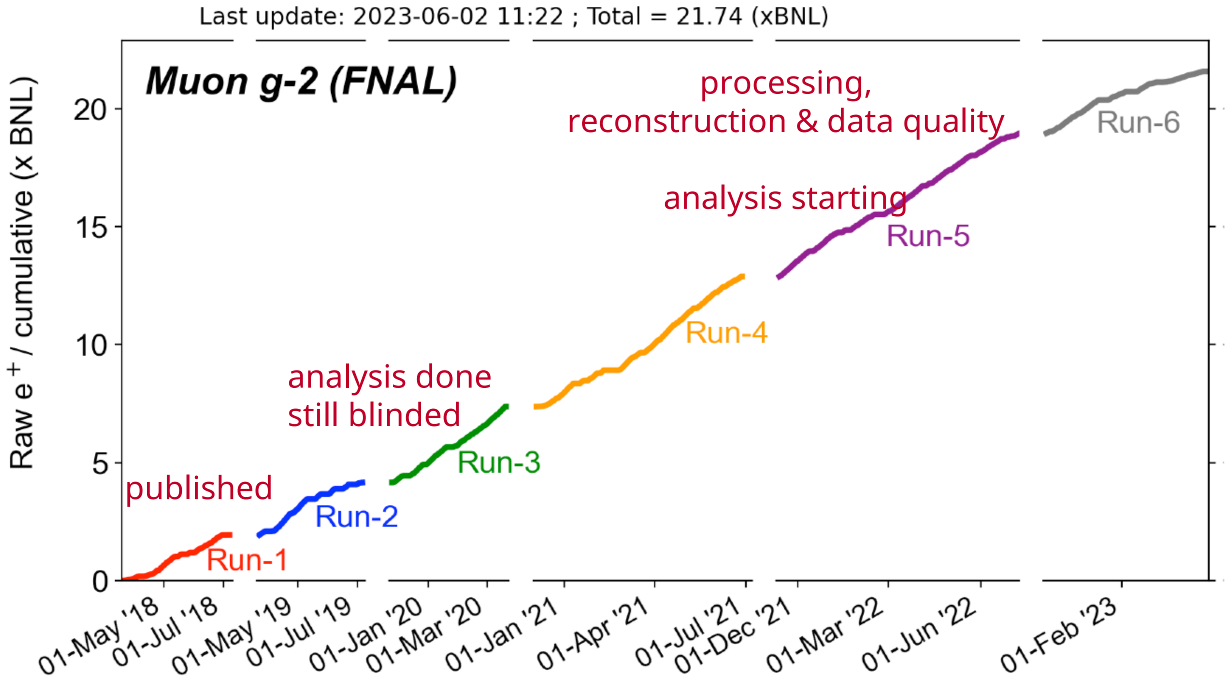

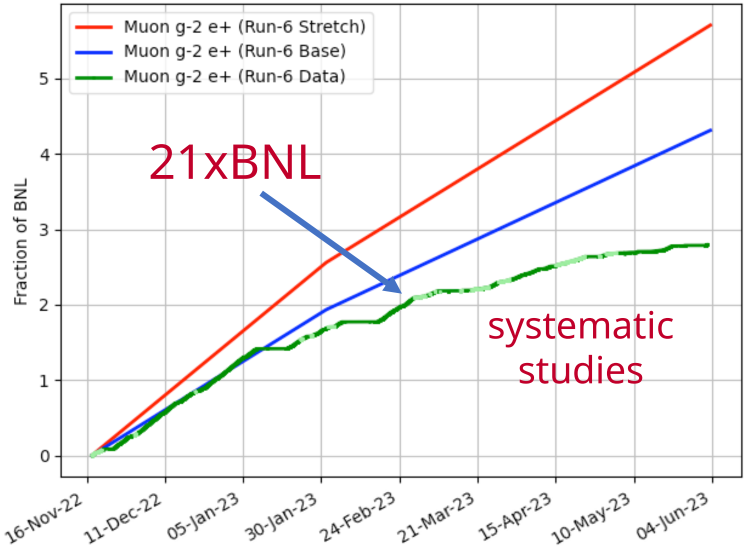

Improvements in Run 2/3

- ESQ transient dominating systematic in run1 (92ppb)
  - New effect (assume mechanical vibrations of quad plates)
  - Spatial & time structure unknown
  - Estimated from measurements in ~20° region
- Summer 2021 measurement campaign
  - Measure field with PEEK NMR probe synchronized to trigger
  - Scan delay between trigger & NMR measurement (20 min)
  - Measure spatial structure repeating at 92 azimuthal locations
  - Total uncertainty ~20ppb

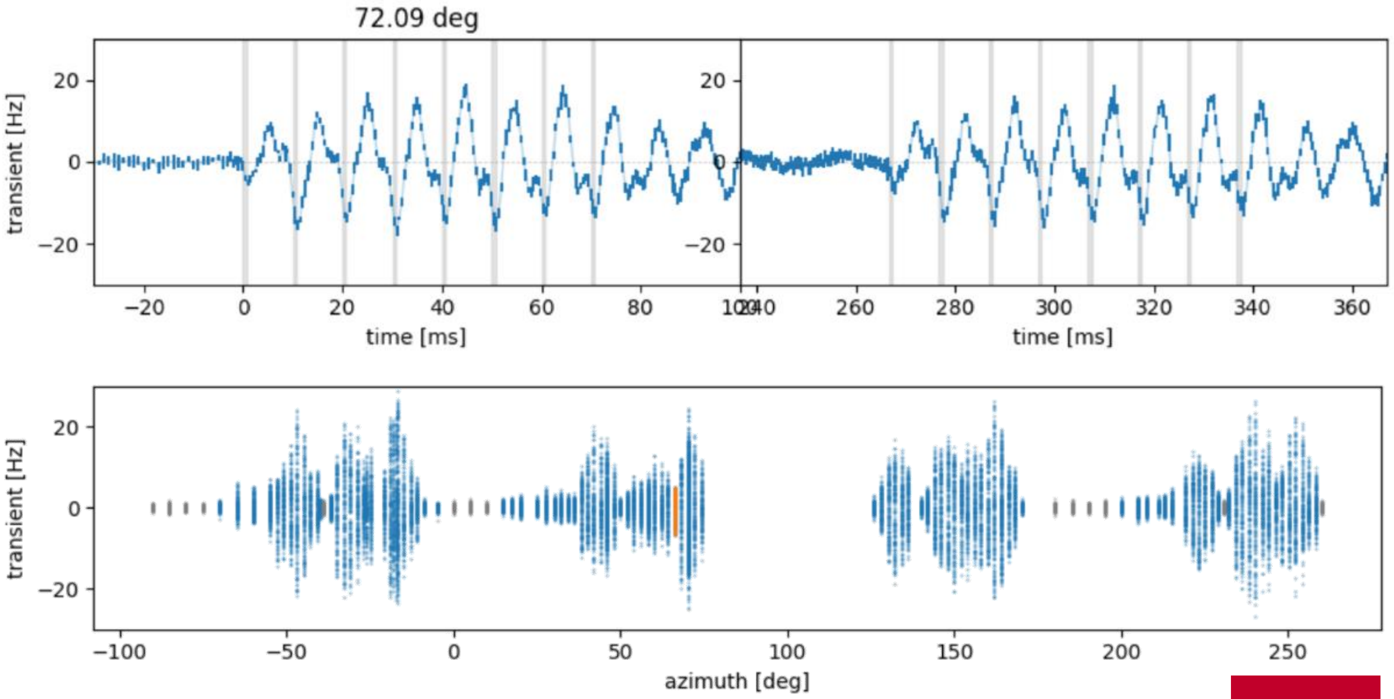

Summary

- High precision measurements of muon g-2 stringent test on SM theory
- First time a three-way comparison of a_μ is possible, very exciting
- Run 2 / 3 result soon
  - four times larger statistics
  - ~1/3 reduction in systematics
- Analysis for EDM on-going as well
- Reached 21 x BNL statistics and detailed systematic datasets
- Run 4/5/6 analysis ramping up

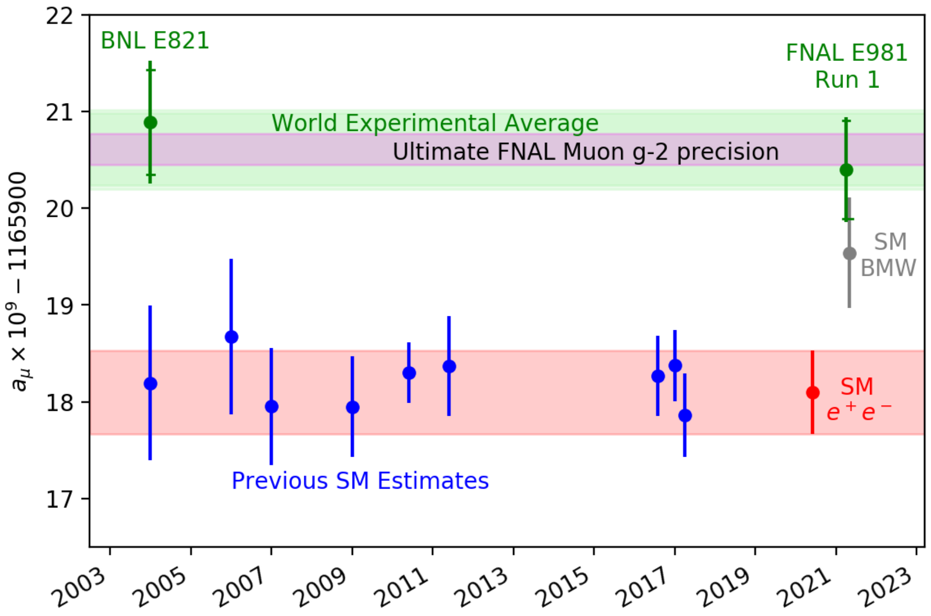

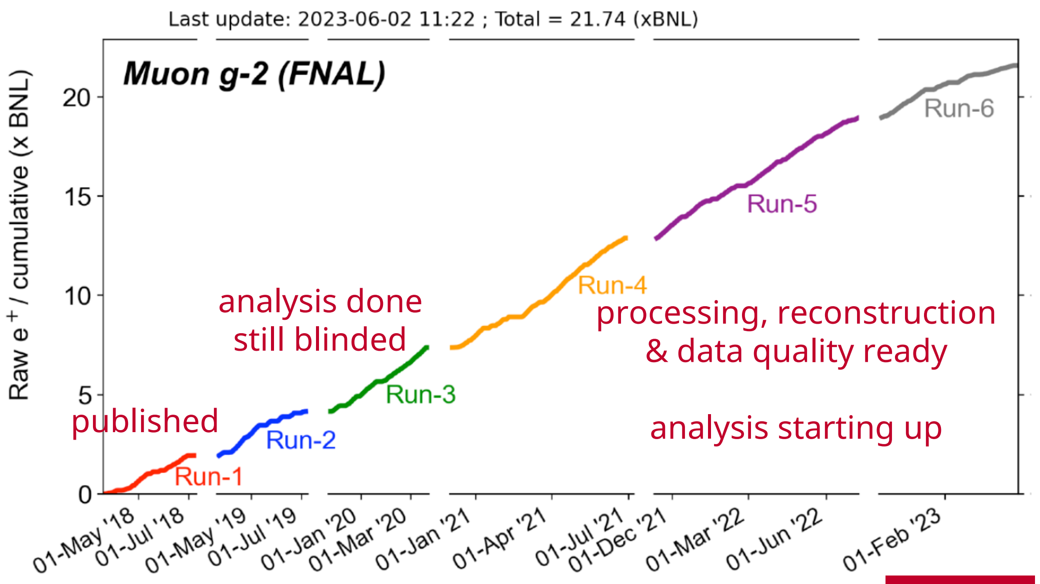

Summary

- High precision measurements of muon g-2 stringent test on SM theory
- First time a three-way comparison of a_μ is possible, very exciting
- Run 2 / 3 result soon
  - four times larger statistics
  - ~1/3 reduction in systematics
- Analysis for EDM on-going as well
- Reached 21 x BNL statistics and detailed systematic datasets
- Run 4/5/6 analysis ramping up

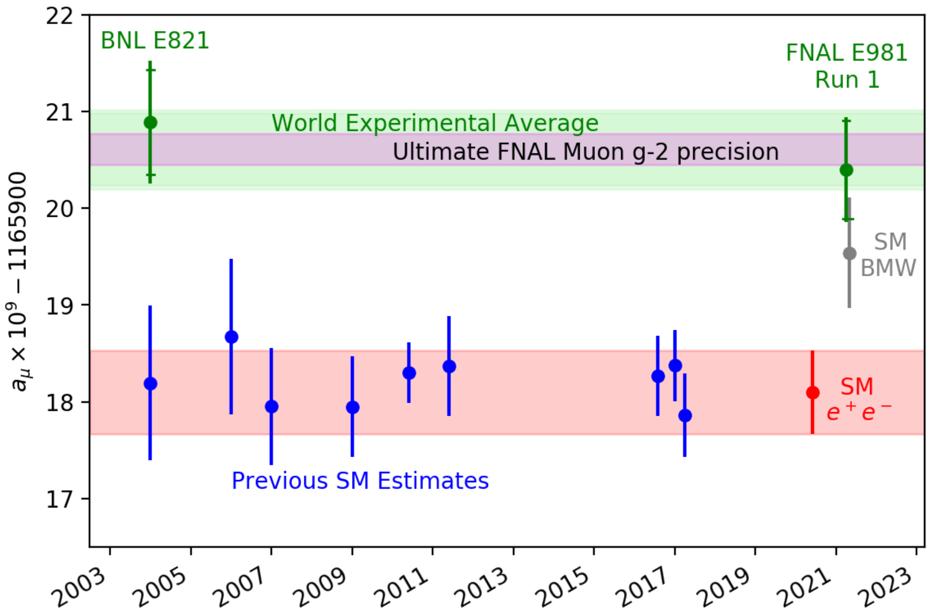

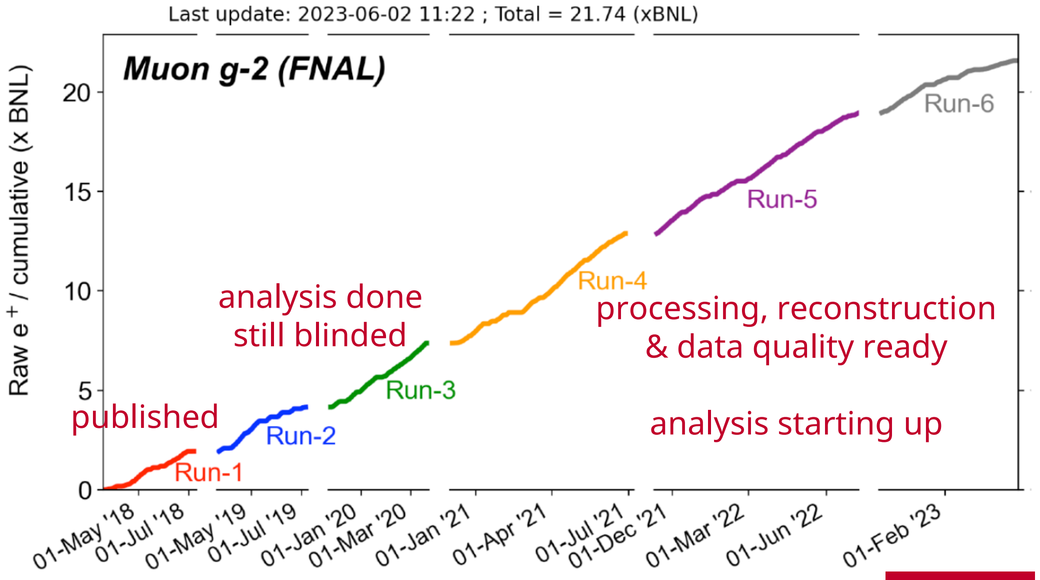

Thank you for your attention!

Backup

EDM with E989

- Muon EDM leads to spin precession as well
- MDM leads to rotation around vertical direction
- EDM leads to rotation around radial direction

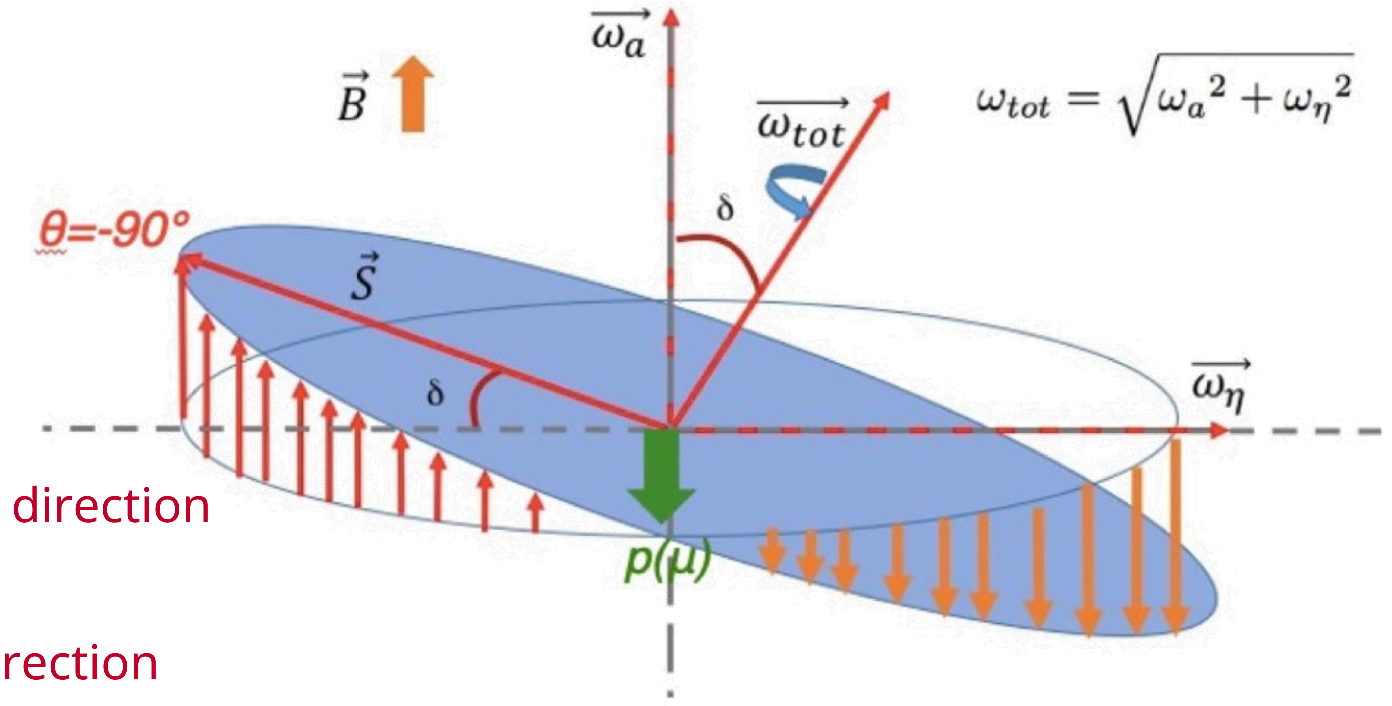

$$\vec{\omega}_s = -\frac{q}{m}\left[a_\mu \vec{B} - \left(a_\mu - \frac{1}{\gamma^2 - 1}\right)\frac{\vec{\beta}\times\vec{E}}{c}\right] + \frac{\eta q}{2mc}\left[\vec{E} + c\vec{\beta}\times\vec{B}\right]$$

MDM
Rotation around vertical

EDM
Rotation around radial

EDM with E989

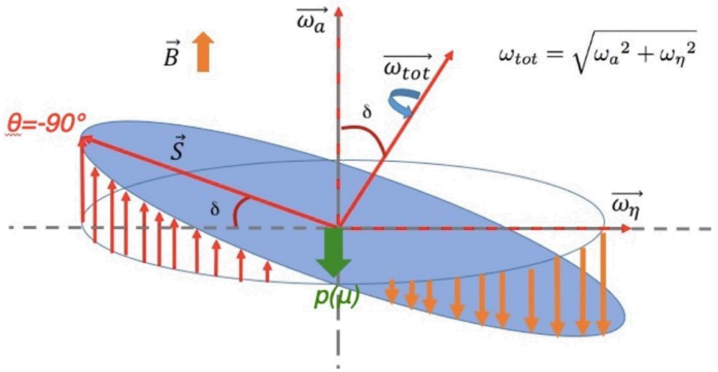

1. Deviation in measured $|\omega_a|$
   - Assuming $a_\mu^{\mathrm{Exp}} - a_\mu^{\mathrm{SM}}$ purly caused by EDM results in $d_\mu = (2.3 \pm 0.3) \times 10^{-19} e \cdot \mathrm{cm}$
   - Exceeds current upper limit of $|d_\mu| < 1.8 \times 10^{-19}\, e \cdot \mathrm{cm}$ at 95% C.L.

$$\vec{\omega}_s = -\frac{q}{m}\left[a_\mu \vec{B} - \left(a_\mu - \frac{1}{\gamma^2 - 1}\right)\frac{\vec{\beta} \times \vec{E}}{c}\right] + \frac{\eta q}{2mc}\left[\vec{E} + c\vec{\beta} \times \vec{B}\right]$$

MDM
Rotation around vertical

EDM
Rotation around radial

EDM with E989

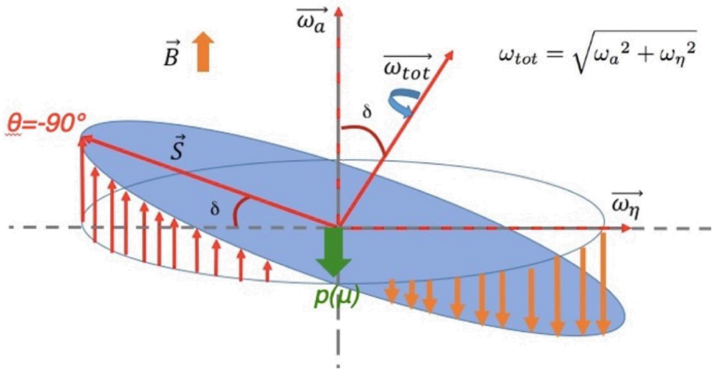

2. Observe vertical decay angle
   - Measure positron momentum vector with tracker
   - Determine vertical decay angle $\theta_y = \arcsin(p_y/p)$
   - EDM signal oscillates with 180° out-of-phase w.r.t ω_a

$$\langle \theta_y \rangle (t) = A_{g-2} \cos(\omega_a t + \phi) + A_{\mathrm{EDM}} \sin(\omega_a t + \phi) + c$$

   - Systematics: tracker acceptance, tracker alignment, radial magnetic field
   - Statistical limited in BNL measurement
   - Run 1 analysis nearly ready but still blinded
   - Limit if A_{EDM}=0 $|d_\mu| < 2.0 \times 10^{-19}\, e \cdot \mathrm{cm}$

$$\vec{\omega}_s = -\frac{q}{m}\left[a_\mu \vec{B} - \left(a_\mu - \frac{1}{\gamma^2 - 1}\right)\frac{\vec{\beta} \times \vec{E}}{c}\right] + \frac{\eta q}{2mc}\left[\vec{E} + c\vec{\beta} \times \vec{B}\right]$$

MDM
Rotation around vertical

EDM
Rotation around radial

EDM with E989

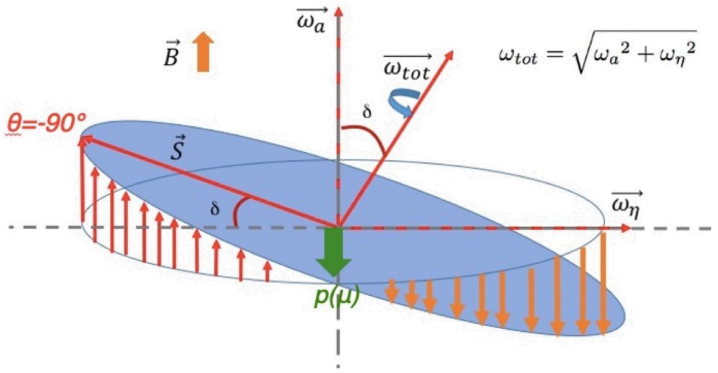

3. Frozen spin Observe vertical decay angle
   - For muon g-2 we operate at magic momentum
   - Idea: apply radial dipolar electric field to vanish MDM contribution
   - Operate E989 with ~300 MeV/c muons, B ~ 0.13 T and E_r~0.77 MV/m
   - No spin rotation in vertical direction (frozen spin)
   - Tested beam line to deliver ~300 MeV/c muons
   - Simulations on-going to investigate measurement principle

=0

$$\vec{\omega}_s = -\frac{q}{m}\left[a_\mu \vec{B} - \left(a_\mu - \frac{1}{\gamma^2 - 1}\right)\frac{\vec{\beta}\times\vec{E}}{c}\right] + \frac{\eta q}{2mc}\left[\vec{E} + c\vec{\beta}\times\vec{B}\right]$$

MDM
Rotation around vertical

EDM
Rotation around radial

View inside the vacuum chambers

Laser calibration system

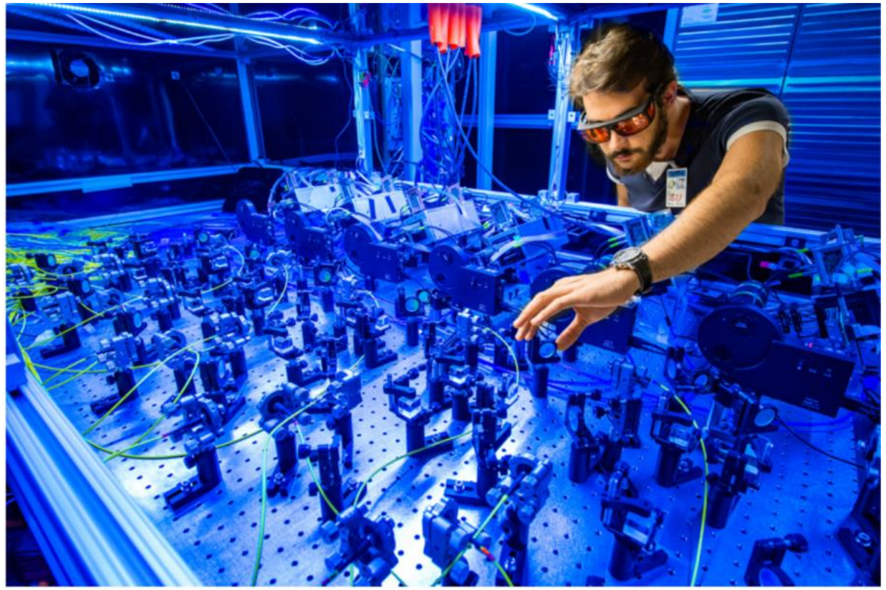

Figure credit: Andrea Fioretti

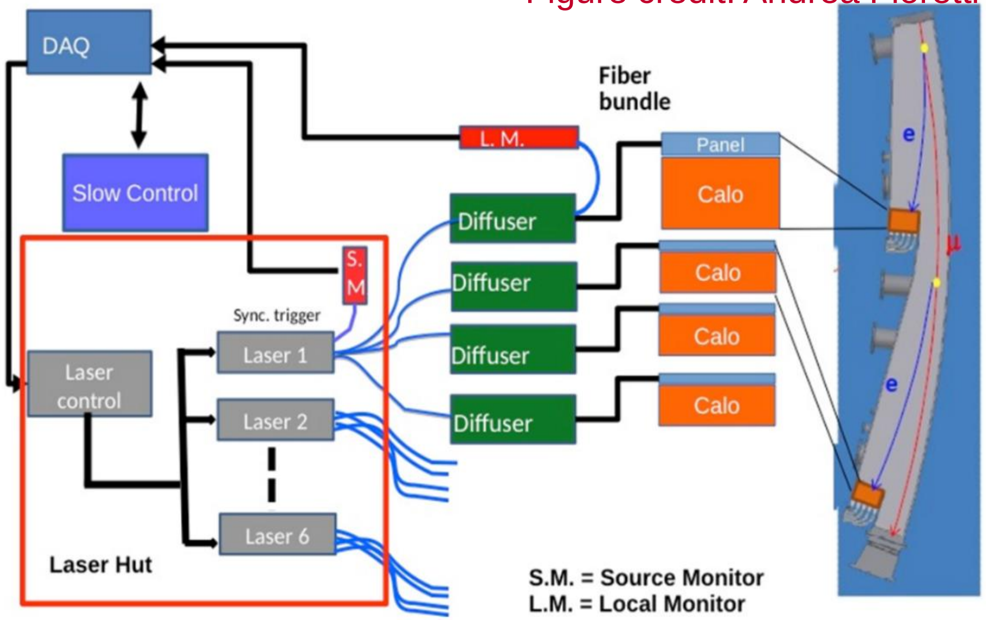

Inject laser pulses systematically also during beam operation (about 10% of time)

Long term gain changes due to temperature changes

Short term gain drops from initial beam flash at injection or consecutive hits

Gain Stability

Long term gain changes due to temperature changes
Long term gain changes can be corrected

Short term gain drops
- Initial beam flash at injection
- Consecutive hits

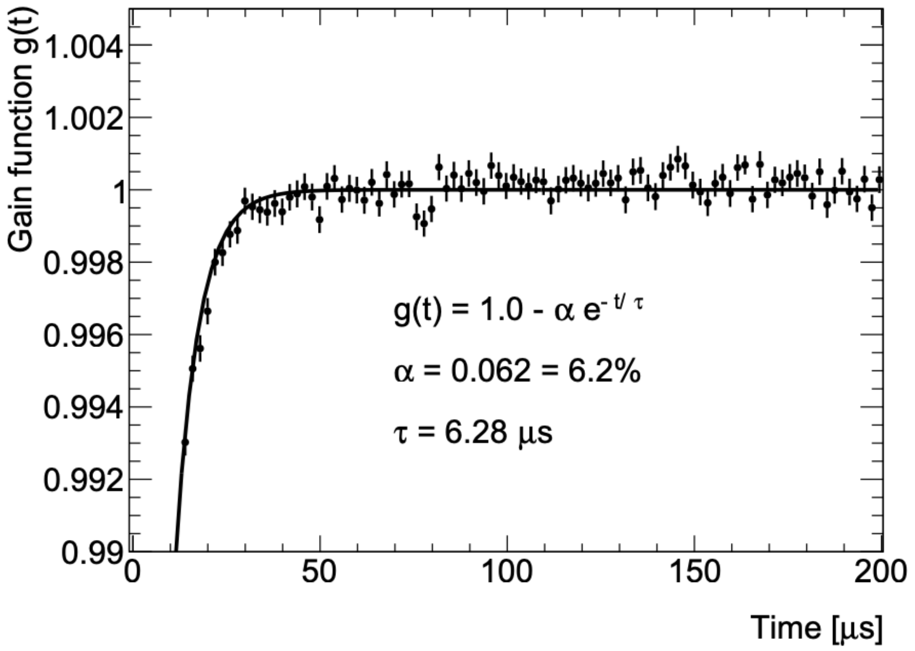

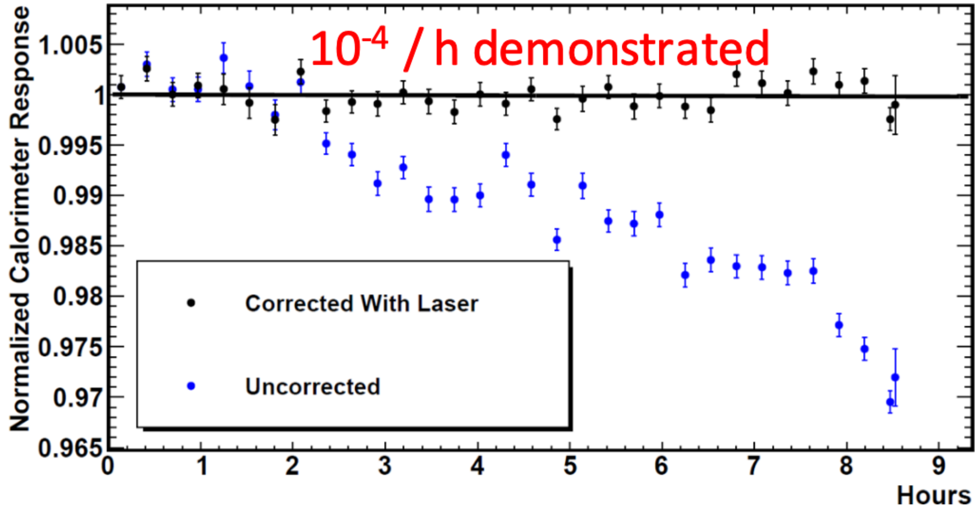

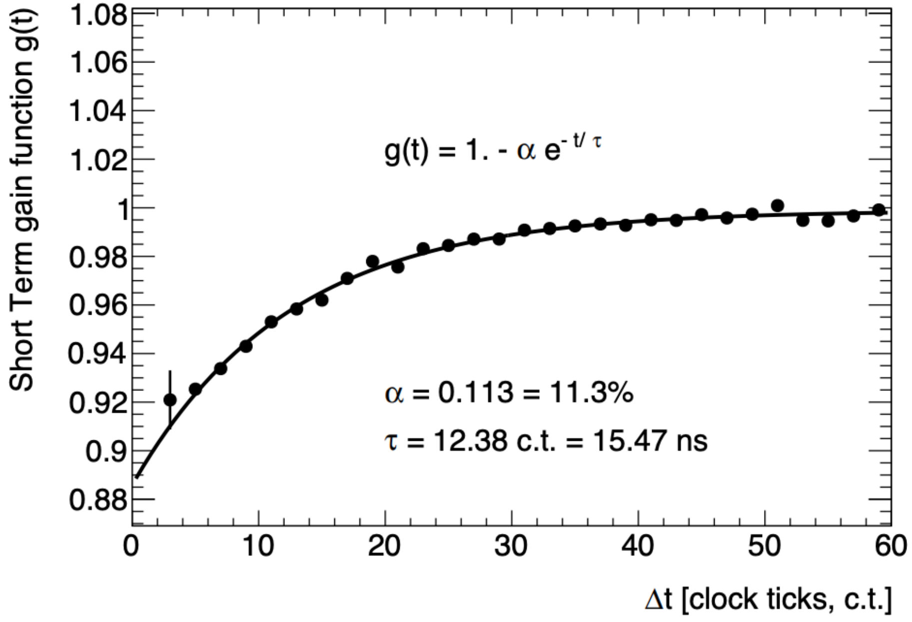

Scaping of beam edges

- Beam dynamics could make muons oscillated into physical objects around the muon storage area
- potential early-to-late in muon loss factor

- First apply small vertical focusing
- Edge of stored muons collide with collimators

- Second apply higher vertical focusing
- Stored muons well separated from collimators

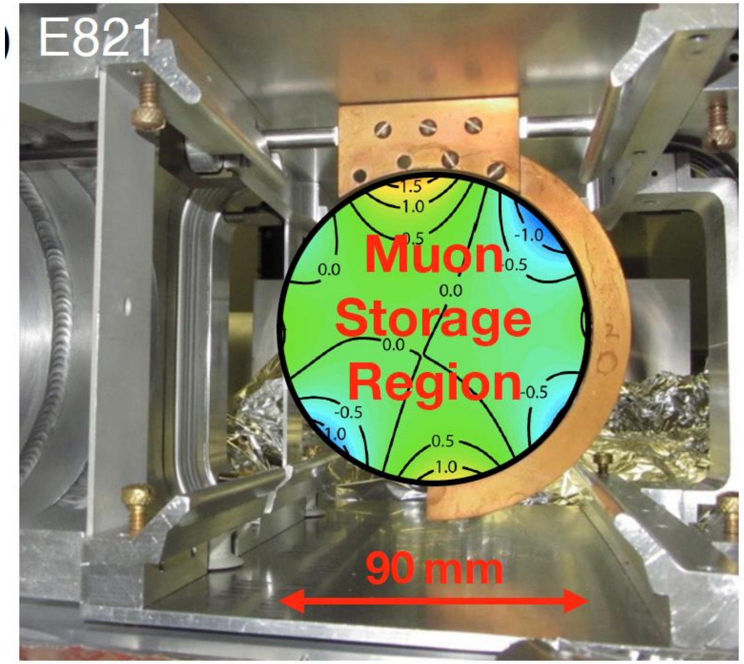

Technique developed over 40 years

Goal: 100ppb statistical ⊕ 100ppb systematic uncertainty

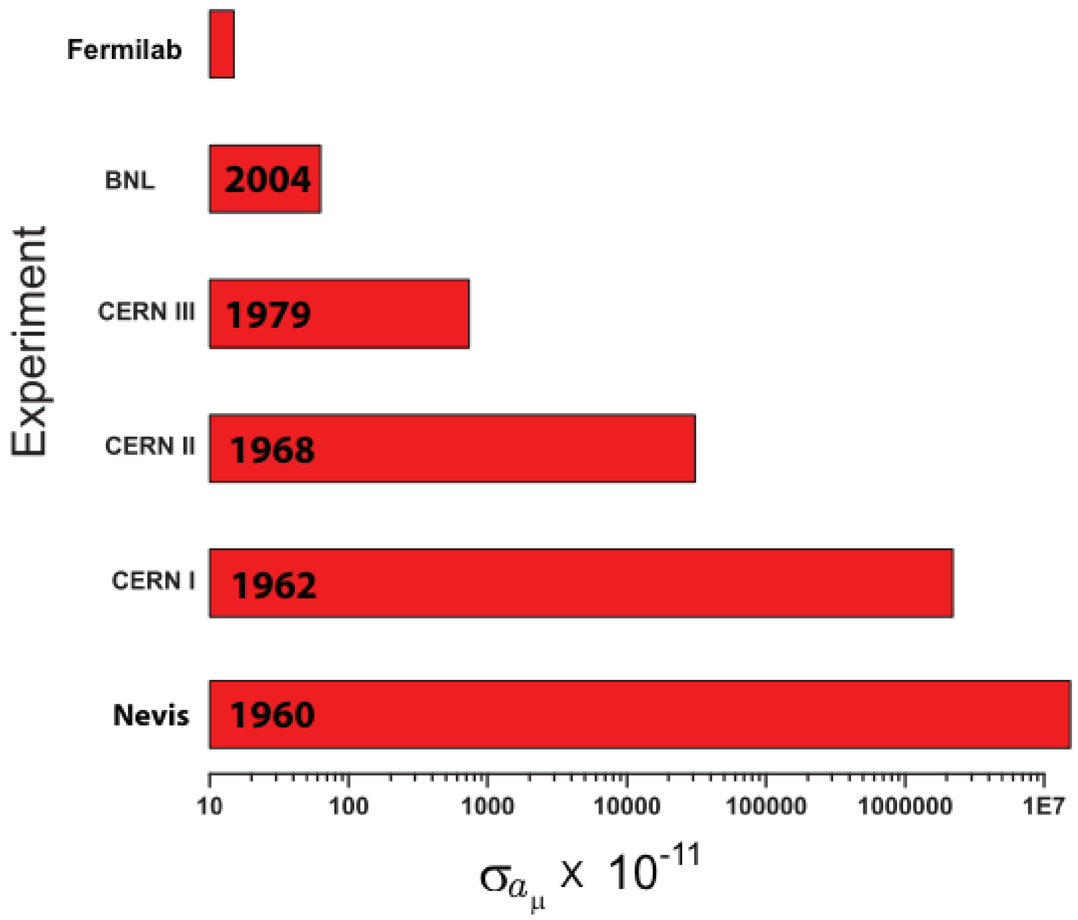

Superconducting storage ring magnet
Muon Injection and magnetic kicker
Superconducting inflector magnet

NMR technique

Magic momentum technique

Storage ring technique to measure g-2

Measured g_μ from muon at rest

The “wiggle” plot

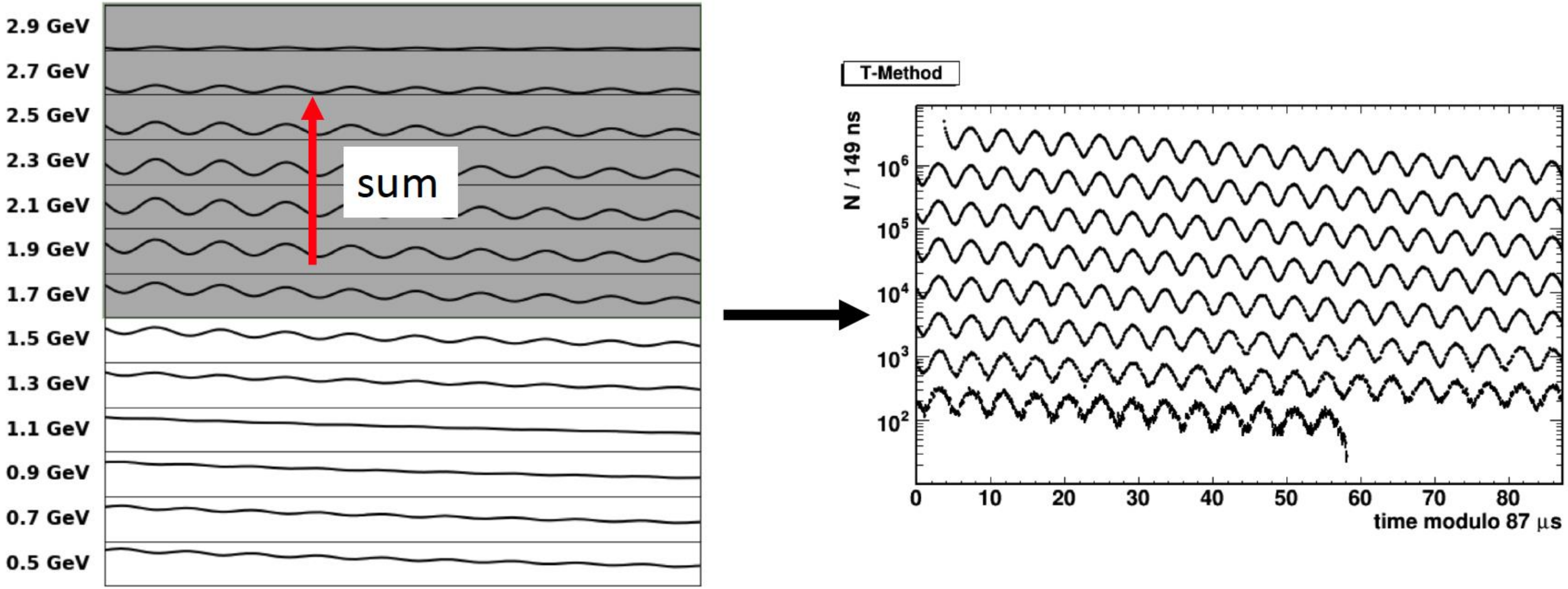

$$N(t) = N_0(E)\, e^{-\frac{t}{\gamma\tau}} \left[1 + A(E)\cos\left(\omega_a t - \phi(E)\right)\right]$$

Exponential decay from muon lifetime modulated with $\omega_a = a_\mu \frac{e}{m_\mu} B$

Beam dynamics corrections

- Electric field correction
  - Finite momentum distribution, not all at magic momentum
  - Debunching
    → determine momentum distribution
    → determine equilibrium radius distribution

$$C_e = -2n(1-n)\beta^2 \frac{\langle x_e^2 \rangle}{R_0^2}$$

- Pitch correction
  - Vertical momentum component of muons
  - Trackers measure vertical oscillation amplitude

$$C_p = \frac{n}{4R_0^2}\langle A^2 \rangle$$

- Muon loss correction
  - Lose muons due to collisions instead of decay
  - Different for low and high energy muons, early-to-late effect

$$C_{ml}$$

- Phase difference depending on decay position
  - Corrected from Beam dynamic simulation

$$C_{\text{pa}}$$

22 parameter fit

$$N_0\, e^{-\frac{t}{\gamma\tau}}\,(1 + A \cdot A_{BO}(t)\cos(\omega_a t + \phi \cdot \phi_{BO}(t))) \cdot N_{\mathrm{CBO}}(t) \cdot N_{\mathrm{VW}}(t) \cdot N_y(t) \cdot N_{2\mathrm{CBO}}(t) \cdot J(t)$$

$$A_{\mathrm{BO}}(t) = 1 + A_A \cos(\omega_{\mathrm{CBO}}(t) + \phi_A)e^{-\frac{t}{\tau_{\mathrm{CBO}}}}$$

$$\phi_{\mathrm{BO}}(t) = 1 + A_\phi \cos(\omega_{\mathrm{CBO}}(t) + \phi_\phi)e^{-\frac{t}{\tau_{\mathrm{CBO}}}}$$

$$N_{\mathrm{CBO}}(t) = 1 + A_{\mathrm{CBO}} \cos(\omega_{\mathrm{CBO}}(t) + \phi_{\mathrm{CBO}})e^{-\frac{t}{\tau_{\mathrm{CBO}}}}$$

$$N_{2\mathrm{CBO}}(t) = 1 + A_{2\mathrm{CBO}} \cos(2\omega_{\mathrm{CBO}}(t) + \phi_{2\mathrm{CBO}})e^{-\frac{t}{2\tau_{\mathrm{CBO}}}}$$

$$N_{\mathrm{VW}}(t) = 1 + A_{\mathrm{VW}} \cos(\omega_{\mathrm{VW}}(t)t + \phi_{\mathrm{VW}})e^{-\frac{t}{\tau_{\mathrm{VW}}}}$$

$$N_y(t) = 1 + A_y \cos(\omega_y(t)t + \phi_y)e^{-\frac{t}{\tau_y}}$$

$$J(t) = 1 - k_{LM}\int_{t_0}^{t} \Lambda(t)dt$$

$$\omega_{\mathrm{CBO}}(t) = \omega_0 t + Ae^{-\frac{t}{\tau_A}} + Be^{-\frac{t}{\tau_B}}$$

$$\omega_y(t) = F\omega_{\mathrm{CBO}(t)}\sqrt{2\omega_c/F\omega_{\mathrm{CBO}}(t) - 1}$$

$$\omega_{\mathrm{VW}}(t) = \omega_c - 2\omega_y(t)$$

Beam dynamics effects have to be considered

22 parameter fit

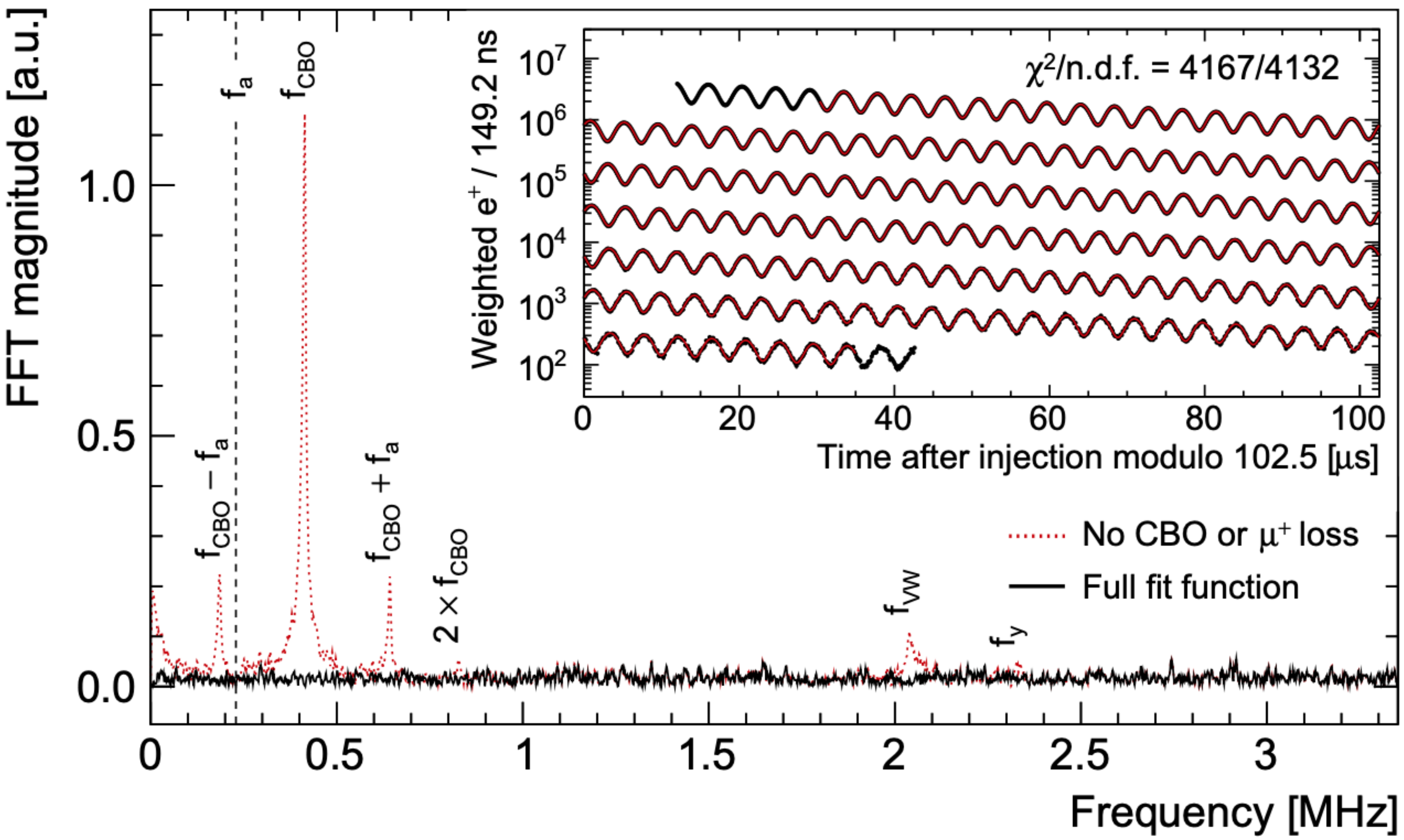

$t) \cdot N_{2CBO}(t) \cdot J(t)$

Beam dynamics effects have to be considered

Asymmetry weighted method

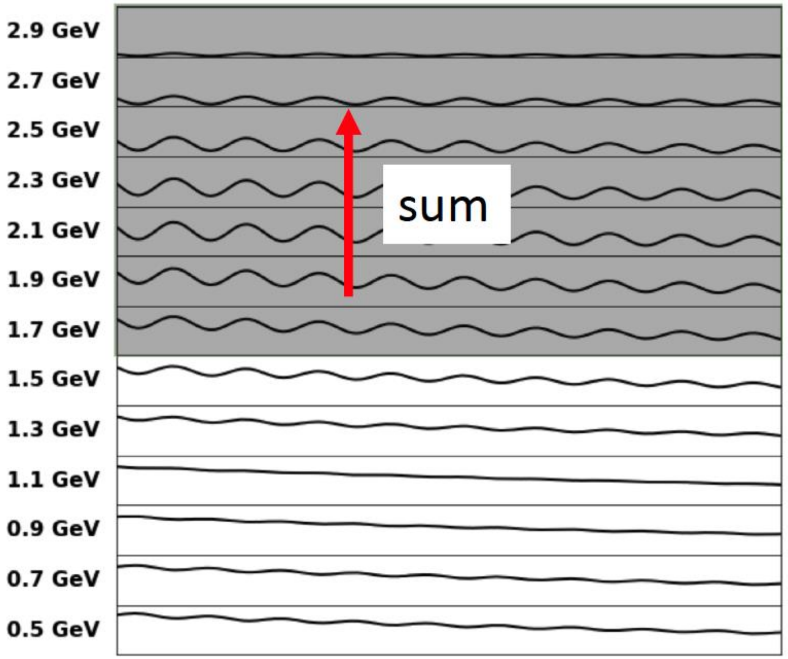

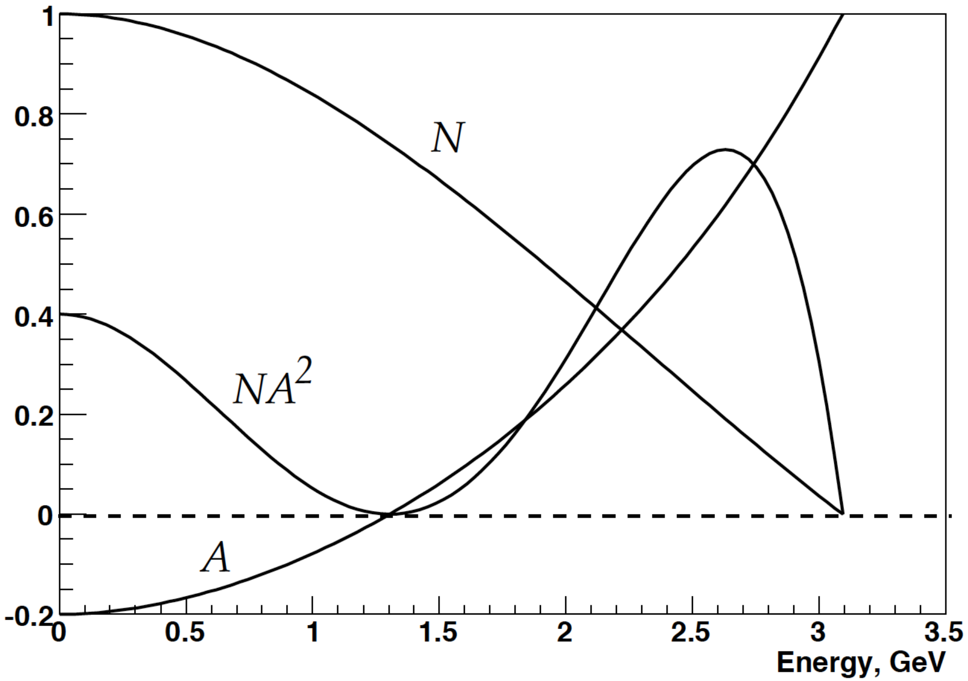

- Asymmetry is energy dependent
- High energy positrons have stronger asymmetry
- Introduce weight proportional to asymmetry

Ratio method

- Split positrons randomly in four sets
- Time shift one set by $+T_a/2$ and one by $-T_a/2$
- Build the ratio

$$r(t) = \frac{[u_+(t) - v_1(t)] + [u_-(t) - v_2(t)]}{[u_+(t) + v_1(t)] + [u_-(t) + v_2(t)]}$$

- Gets rid of exponential decay and any slow drift

$$r(t) = A\cos\left(\omega_a^m t + \phi\right) - \frac{1}{16}\left(\frac{T_a}{\gamma\tau_\mu}\right)^2 + \mathcal{O}((T_a/(4\gamma\tau_\mu))^4)$$

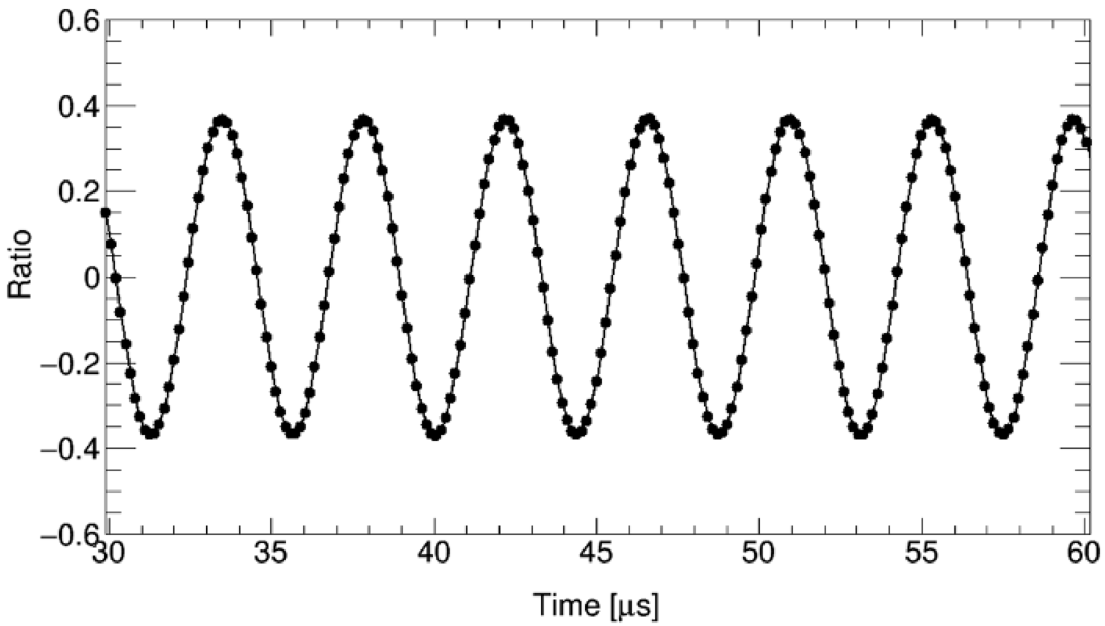

$$u_+(t) = \frac{1}{4}n(t + T_a/2),$$

$$u_-(t) = \frac{1}{4}n(t - T_a/2),$$

$$v_1(t) = \frac{1}{4}n(t),$$

$$v_2(t) = \frac{1}{4}n(t).$$

Finite beam length

- Individual calorimeters see has oscillation with frequency ω_c caused by bunch distribution
- Add time offset uniformly distributed between $-T_c/2, T_c/2$
- With time bunch decoheres because of momentum spread of initial beam
- Used to calculate momentum distribution → corresponds to equilibrium radius
- Used to calculate electric field correction

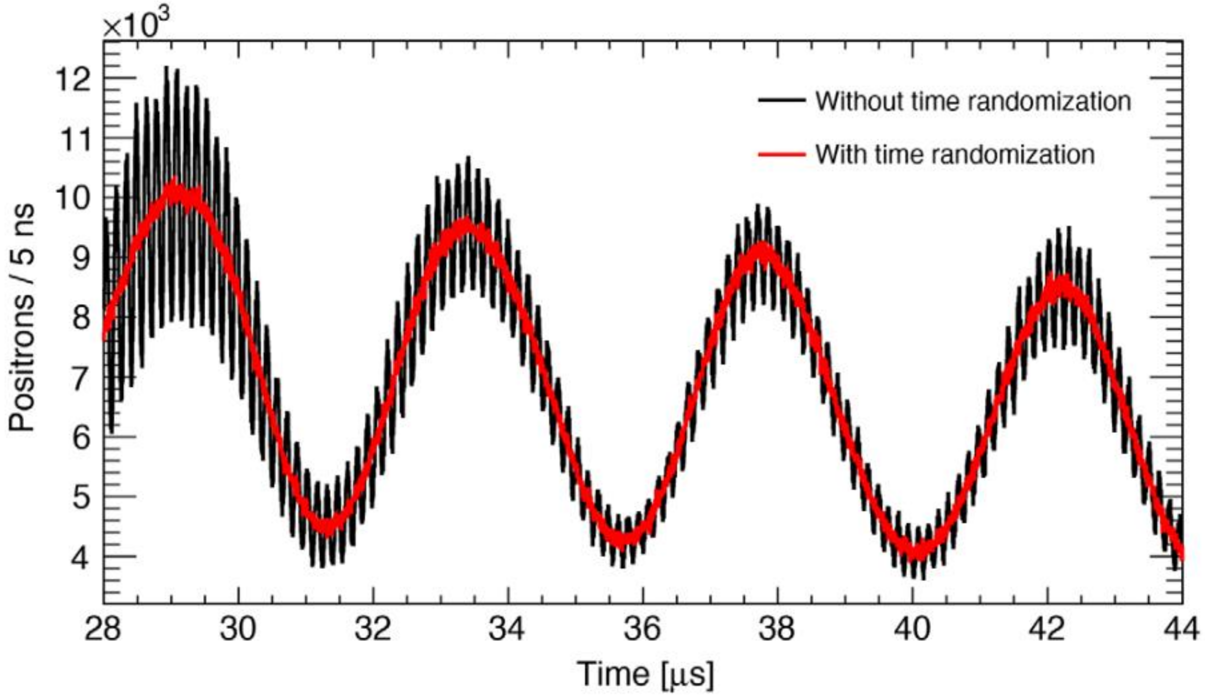

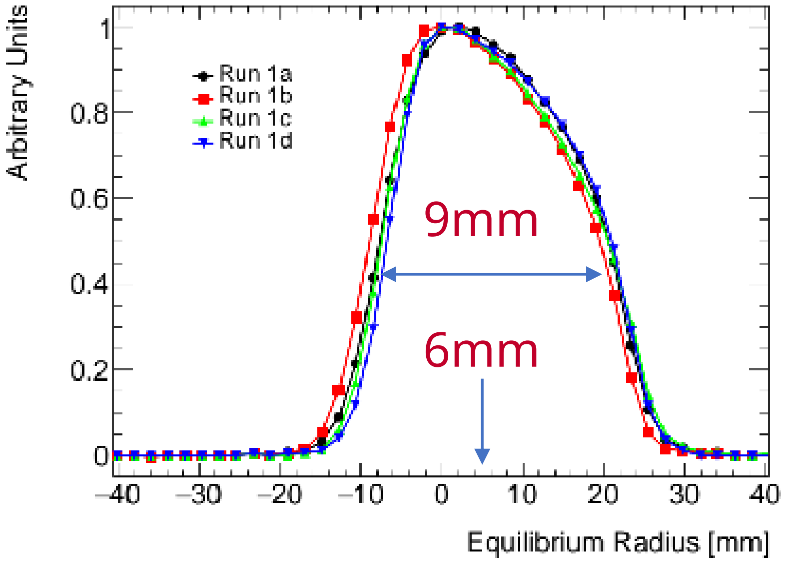

Electric field correction

$$\vec{\omega}_a = \frac{e}{m}\left[a_\mu \vec{B} - a_\mu \left(\frac{\gamma}{\gamma+1}\right)\left(\vec{\beta}\cdot\vec{B}\right)\vec{\beta} - \left(a_\mu - \frac{1}{\gamma^2-1}\right)\frac{\vec{\beta}\times\vec{E}}{c}\right]$$

- Off-center beam sees electric field
- Correction given by

$$C_e = -2n(1-n)\beta^2 \frac{\langle x_e^2 \rangle}{R_0^2}$$

  - n given by ESQ HV settings
  - β known from magic momentum
  - R_0 nominal orbit radius

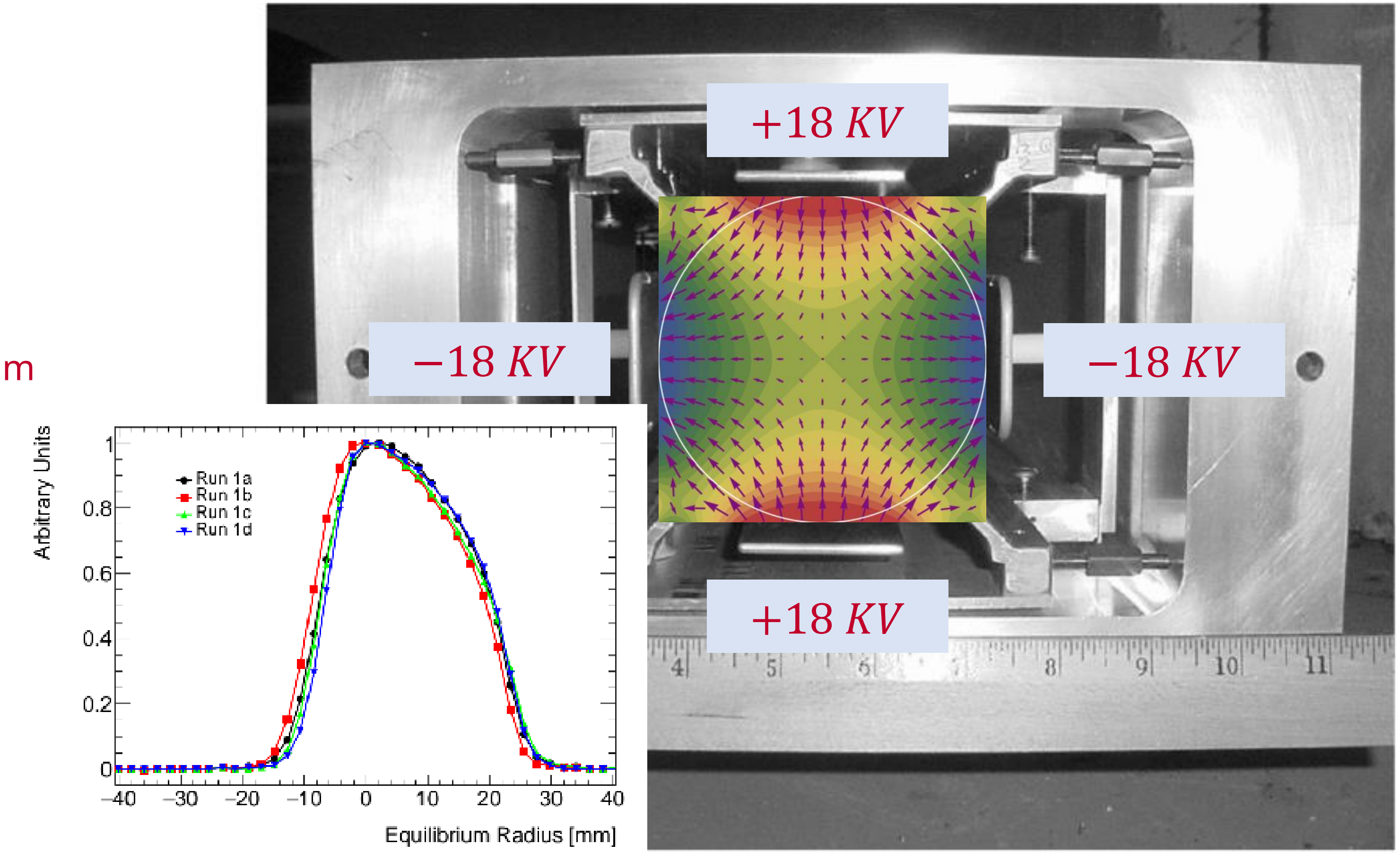

Pitch correction

- Muons have transversal momentum (pitch)

$$\frac{e}{m}\left[a_\mu \vec{B} - a_\mu \left(\frac{\gamma}{\gamma+1}\right)\left(\vec{\beta}\cdot\vec{B}\right)\vec{\beta} - \left(a_\mu - \frac{1}{\gamma^2-1}\right)\frac{\vec{\beta}\times\vec{E}}{c}\right]$$

- Vertical beam motion simulated by three different beam dynamics simulations

- Using tracker beam distribution as input and cross-check

- Correction given by mean acceptance-corrected vertical amplitude

$$C_p = \frac{n}{4R_0^2}\langle A^2\rangle$$

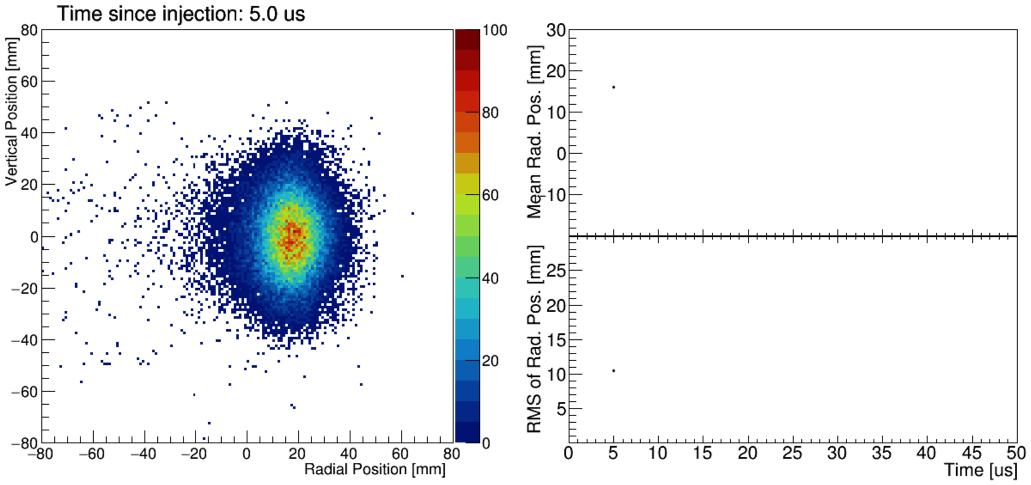

Lost muons

- Beside decay muons get lost by interaction with obstacles or collimators
- Lost muons pass through several calorimeters
- Deposited energy of a MiP with ~170MeV
- Successive calorimeter hits separated by 6.15ns
- Require measurement in three successive calorimeters to reduce random coincidences
- Monitors rate up to overall factor
- Low momentum muon lost faster
  → Early to late effect
- Needs to be corrected

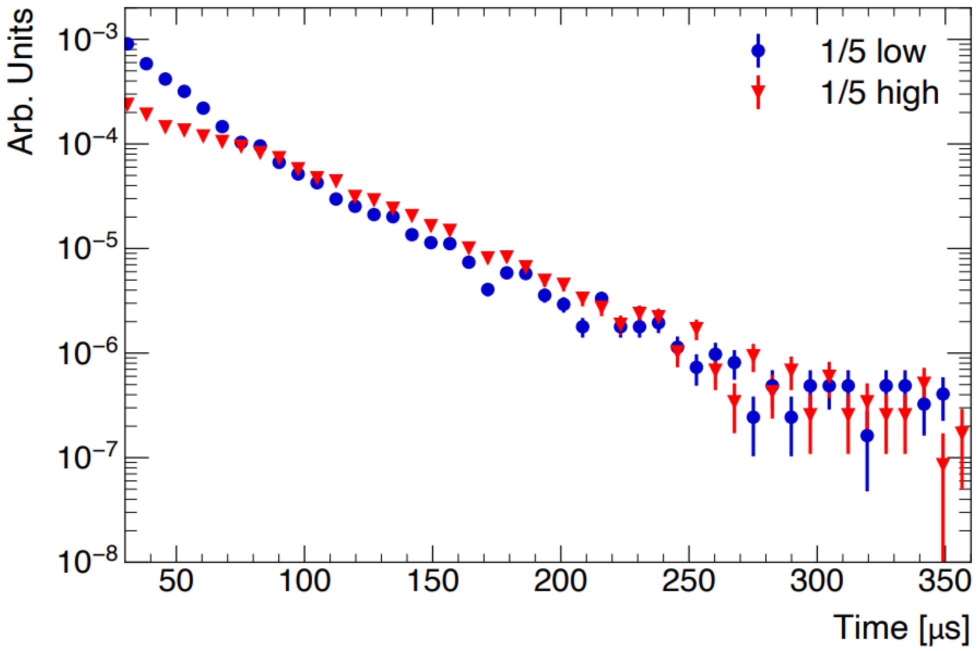

Finite Calorimeter Acceptance

- Since finite calorimeter acceptance we are sensitive to muon decay position

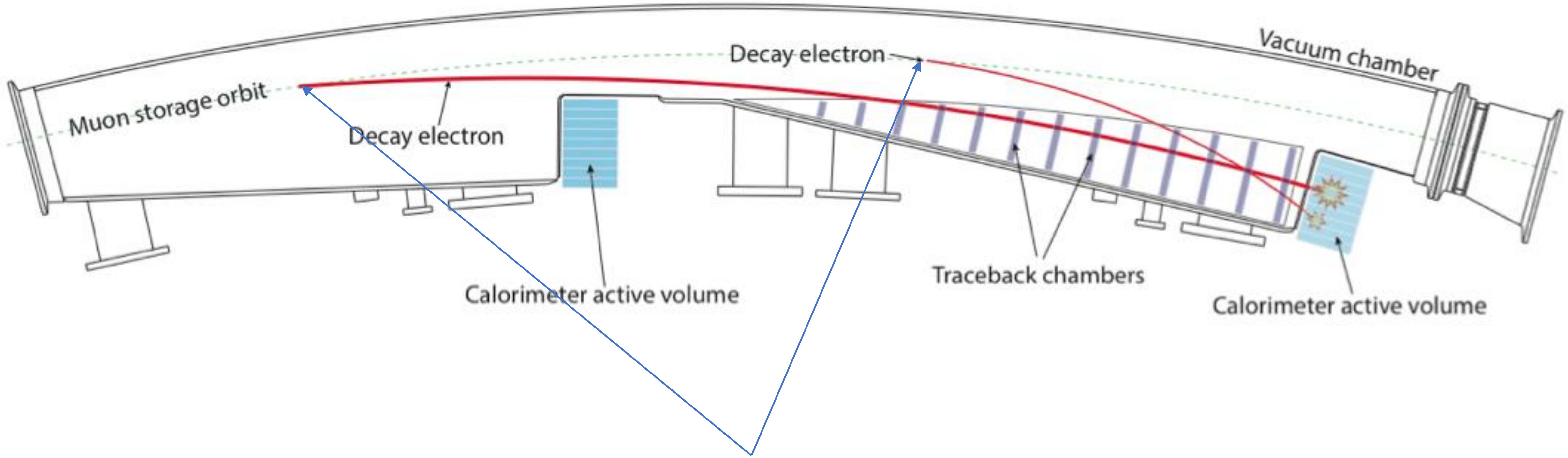

Muon spin has precessed a bit further

Phase acceptance

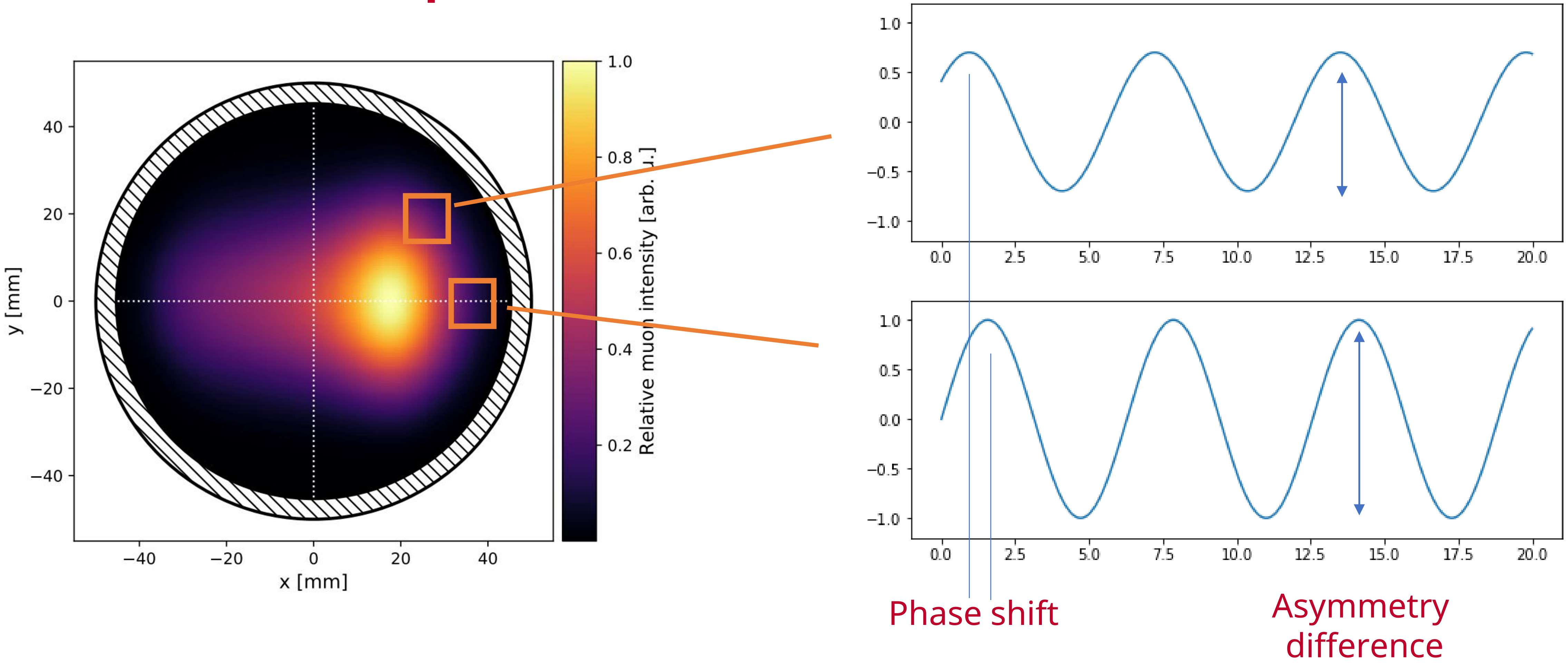

Depends on energy and time
Beam profile must be well-understood during measurement period

Phase acceptance

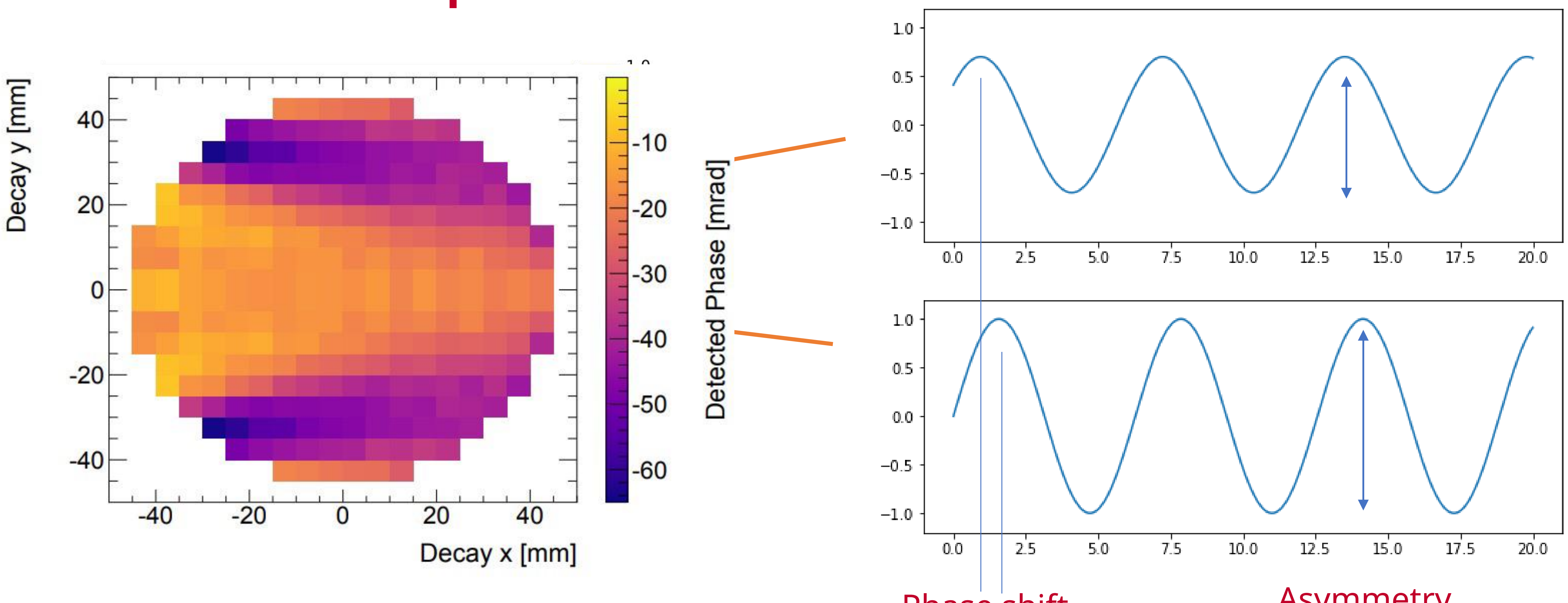

Depends on energy and time

Beam profile must be well-understood during measurement period

Calorimeter requirements

Fraction of positrons above a threshold energy in a calorimeter is given by

$$f(t) \propto \int_{E_{\mathrm{thresh}}}^{E_{\mathrm{max}}} N_0 e^{-\frac{t}{\gamma\tau}} N(E)\left[1 + A(E)\cos\left(\omega_{\mathrm{a}} t - \phi(E)\right)\right] dE$$

But can be written as an effective function

$$f(t) \propto N_0 e^{-\frac{t}{\gamma\tau}} \left[\langle N\rangle_{\mathrm{thresh}} + \langle A\rangle_{\mathrm{thresh}} \cos\left(\omega_{\mathrm{a}} t - \langle\phi\rangle_{\mathrm{thresh}}\right)\right]$$

Any remaining time dependence of $\langle\phi\rangle_{\mathrm{thresh}}$ will bias ω_a!

$$\cos\left(\omega_{\mathrm{a}} t - \langle\phi\rangle_{\mathrm{thresh}}(t)\right) \approx \cos\left[\left(\omega_{\mathrm{a}} - \frac{d\langle\phi\rangle_{\mathrm{thresh}}}{dt}\right) t - \langle\phi\rangle_{\mathrm{thresh}}(0)\right]$$

Early to late effect

Calorimeter requirements

Assume two energy bins

$$N(t) = N_{1,0}(E_1)\, e^{-\frac{t}{\gamma_1 \tau_1}} \left[1 + A_1(E_1)\cos\left(\omega_\mathrm{a} t - \phi(E_1)\right)\right] + N_{2,0}(E_2)\, e^{-\frac{t}{\gamma_2 \tau_2}} \left[1 + A_2(E_2)\cos\left(\omega_\mathrm{a} t - \phi(E_2)\right)\right]$$

Phase of summed signal

$$\tan(\phi_\mathrm{sum}) = \frac{N_{1,0}(E_1)\, e^{-\frac{t}{\gamma_1 \tau_1}} A_1(E_1)\sin(\phi(E_1)) + N_{2,0}(E_2)\, e^{-\frac{t}{\gamma_2 \tau_2}} A_2(E_2)\sin(\phi(E_2))}{N_{1,0}(E_1)\, e^{-\frac{t}{\gamma_1 \tau_1}} A_1(E_1)\cos(\phi(E_1)) + N_{2,0}(E_2)\, e^{-\frac{t}{\gamma_2 \tau_2}} A_2(E_2)\cos(\phi(E_2))}$$

Any differential change between both energy groups will bias the frequency if it is time dependent!

- different storage times for different muon energies, phase-space dependent loss rates
- Detector gain change: $A_{1,2}$ are energy-dependent
- Detector pile up: wrong energy reconstruction

Pitch correction

- Muons have transversal momentum components

$$\Delta\vec{\omega}_{\mathrm{a,pitch}} = -a_\mu \frac{e}{m}\left(\frac{\gamma}{\gamma+1}\right)\left(\vec{\beta}\cdot\vec{B}\right)\vec{\beta}$$

- Transversal component oscillates with $\omega_{\mathrm{y}} = \sqrt{n}\omega_{\mathrm{c}}$

- Effect mainly averages out to first order, but second order effect is

$$\left\langle \frac{\Delta\omega_{\mathrm{a}}}{\omega_{\mathrm{a}}} \right\rangle_{\mathrm{pitch}} = -\frac{\left\langle \psi^2 \right\rangle}{2} = -\frac{n\left\langle y^2 \right\rangle}{2R_0^2}$$

- Introduces always a negative bias
- Correction can be derived from measurements of the muon beam distribution

Muon beam dynamics in storage ring

- Electrostatic quadrupoles imprint harmonic potential around their central position
- Muon storage close to central position
  - Perturbative approach
- Newton's second law and Lorentz force

$$\frac{d\vec{p}}{dt} = e\left(\vec{E} + \frac{d\vec{v}}{dt} \times \vec{B}\right)$$

- Three differential equations
- Harmonic oscillator in vertical direction $\omega_{\mathrm{y}} = \sqrt{n}\omega_{\mathrm{c}}$
- Harmonic oscillator in horizontal direction $\omega_{\mathrm{x}} = \sqrt{1-n}\,\omega_{\mathrm{c}}$

Muon beam dynamics in storage ring

- Electrostatic quadrupoles imprint harmonic potential around their central position
- Muon storage close to central position
  - Perturbative approach
- Newton's second law and Lorentz force

$$\frac{d\vec{p}}{dt} = e\left(\vec{E} + \frac{d\vec{v}}{dt} \times \vec{B}\right)$$

- Three differential equations
- Harmonic oscillator in vertical direction $\omega_{\mathrm{y}} = \sqrt{n}\omega_{\mathrm{c}}$
- Harmonic oscillator in horizontal direction $\omega_{\mathrm{x}} = \sqrt{1-n}\,\omega_{\mathrm{c}}$
- *n* depends on quadrupole HV settings

Muon beam dynamics in storage ring

- Electrostatic quadrupoles imprint harmonic potential around their central position
- Muon storage close to central position
    - Perturbative approach
- Newton's second law and Lorentz force

$$\frac{d\vec{p}}{dt} = e\left(\vec{E} + \frac{d\vec{v}}{dt} \times \vec{B}\right)$$

- Three differential equations
- Harmonic oscillator in vertical direction $\omega_\mathrm{y} = \sqrt{n}\omega_\mathrm{c}$
- Harmonic oscillator in horizontal direction $\omega_\mathrm{x} = \sqrt{1-n}\,\omega_\mathrm{c}$
- *n* depends on quadrupole HV settings
- Resonant condition for

$$M\nu_\mathrm{x} + N\nu_\mathrm{y} = P \quad \mathrm{with\,M,N} \in \mathbb{Z}\,\mathrm{and\,P} \in \mathbb{N}$$

- Avoid ω_a interference

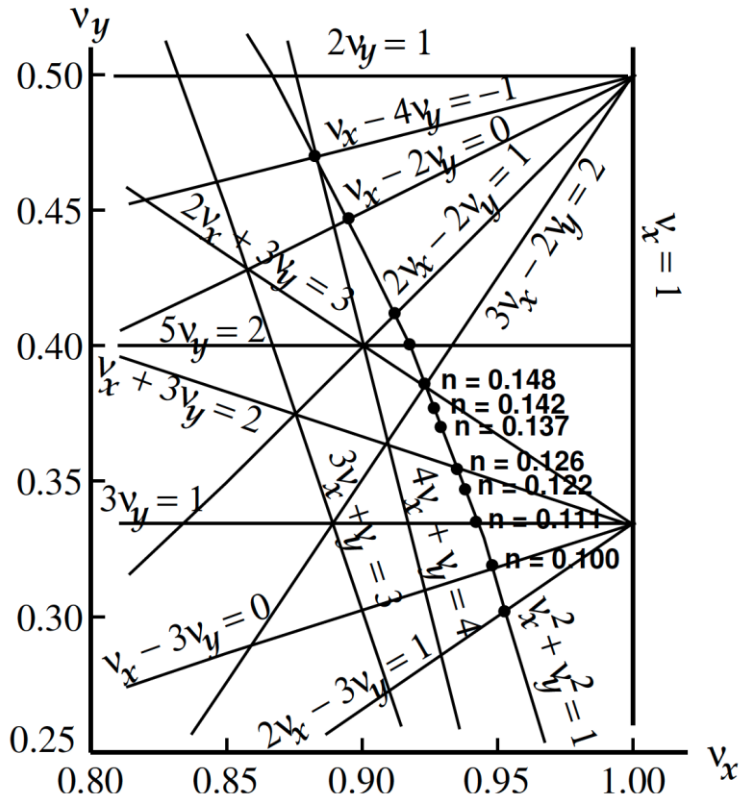

Spatial dependence of B-field

$$B(r,\theta) = B_0 + \sum_{n=1}^{4}\left(\frac{r}{r_0}\right)^n [a_n\cos(n\theta) + b_n\sin(n\theta)]$$

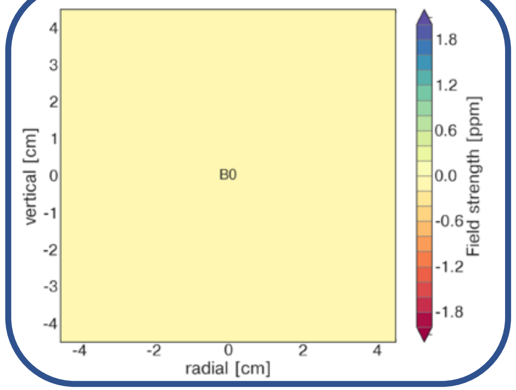

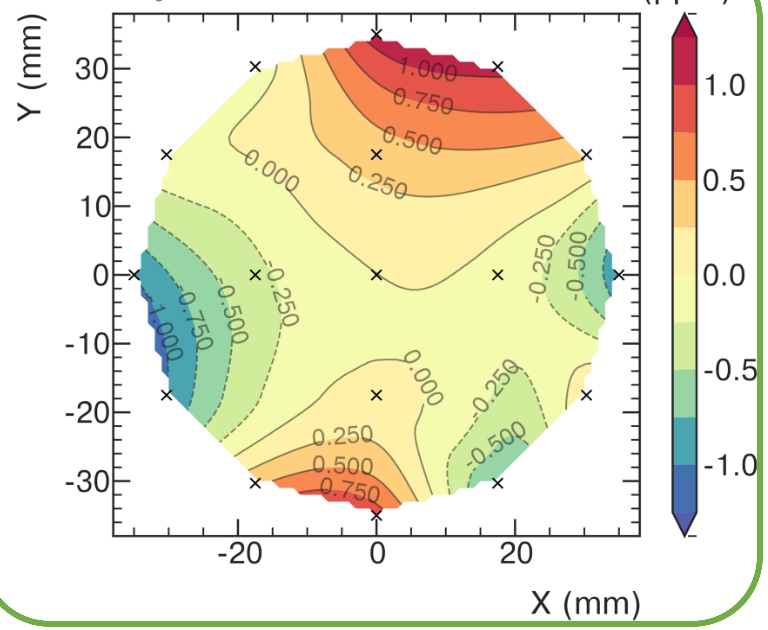

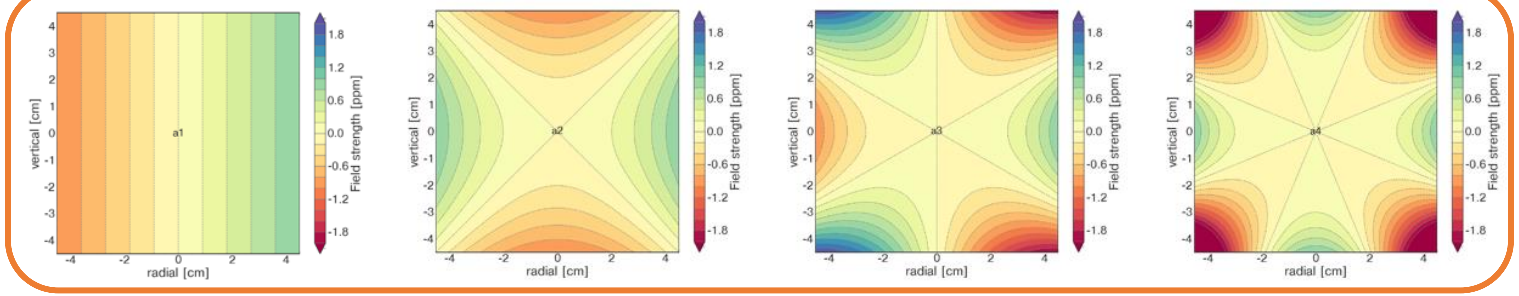

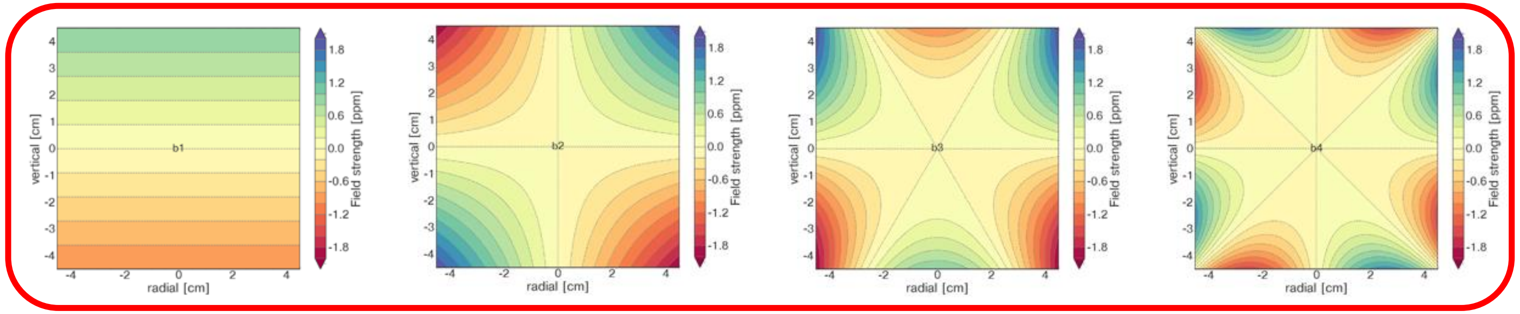

2D B-field contour map can be described by the terms in a multipole expansion

Magnetic field stability

Improved operating conditions

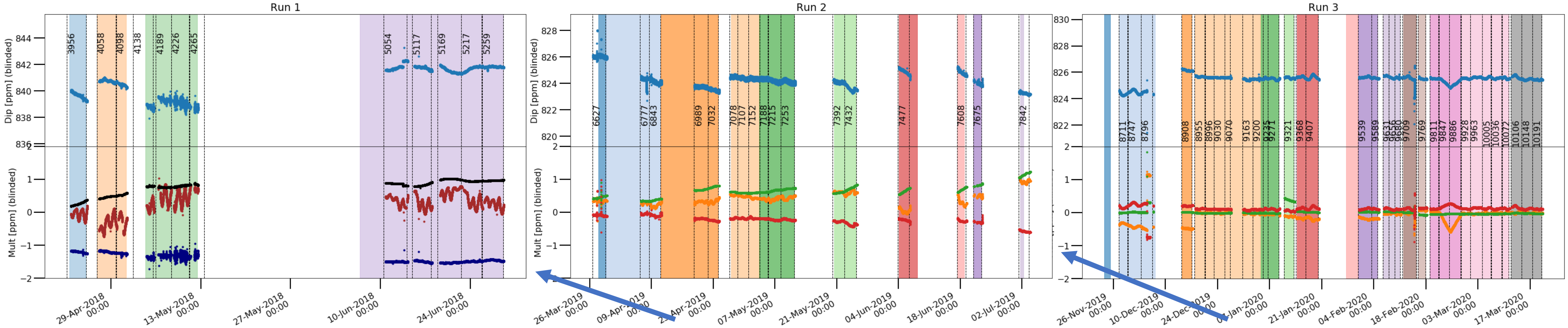

Magnet insulation

Upgrade Air Conditioning System

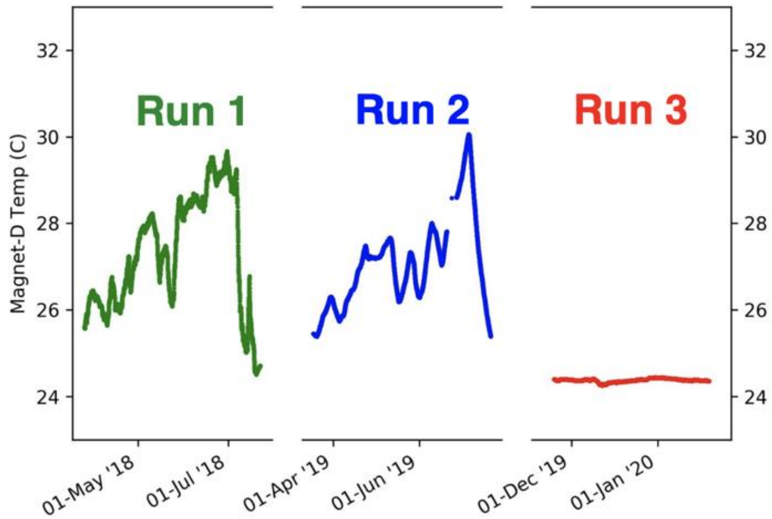

Hall temperature changes caused field changes

See diurnal field variation

Influences magnetic field systematic

Effect of Magnet Cycling

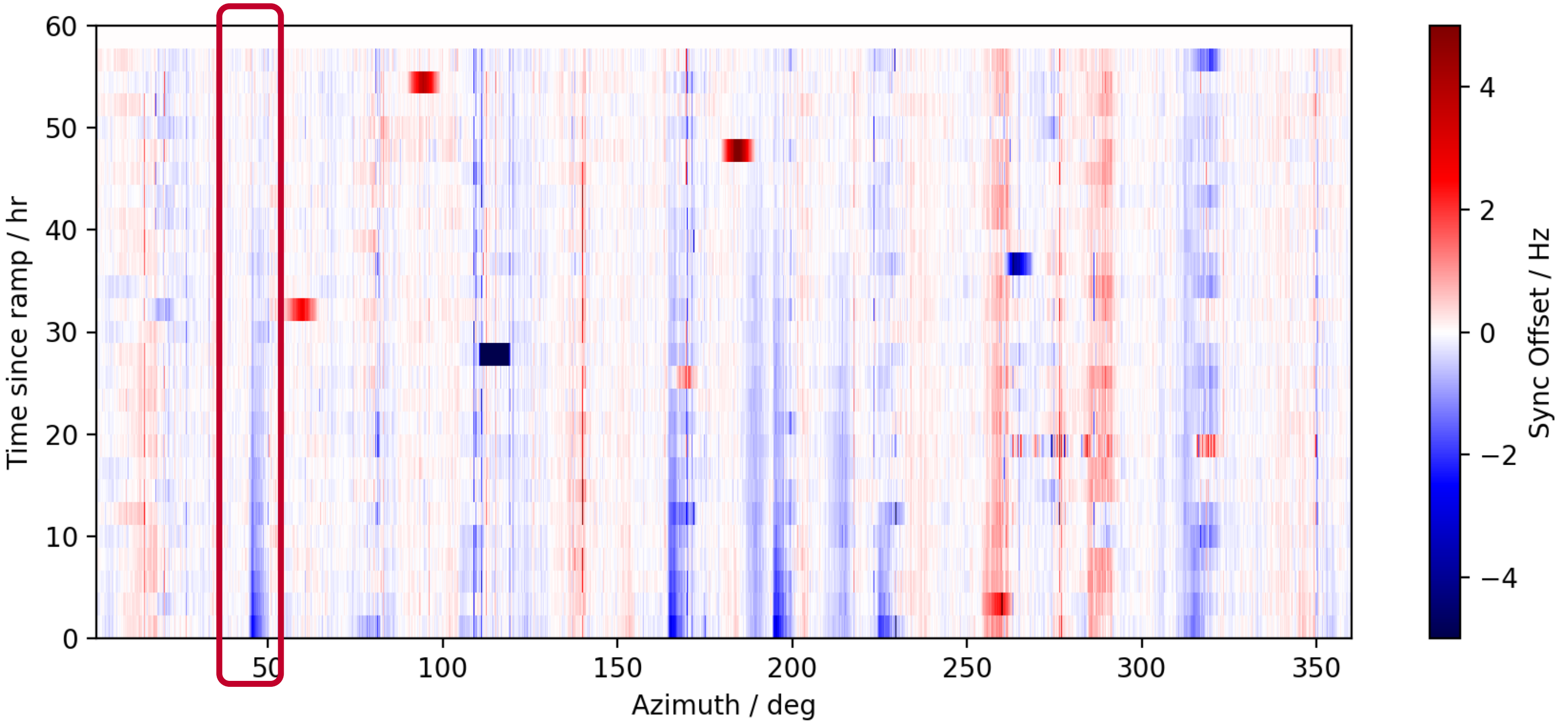

- Magnet cycling while operation necessary for cryo-maintenance, repairs, special studies, …

- Special study: Ramp magnet on purpose, perform trolley measurements for 60 h
- Azimuthal resolved sync offset always w.r.t. the last trolley run

→ Effects at 12 yoke boundaries visible

→ Time dependence of magnetic field visible

Field at Yoke Boundary B/C

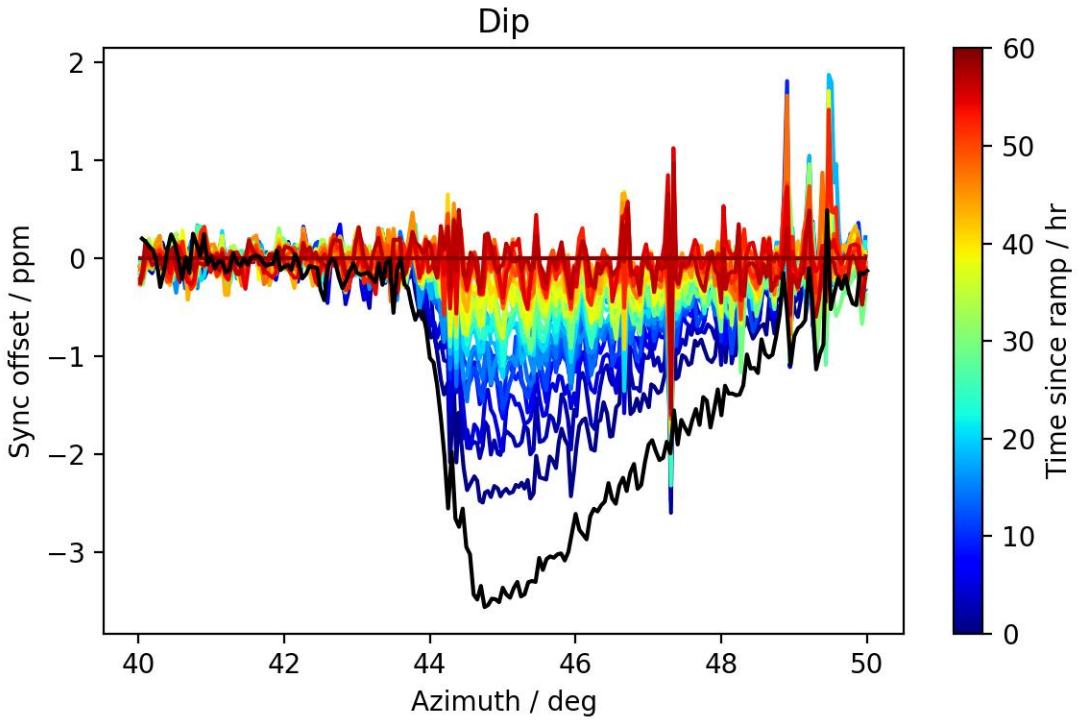

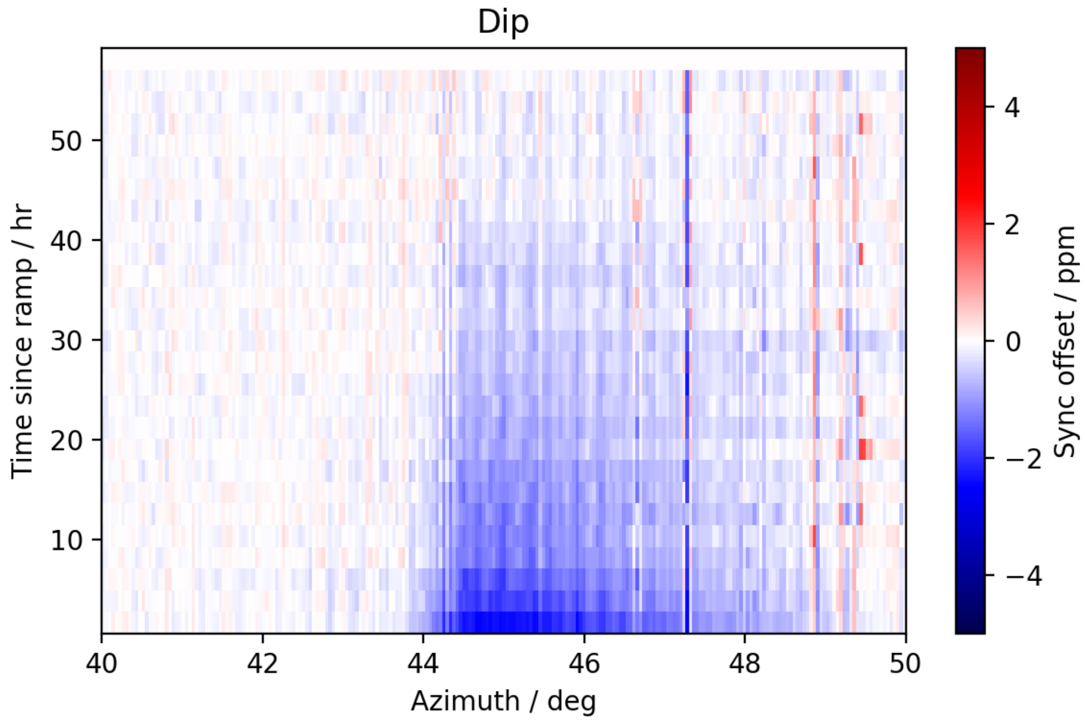

- Increased and time depended sync offsets at yoke boundary region
- Characteristic shape of untracked field changes
- Untracked field changes get smaller over time

Field at Yoke Boundary B/C

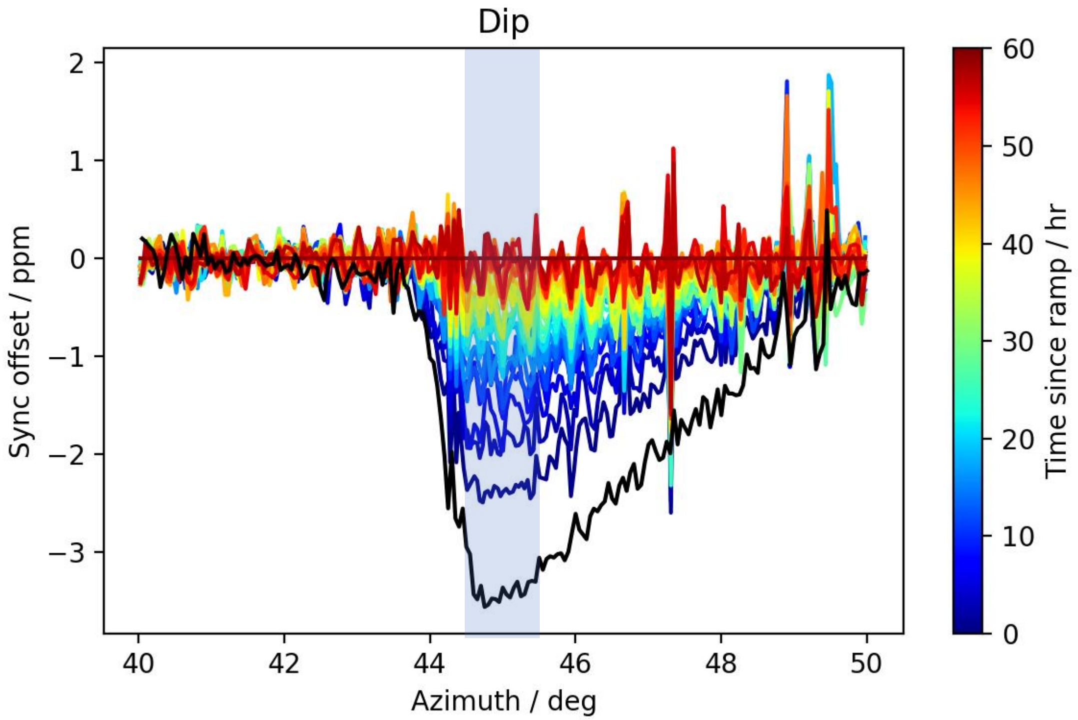

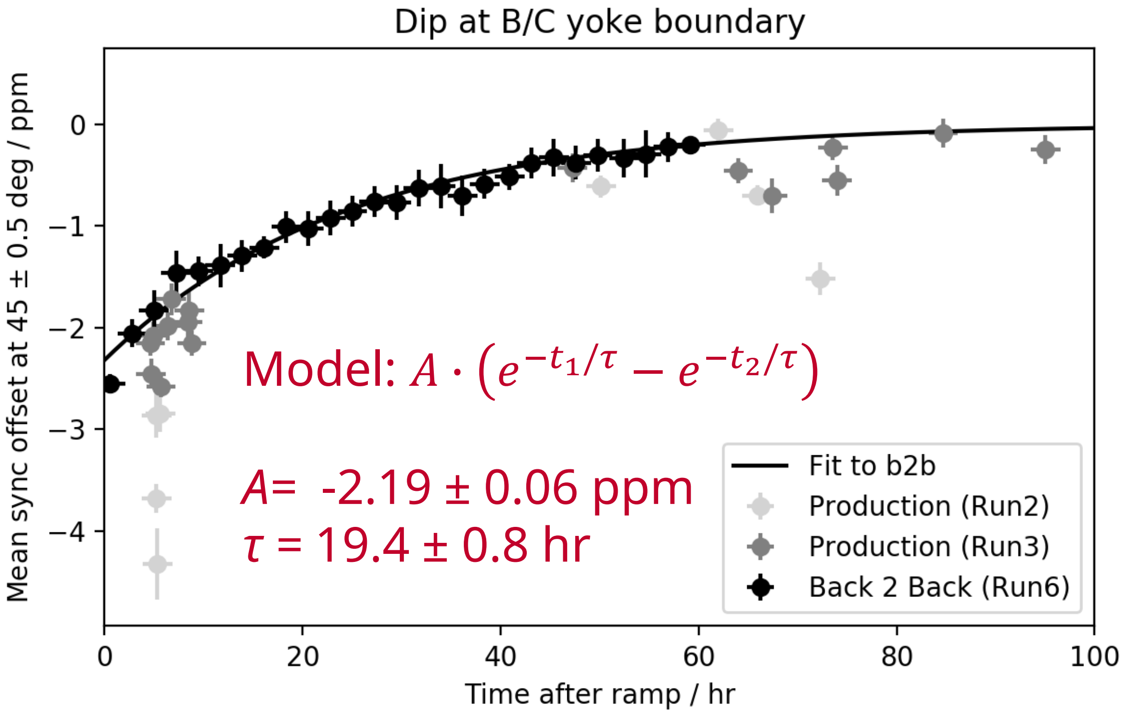

- Fitting amplitude of effect with exponential function
- Time constants of ~20 h

Trolley Probe Calibration

- Absolute calibrated water probe
- Cross-calibrated at Argonne National Lab test magnet

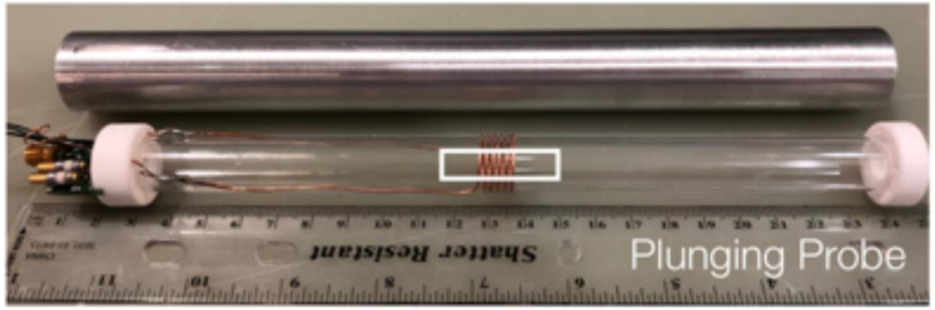

- Probe can be placed in ring by 3D translation stage
- Swap trolley and calibration probe to get calibration constant
- Derive calibration constants for each trolley probe

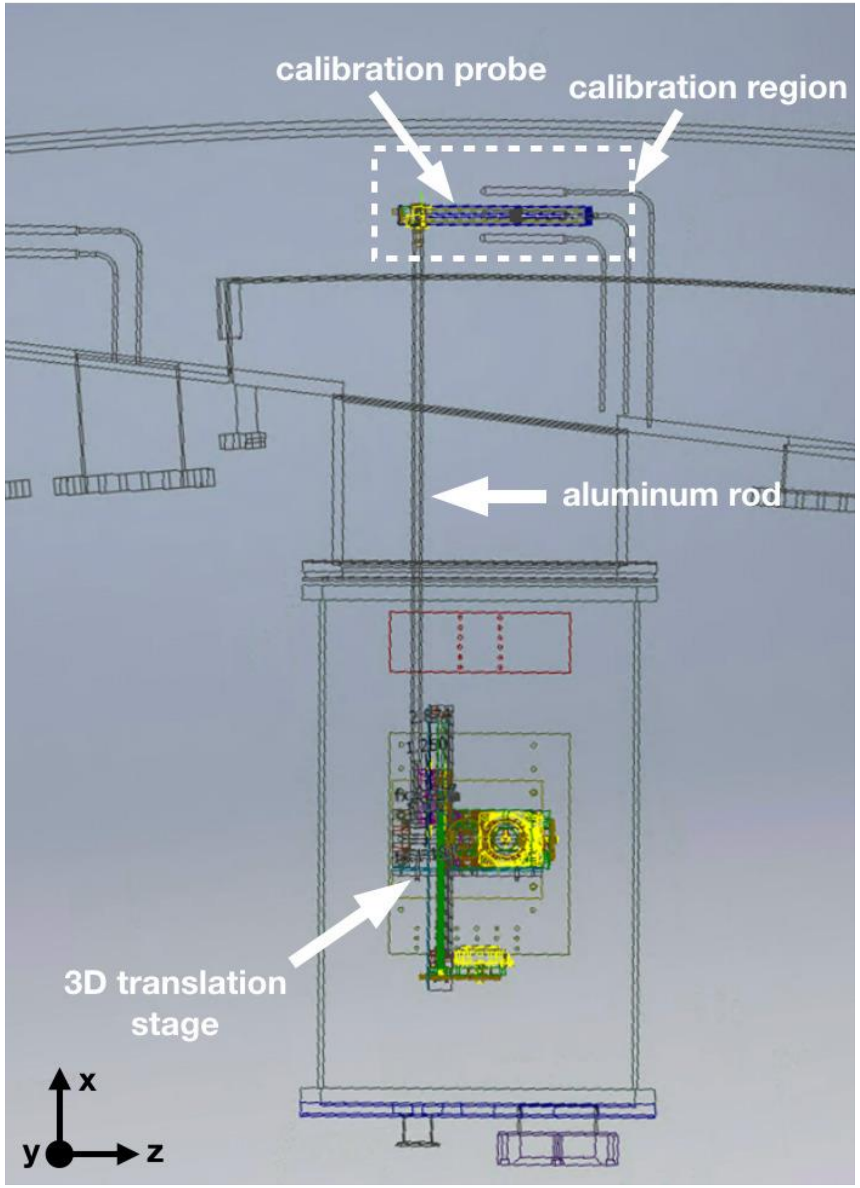

Improvements
- Study of temperature effects
- Calibration twice a year with automated procedure
- Consistent results

Muon weighted average magnetic field

Using tracker profiles and beam dynamics simulation

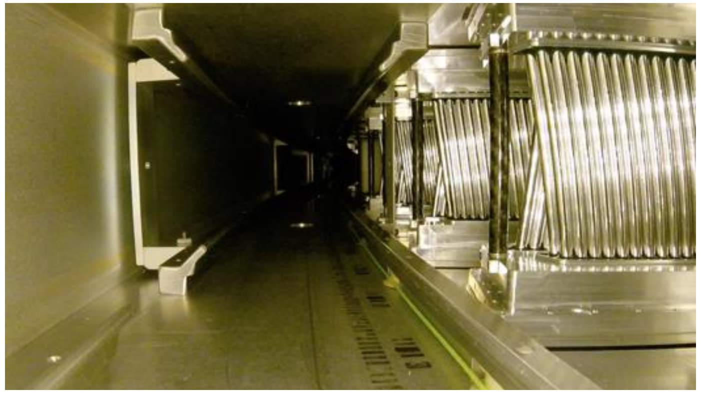

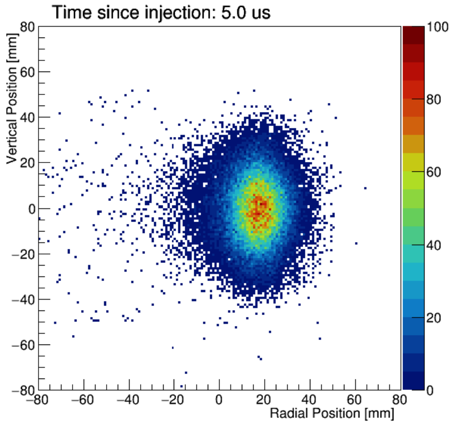

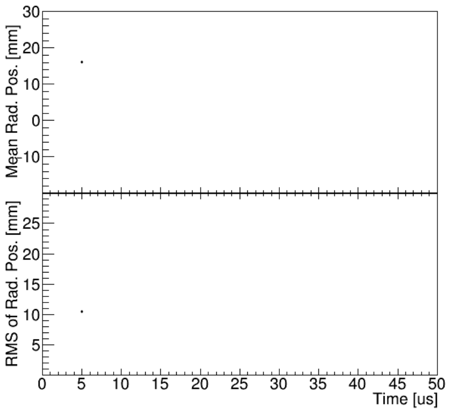

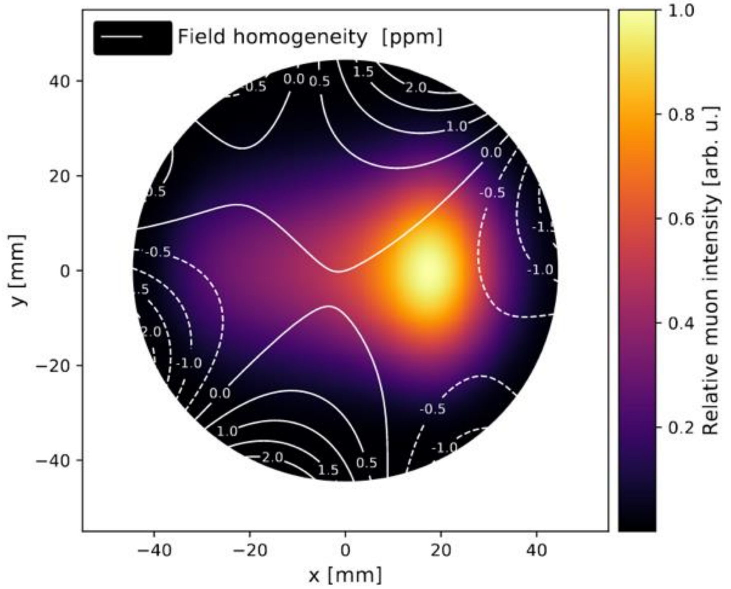

Improvements

- Better placement of beam, due to replacing broken resistors
- Better placement of beam, due to stronger kick
- CBO reduction due to quad RF (run 5)

Trolley Footprint Removal

Phys. Rev. A **103**, 042208 (2021)

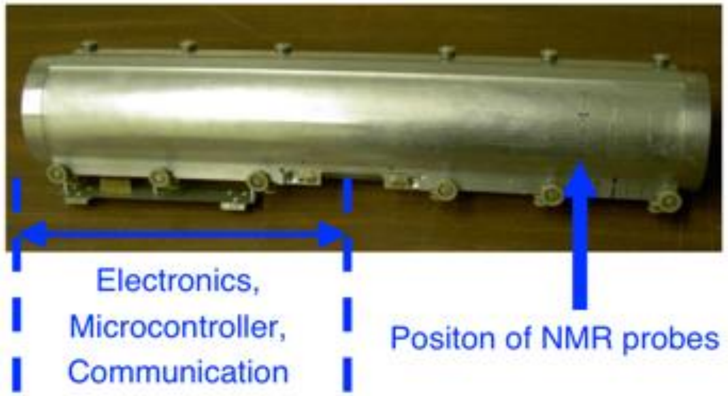

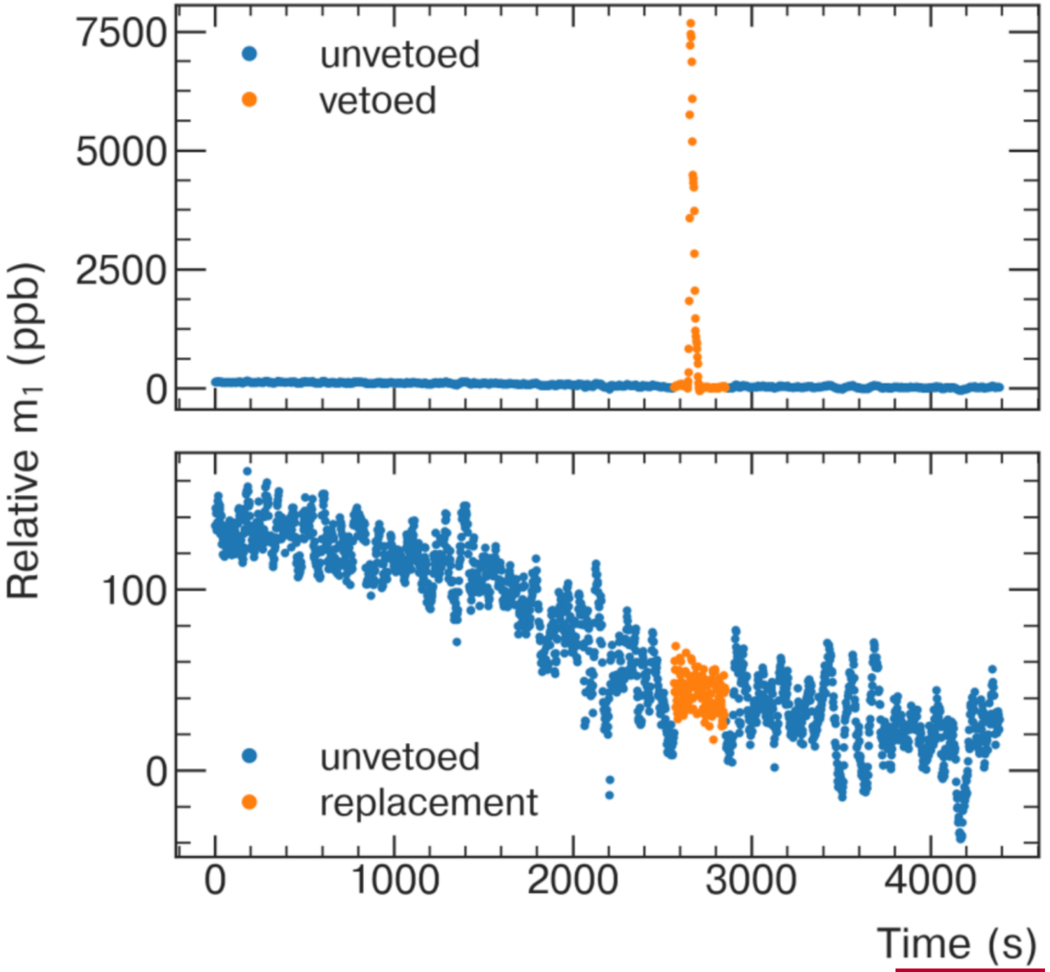

- trolley electronics disturbs field (footprint)
- veto measurements
- interpolate from neighboring probes

Tracking Uncertainty

- Fixed Probe drift: Random walk
- End point known: Brownian bridge model

$$\sigma(t_1, t_2) = M\frac{(T - t_2)t_1}{T}$$

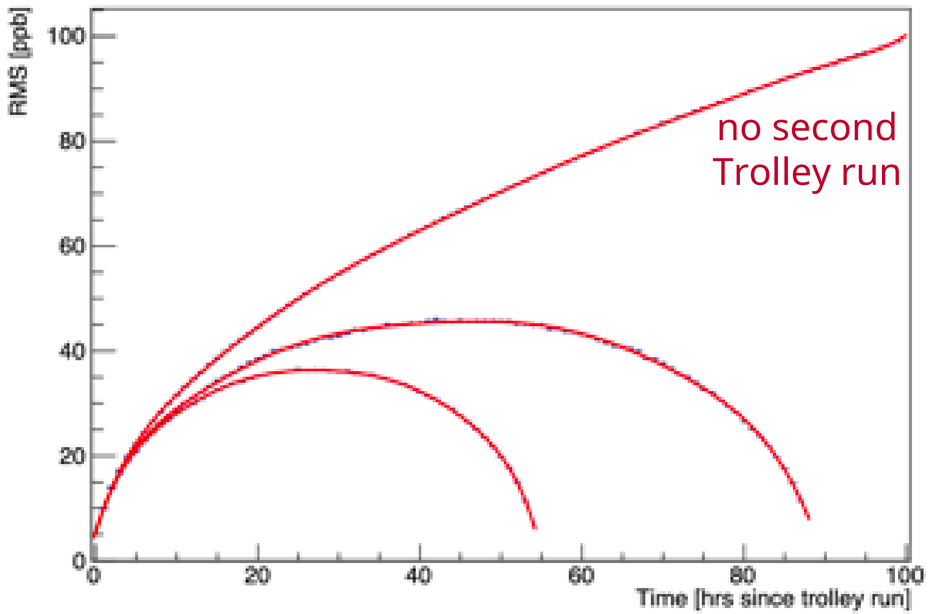

Uncertainty vs time

Improvements

- improved position determination
- continues azimuthal treatment (virtual trolley, Fourier method)
- improved trolley footprint removal
- more trolley runs
- improved field stability by temperature regulation

Nuclear Magnetic Resonance (NMR) technique

Material in external magnetic field

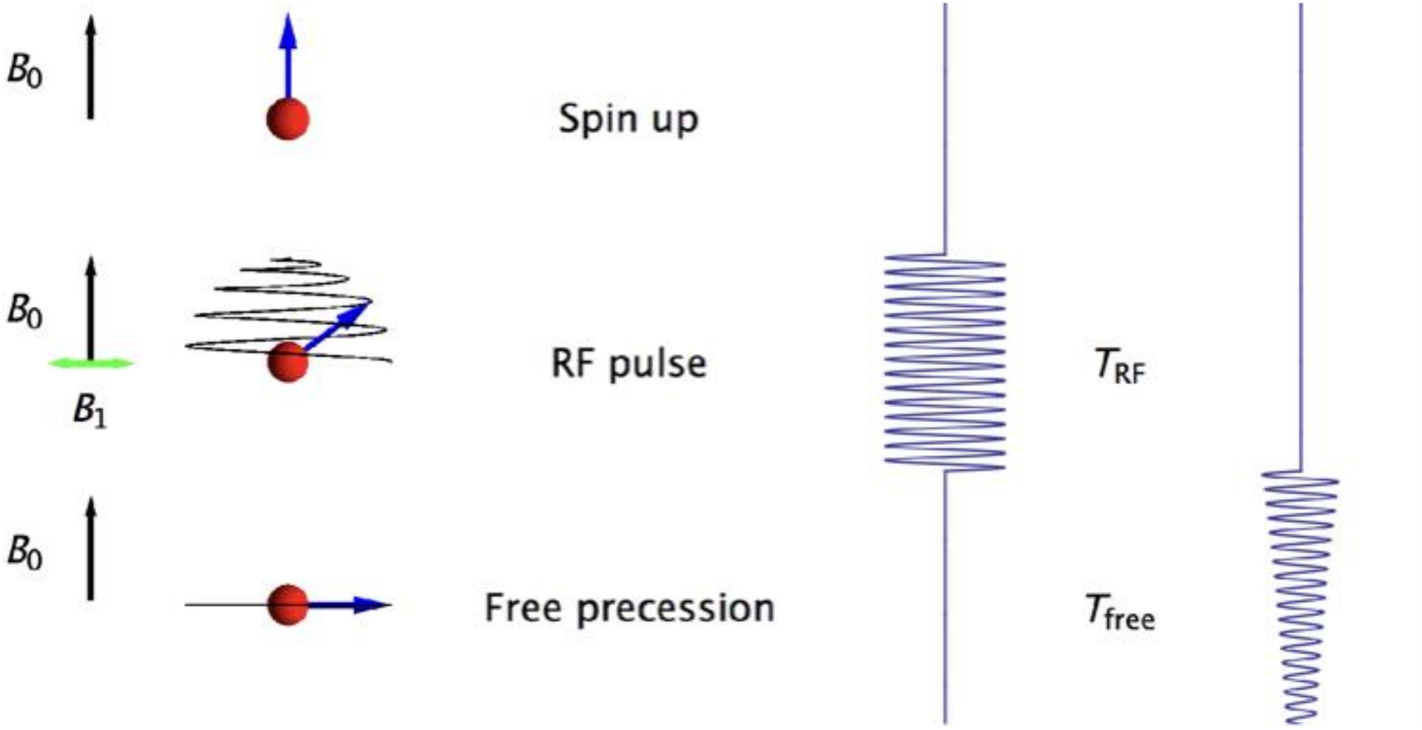

thermal equilibrium polarization: ~ 10^{-6}

RF pulse perpendicular to main field close to proton Larmor frequency tilts the p spin

Pick up induction signal of precising magnetization with the excitation coil

NMR technique

- Lamor precession frequency

$$\omega_L = -\gamma B$$

  with gyromagnetic ratio γ

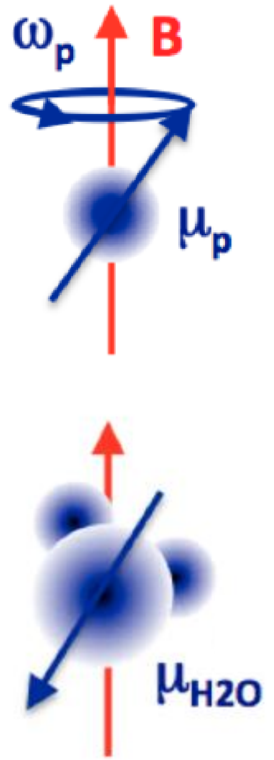

- Gyromagnetic ratio of free proton is 2.6752218744 $\cdot 10^8$ Hz/T

- Reference gyromagnetic ratio of pure water in spherical sample

- Two types of probes
  - Ultra pure water in cylinder volume for calibration
  - Petroleum jelly in cylinder volume for normal measurement

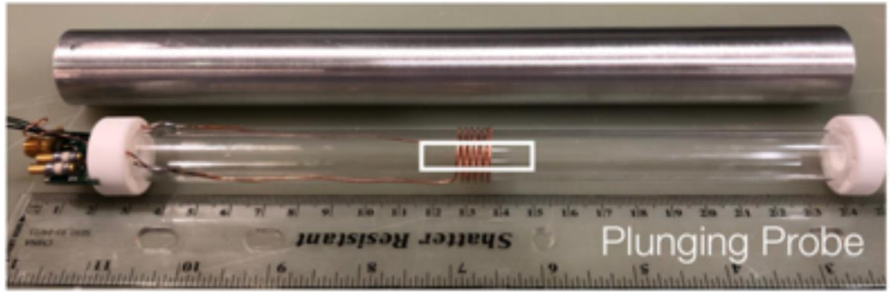

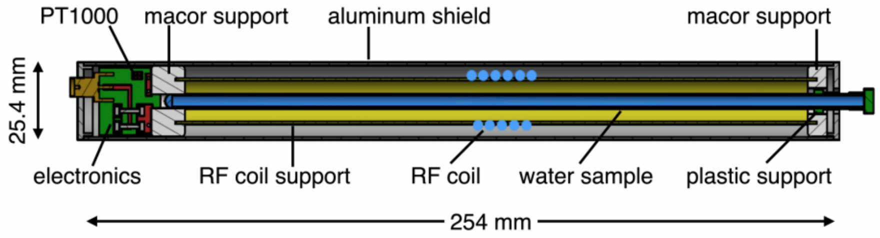

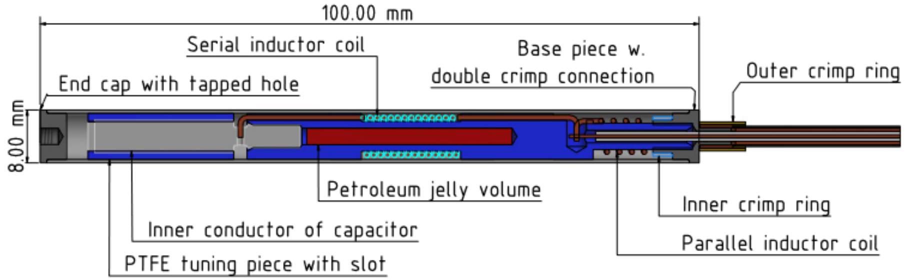

Free Induction Decay

- At 1.45 T field proton spin precession frequency if about 61.79 MHz
- Mixed down frequency to ~50kHz for digitization
- Free induction decay signal oscillates at Lamor frequency
- Decoherence of spins in sample lead to envelop decay
- Using Hilbert transformation to extract phase
- Frequency is given by slope of phase at time t=0
- Subtract template → measure field differences

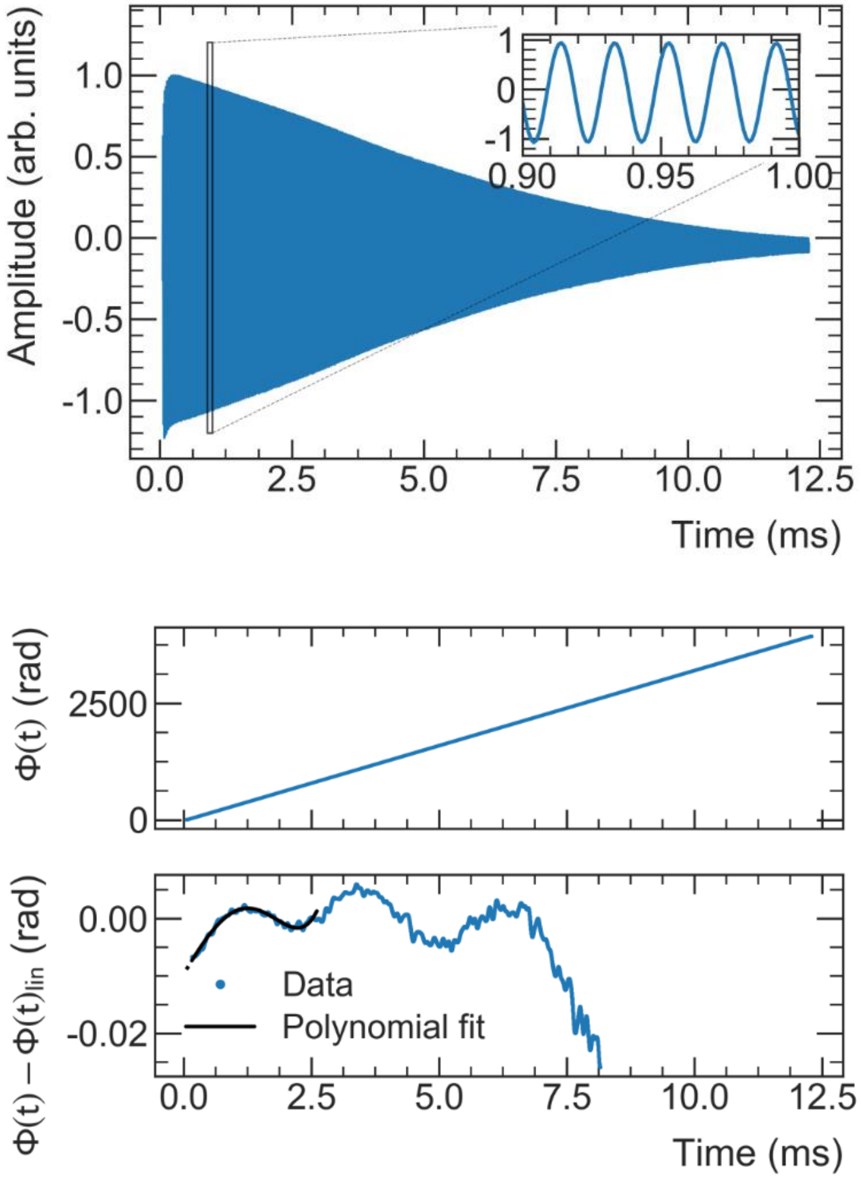

Shimming trolley

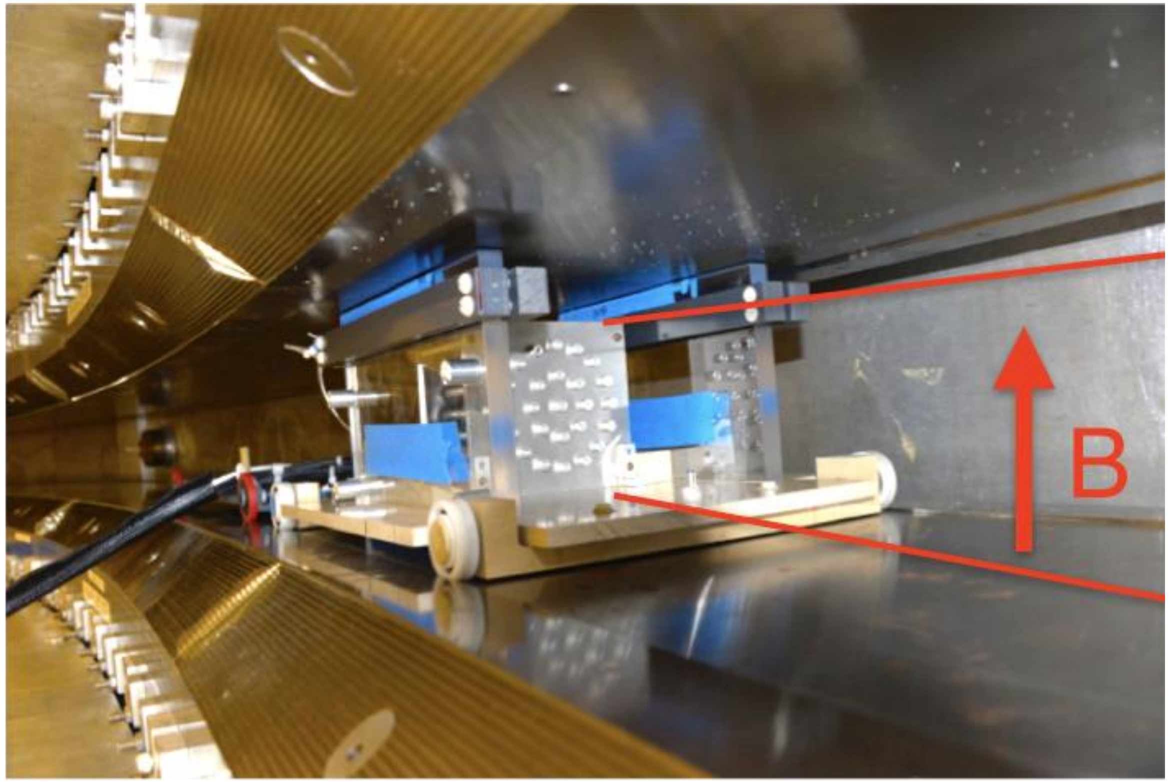

- 25 NMR probes on movable platform
- Used to measure field while assembly

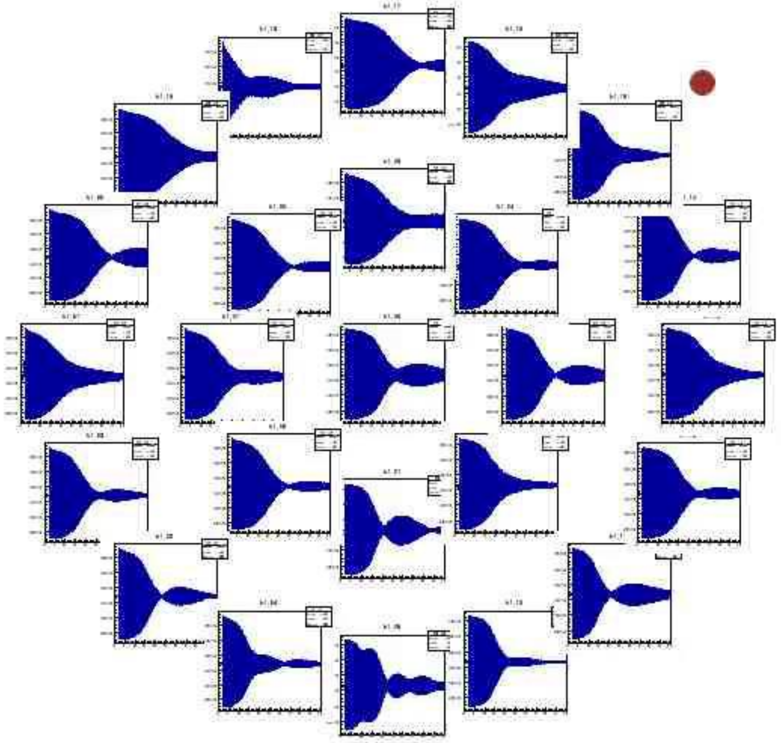

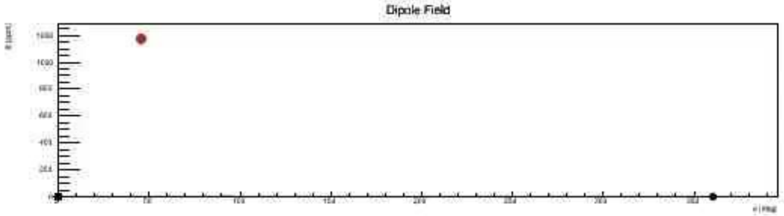

Getting a homogeneous field

First adjust height and tilt of pole pieces

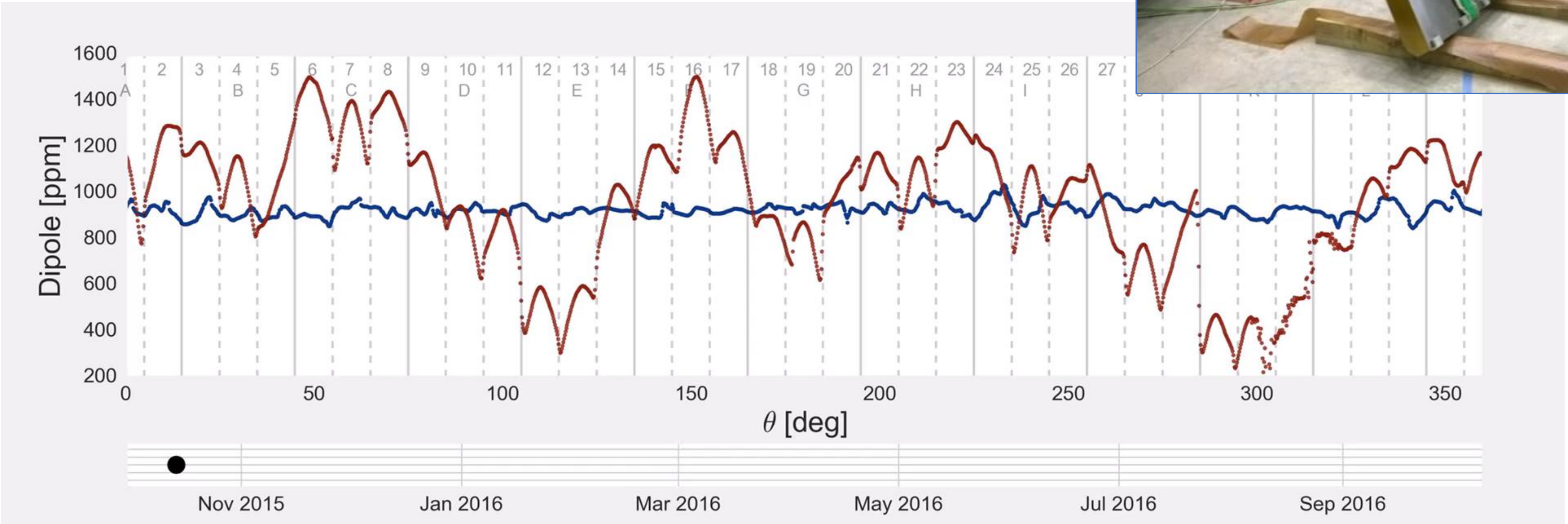

Getting a homogeneous field

Second top hats and wedge shims

Top hats gap changes effective permeability in the magnetic circuit

Radial position of wedges to adjust dipole and compensate quadrupole

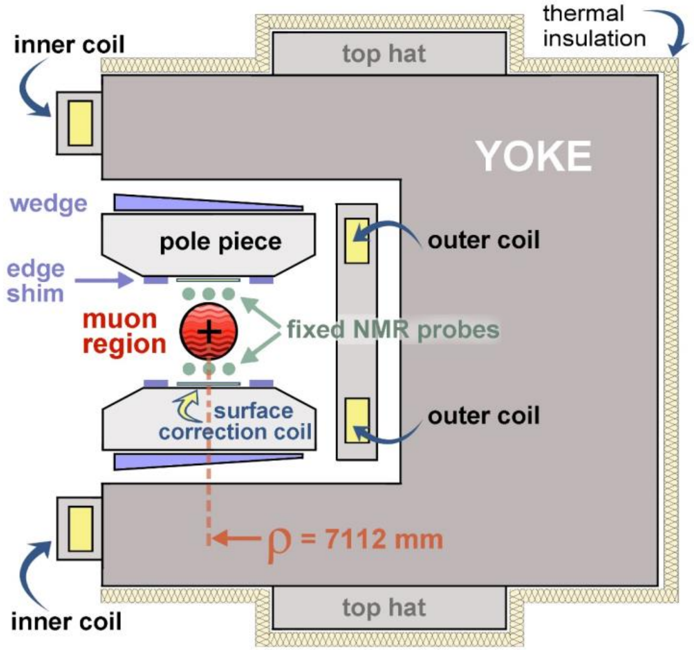

g-2 Magnet in Cross Section

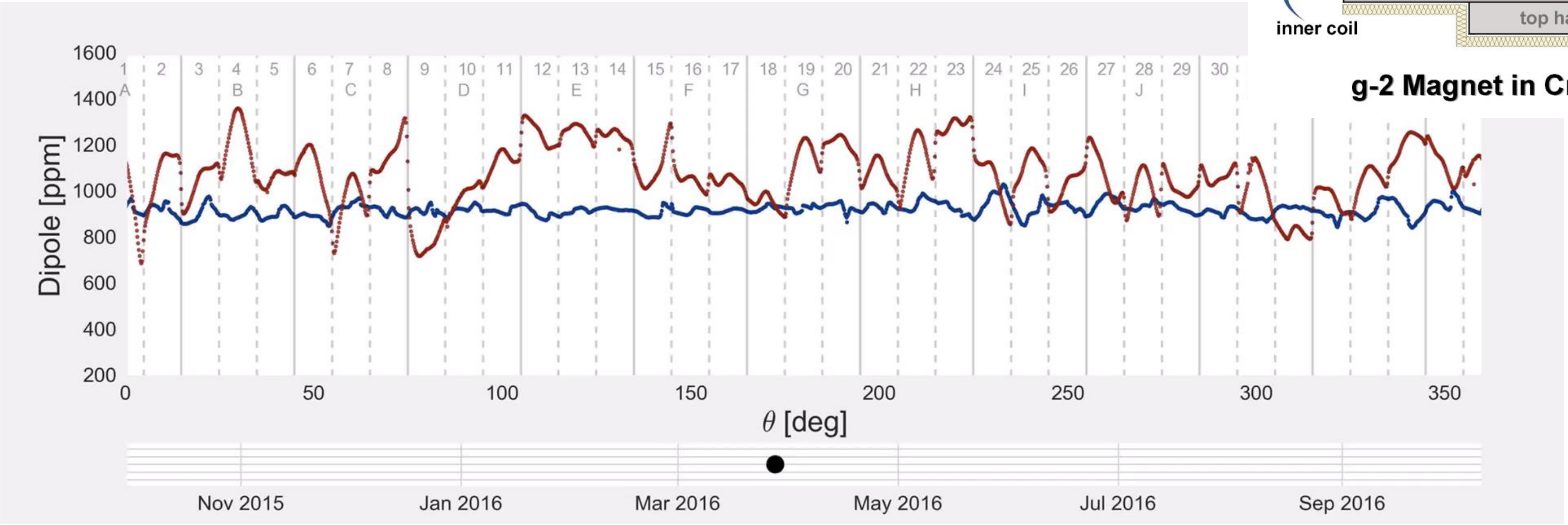

Getting a homogeneous field

Add IR laser cut iron foils

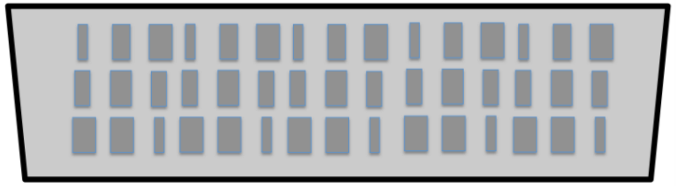

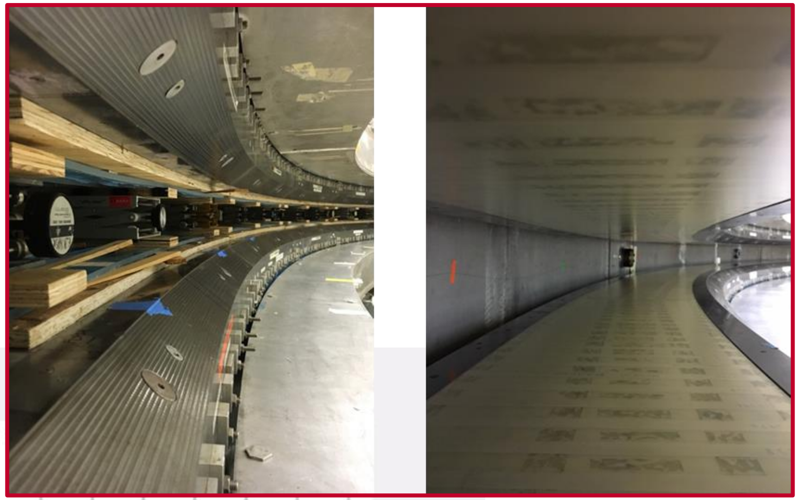

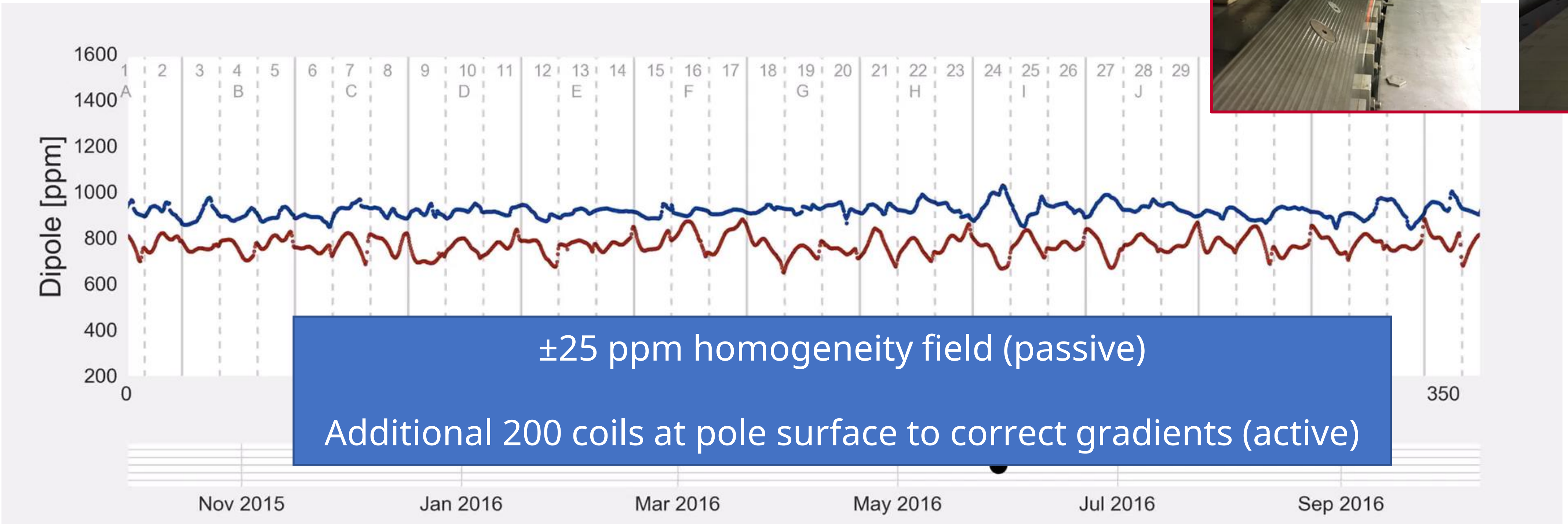

±25 ppm homogeneity field (passive)

Additional 200 coils at pole surface to correct gradients (active)

Blinded results from 4 data periods

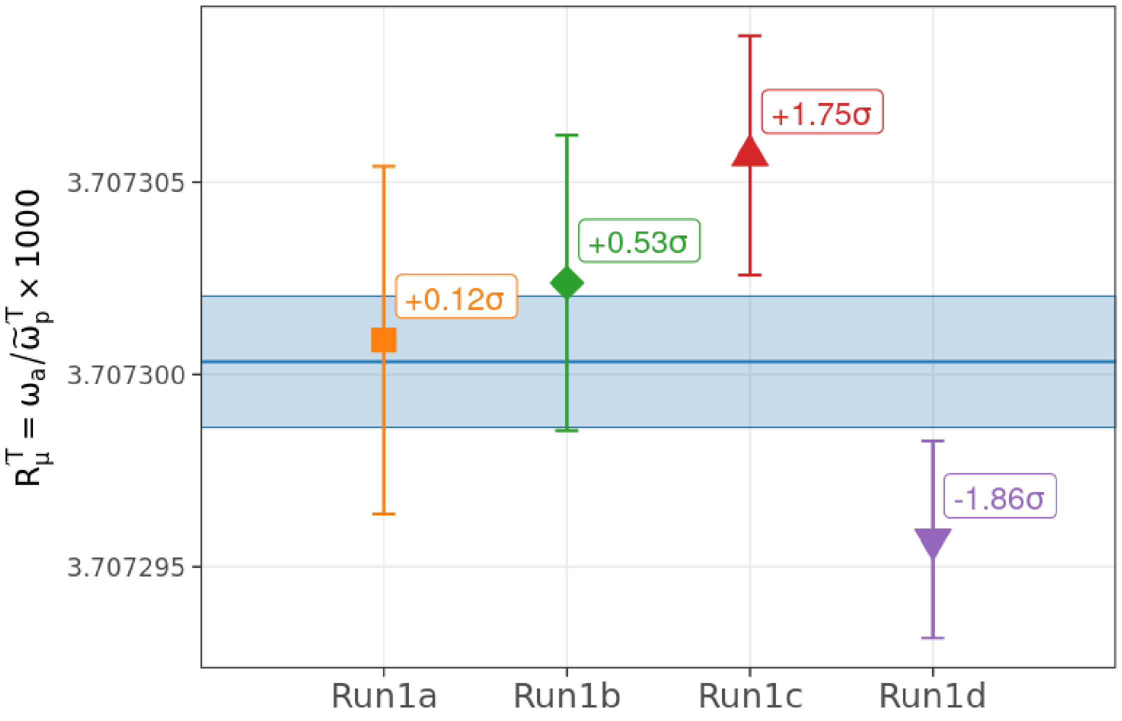

- Correction factors and analysis depend on kicker strength and ESQ HV settings (beam tune)
- Four different settings in run 1
- Results consistent with χ^2/ndf=6.8/3 P(χ^2)=7.8%
- Result still hardware blinded

Blinding of master clock

… by Greg Bock and Joe Lykken in 2018 (no members of Muon g-2 collaboration)

ω_a reference clock supposed to be at 40 MHz but slightly detuned

$$\frac{\omega_a}{\tilde{\omega}'_p} = \frac{\boxed{f_{\text{clock}}}\,\omega_a^{\text{meas}}\left(1 + C_e + C_p + C_{ml} + C_{pa}\right)}{f_{\text{calib}}\left\langle M(x,y,\phi)\,\omega'_p(x,y,\phi)\right\rangle\left(1 + B_k + B_q\right)}$$

Hardware blinding of master clock

… by Greg Bock and Joe Lykken in 2018 (no members of Muon g-2 collaboration)

ω_a reference clock supposed to be at 40 MHz

$$\frac{\omega_a}{\tilde{\omega}'_p} = \frac{\boxed{f_{\mathrm{clock}}}\,\omega_a^{\mathrm{meas}}\,(1 + C_e + C_p + C_{ml} + C_{pa})}{f_{\mathrm{calib}}\,\langle M(x,y,\phi)\,\omega'_p(x,y,\phi)\rangle\,(1 + B_k + B_q)}$$

Hardware blinding of master clock

… by Greg Bock and Joe Lykken in 2018 (no members of Muon g-2 collaboration)

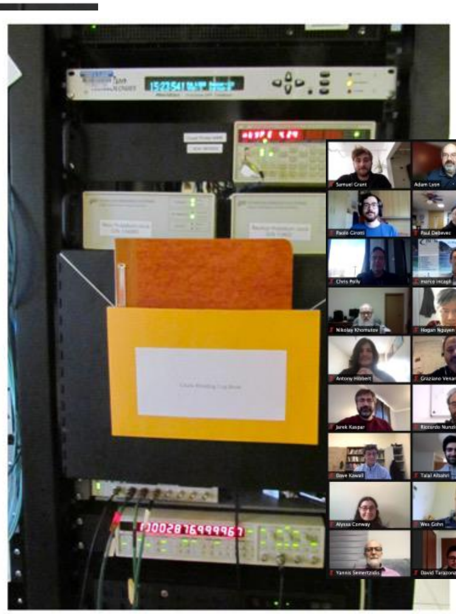

… on February 25th, 2021!

ω_a reference clock supposed to be at 40 MHz

$$\frac{\omega_a}{\tilde{\omega}'_p} = \frac{\boxed{f_{\text{clock}}}\,\omega_a^{\text{meas}}\left(1 + C_e + C_p + C_{ml} + C_{pa}\right)}{f_{\text{calib}}\left\langle M(x,y,\phi)\,\omega'_p(x,y,\phi)\right\rangle\left(1 + B_k + B_q\right)}$$

Hardware blinding of master clock

... by Greg Bock and Joe Lykken in 2018 (no members of Muon g-2 collaboration)

... on February 25th, 2021!

ω_a reference clock supposed to be at 40 MHz but was set to 39.997 844 MHz

$$\frac{\omega_a}{\tilde{\omega}'_p} = \frac{\boxed{f_{\text{clock}}}\,\omega_a^{\text{meas}}\left(1 + C_e + C_p + C_{ml} + C_{pa}\right)}{f_{\text{calib}}\left\langle M(x,y,\phi)\,\omega'_p(x,y,\phi)\right\rangle\left(1 + B_k + B_q\right)}$$

Hardware blinding of master clock

... by Greg Bock a ... ation)

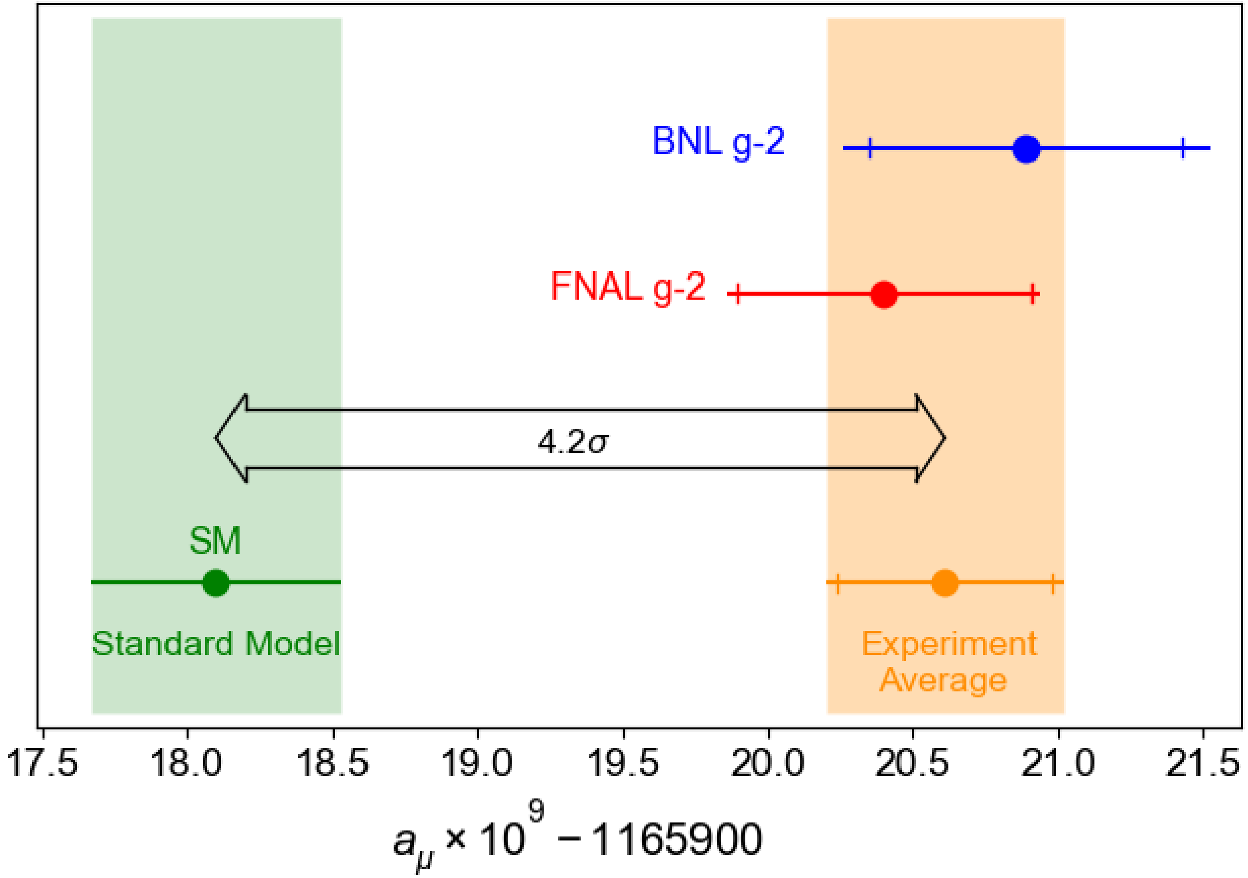

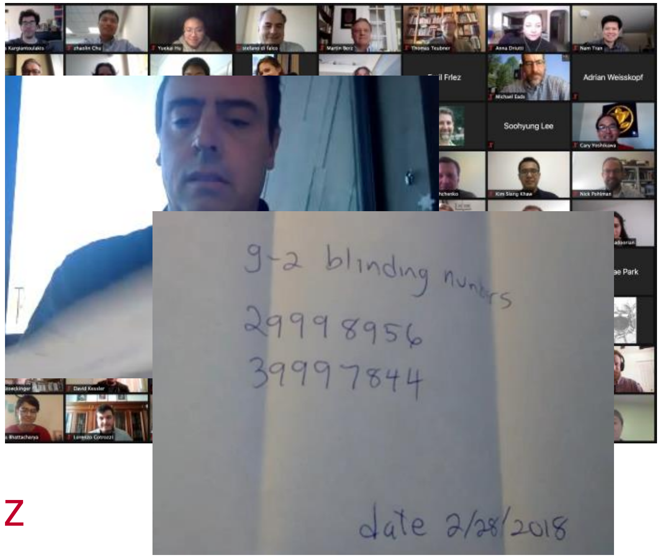

ω_a reference cloc ... z

$$\tilde{\omega}'_p \quad f_{\text{calib}} \langle M(x,y,\phi)\omega'_p(x,y,\phi)\rangle (1 + B_k + B_q)$$

Dynamic theory situation

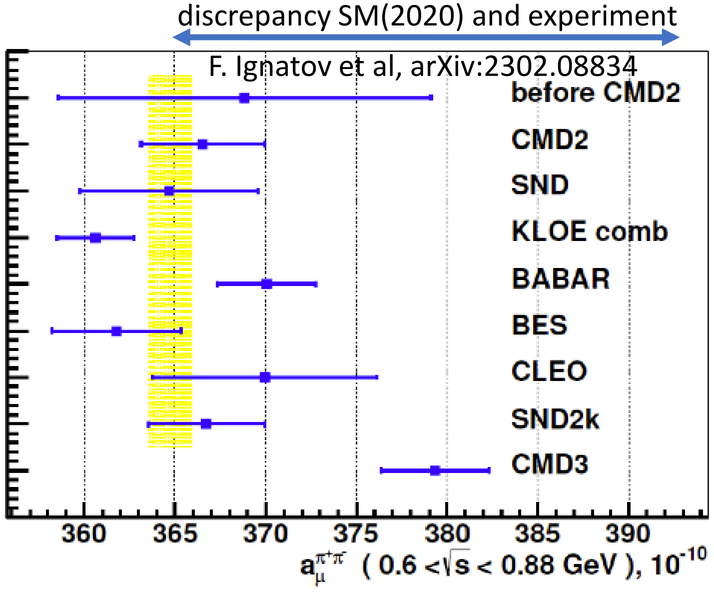

A new experimental input to the SM prediction was recently released!

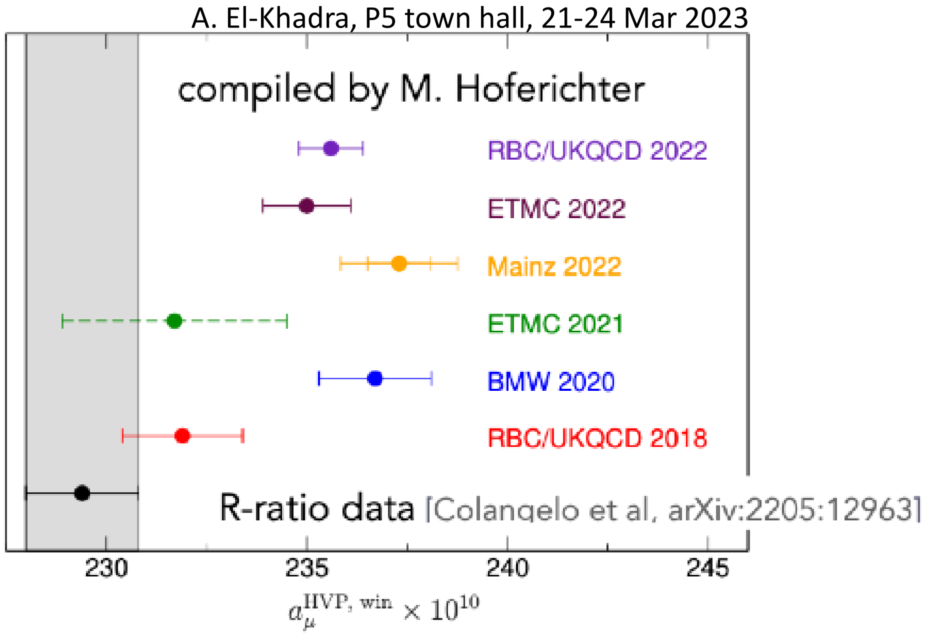

Huge progress in ab-initio calculation of hadronic physic contributions using lattice QCD

Three lepton processes: Naïve scaling

g-2

$$a_l = \frac{g_l - 2}{2} \propto m_l^2$$

EDM

$$d_l \propto m_l$$

LFV

$$\mathcal{B}\nabla(l \to lX) \propto (m_l)^0$$

Dispersive approach

The diagram to be evaluated:

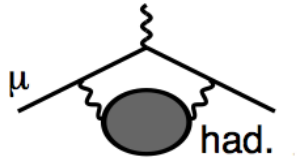

pQCD not useful. Use the dispersion relation and the optical theorem.

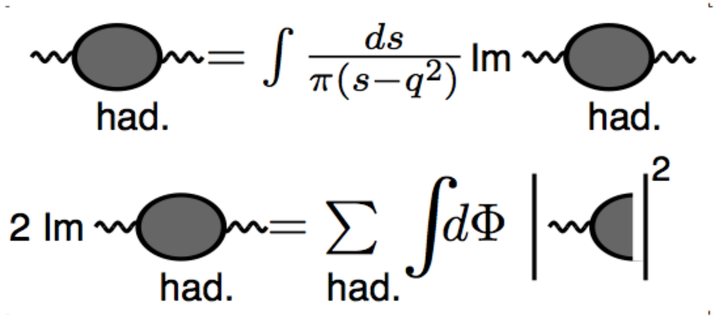

Follows from causality → analyticity

Follows from unitarity of scattering matrix

$$a_\mu^{\mathrm{had,LO}} = \frac{m_\mu^2}{12\pi^3} \int_{s_{\mathrm{th}}}^{\infty} ds \, \frac{1}{s} \hat{K}(s) \sigma_{\mathrm{had}}(s)$$

Weight function K(s) from loop integral $\int d^4q$

Low energies more important

$\pi^+ \pi^-$ contribute 73% to LO

need to know total hadronic cross-section $\sigma_{\mathrm{had}}(s)$

Credit: Thomas Teubner

Dispersive approach

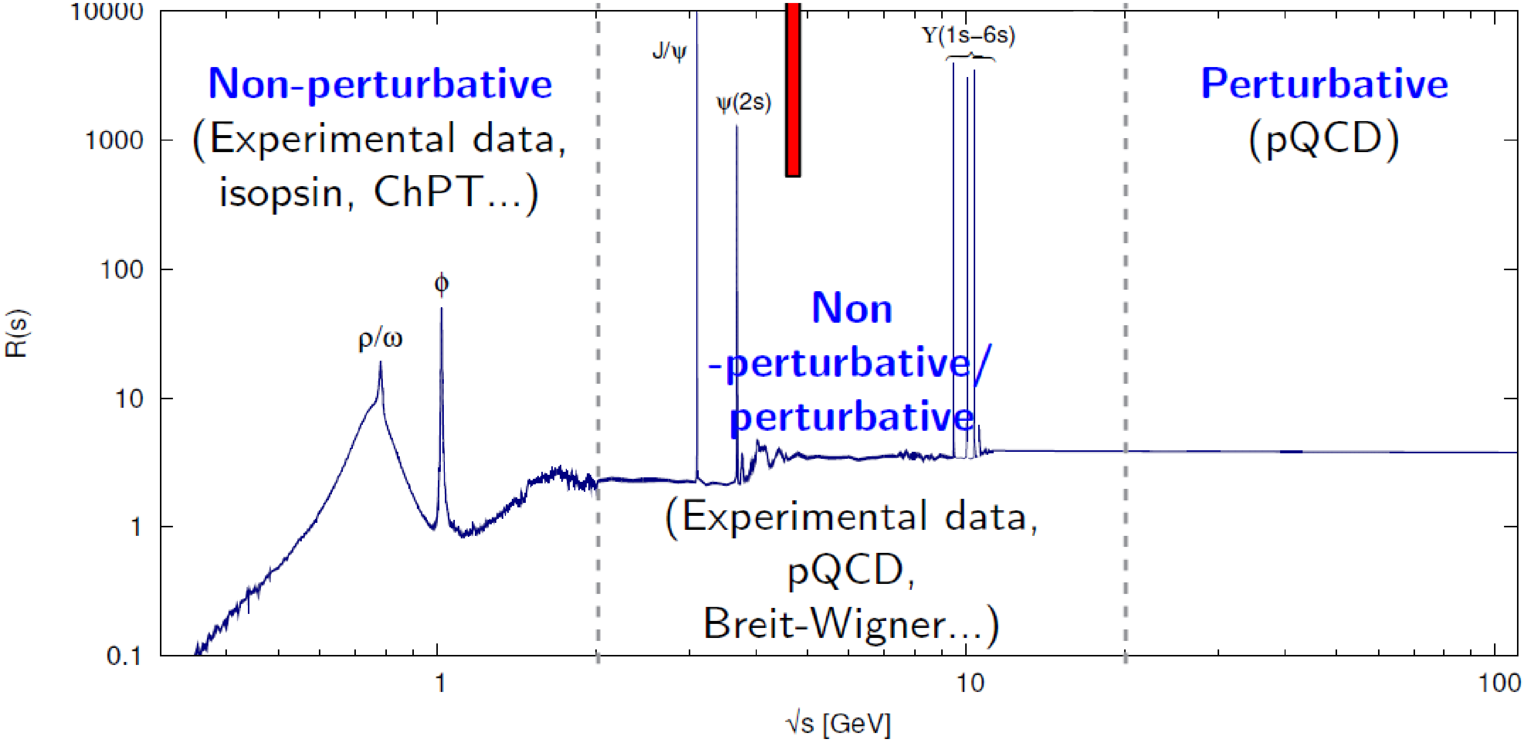

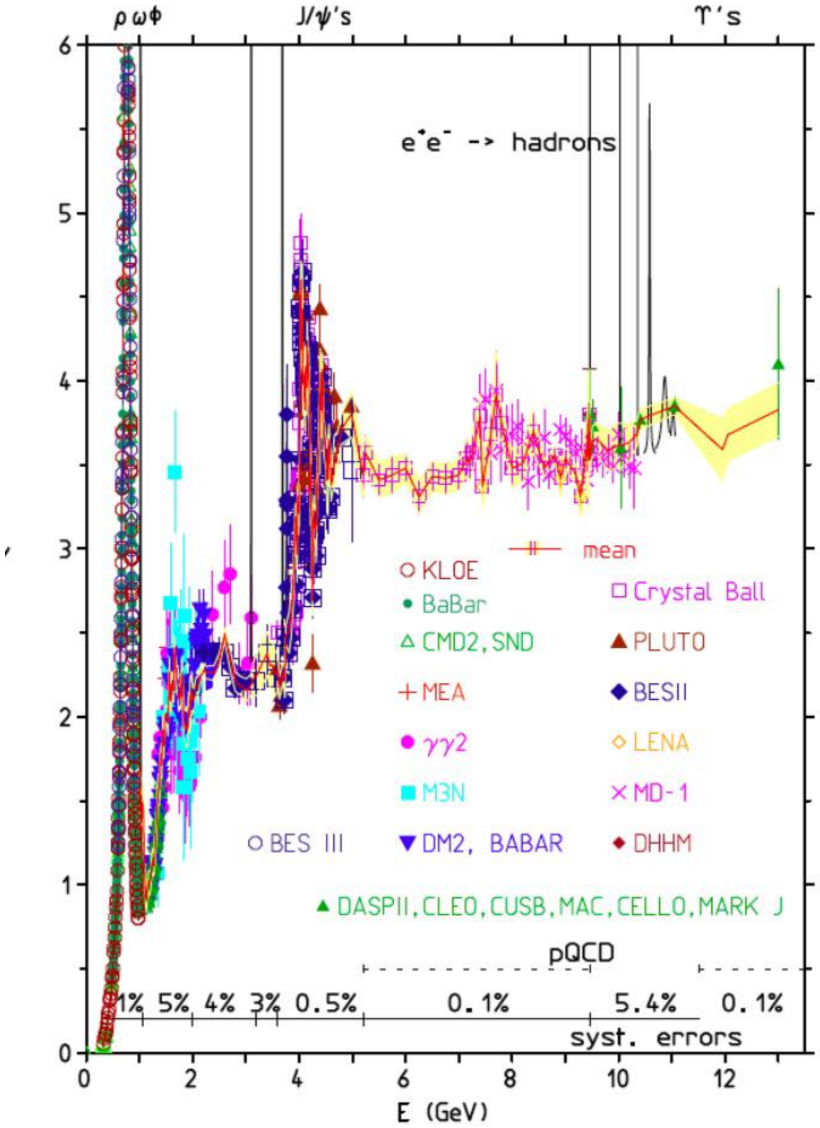

- >100 datasets from $e^+e^- \rightarrow$ hadrons in > 35 final states
- Data from BELLE-II, BES-III, KLOE, BaBar, SND, CMD-3 and KEDR

Lattice approach

- First principal calculation by discretizing Euclidian space-time
- BMW is presently the only sub 1% (HVP) lattice calculation in the full kinematic region
- Cross-checks recently performed but only **in limited** (30%) (distance) region.

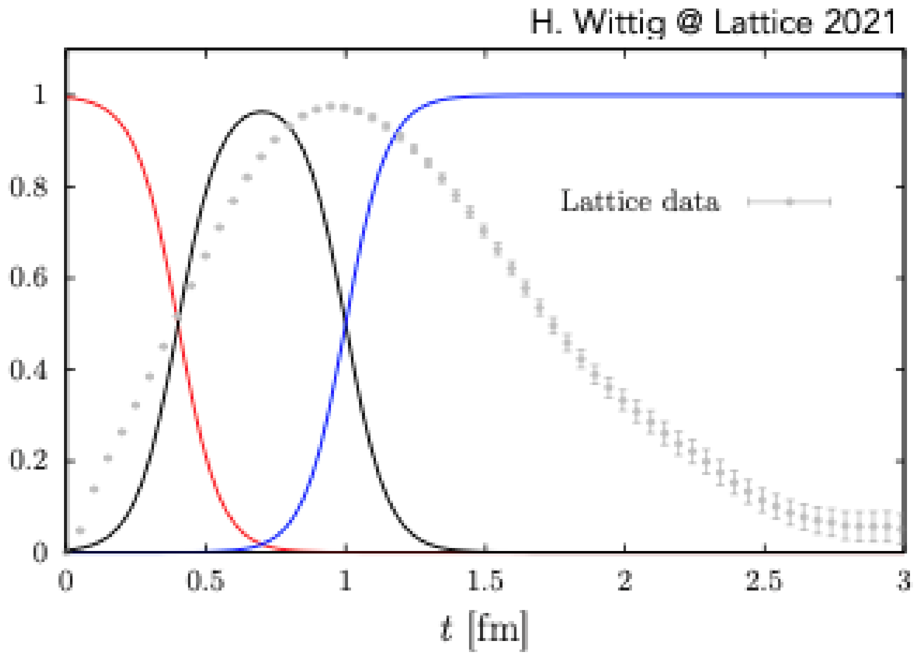

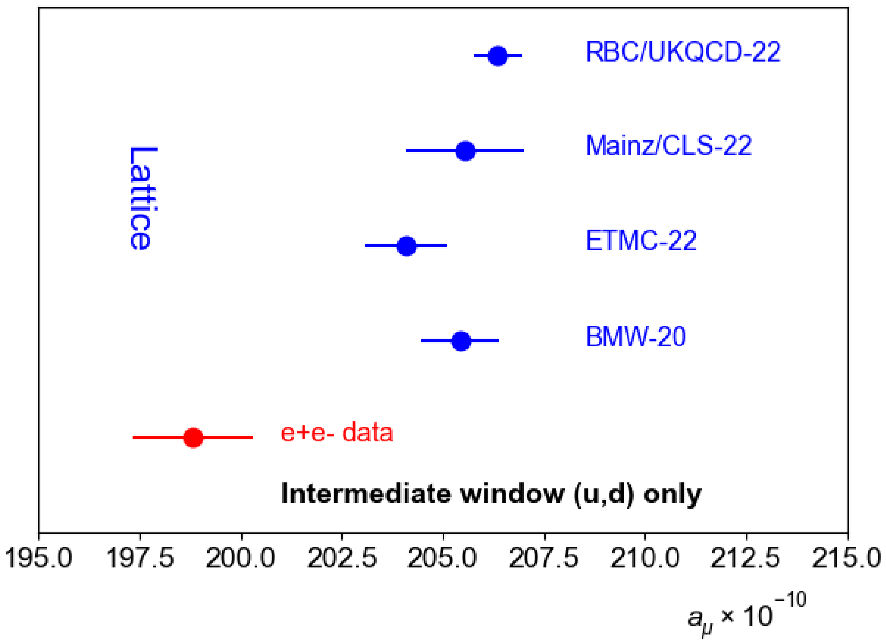

Dispersive vs Lattice Approach

- Implication of BMW results is that there are issues with the e^+e^- measurements (below 0.7 GeV) or a flaw in the e^+e^- or lattice theory
- If this is true then is affected and so are the global EWK fits since they use e^+e^- data
- Tension in SM M_W, M_H vs measured M_W, M_H

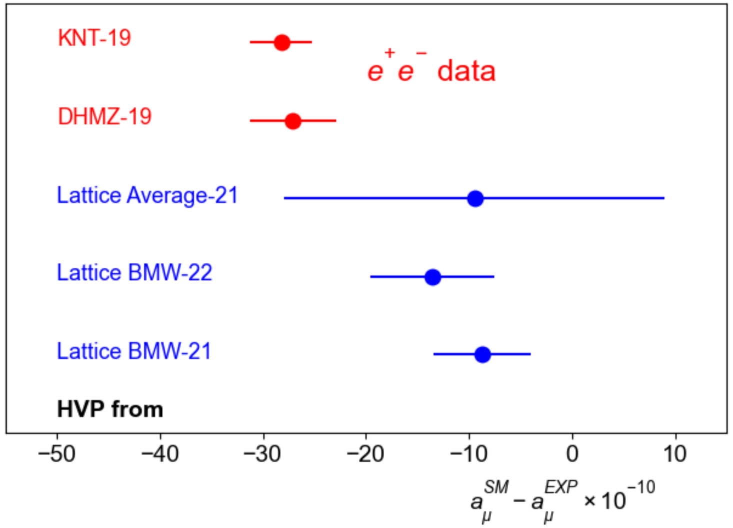

- The analysis of e^+e^- data can be made to match the BMW lattice prediction if the measured cross sections below 0.7 GeV **are shifted by 7%.**
- In this region there is data from 9 independent experiments: the most precise experiments (KLOE, BaBar, CMD, SND, ….) quote **cross section uncertainties of 0.5-1%…**

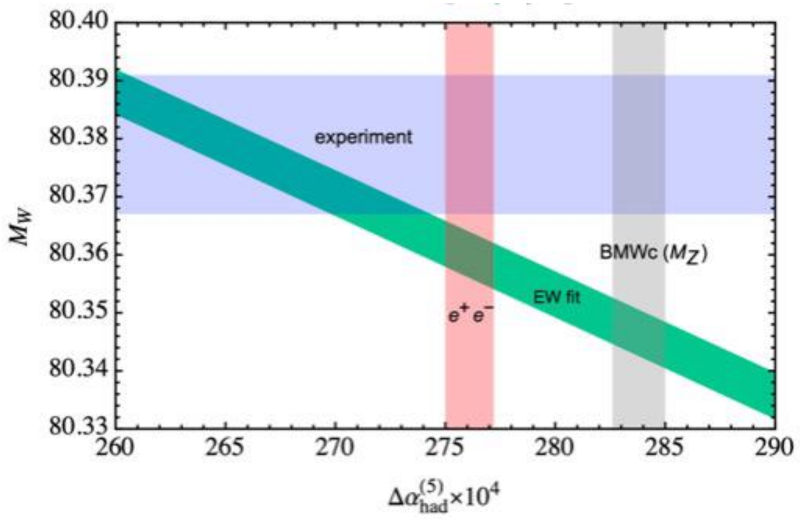

A new era of a_μ comparisons

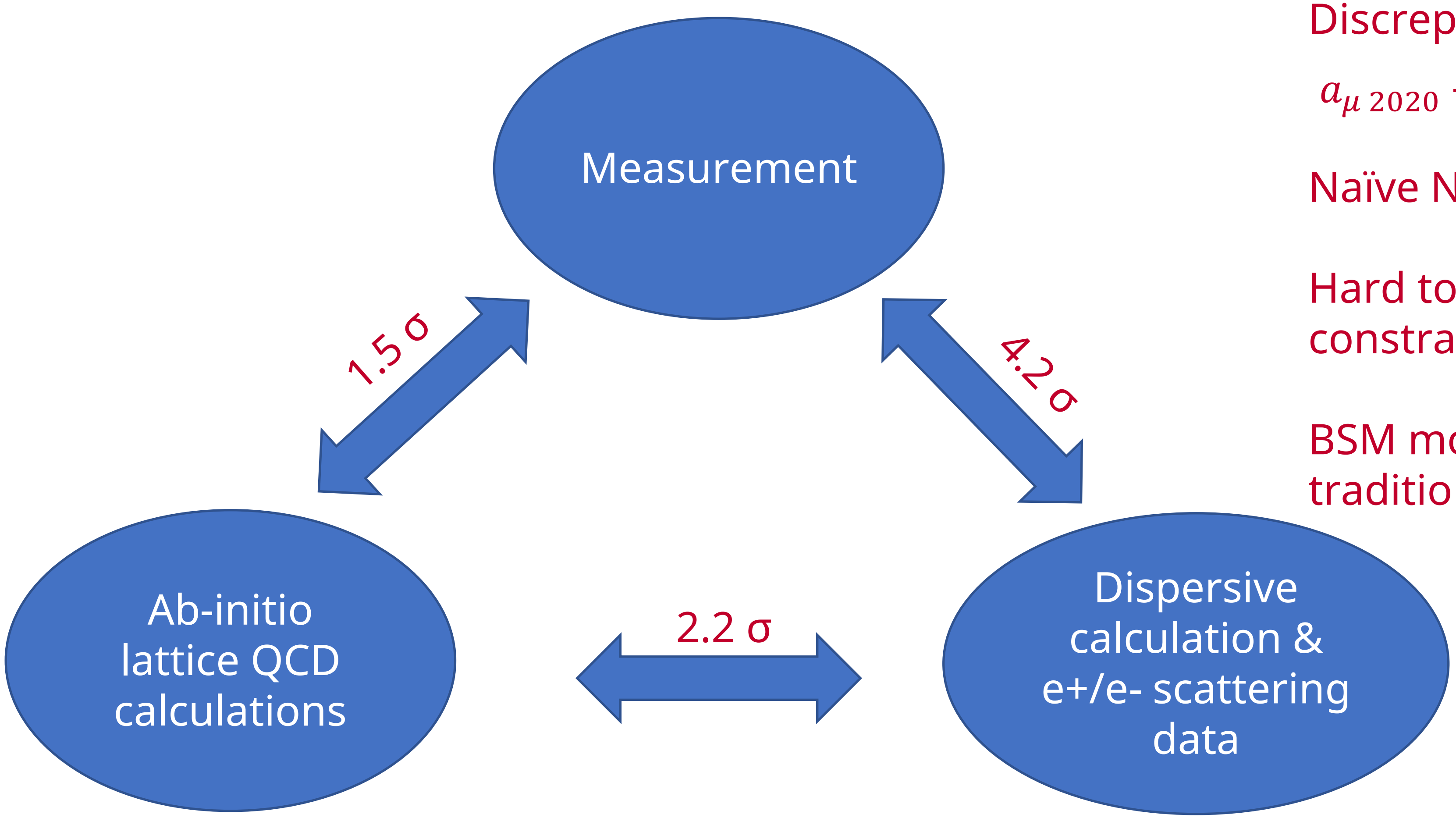

Discrepancy is large

$a_{\mu\ 2020} - a_{\mu\ dispersive} \sim 1.7\ a_{\mu\ Weak}$

Naïve NP scaling $M_{BSM} < O(2.1\ \mathrm{TeV})$

Hard to accomodate with LHC and DM constraints

BSM models tend to be in non-traditional parameter regions

Muon g-2 in SM

			a_μ^{SM} portion	$\delta a_\mu^{\mathrm{SM}}$ portion
QED	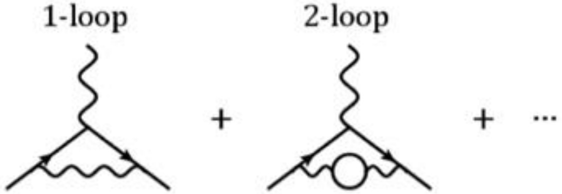	Perturbative (Known to five-loop)	$\sim 99.99\%$	$\sim 0.001\%$
EW	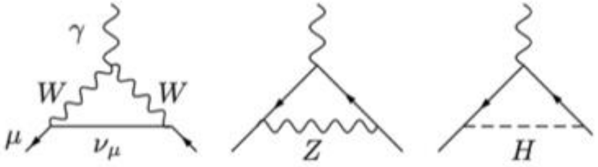	Perturbative (Known to two-loop)	~ 1 ppm	$\sim 0.2\%$
HVP	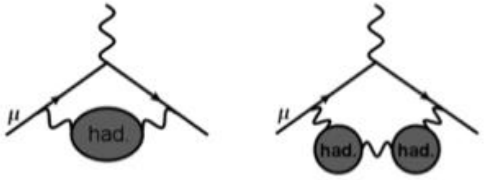	Non-perturbative (Data-driven & lattice)	~ 59 ppm	$\sim 84\%$
HLbL	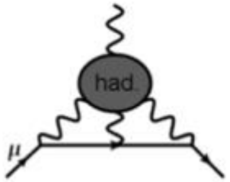	Non-perturbative (Data-driven & lattice)	~ 1 ppm	$\sim 16\%$

Muon g-2 in SM

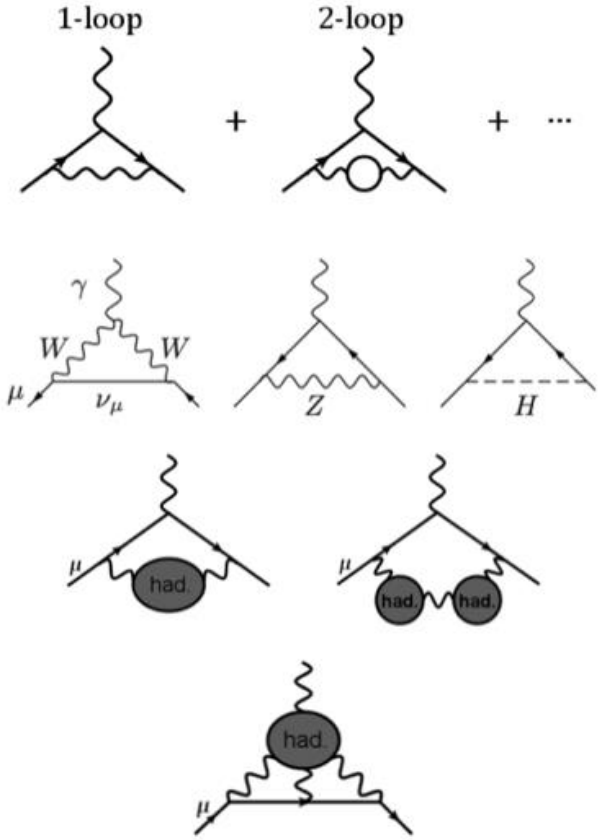

QED — Perturbative (Known to five-loop)

EW — Perturbative (Known to two-loop)

HVP — Non-perturbative (Data-driven & lattice)

HLbL — Non-perturbative (Data-driven & lattice)

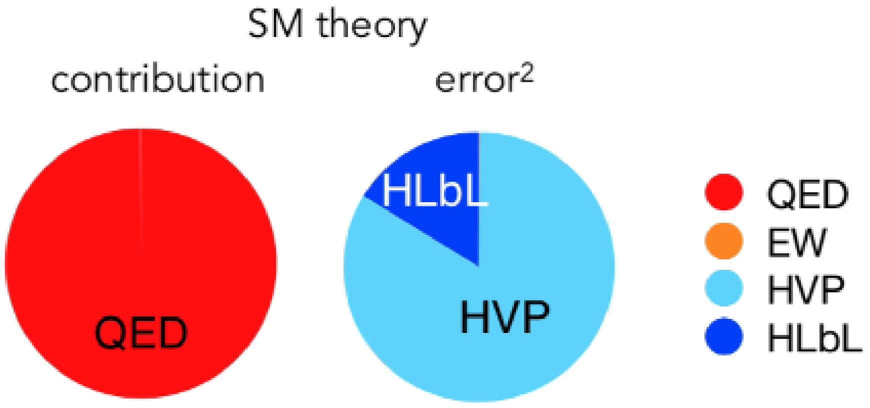

Beyond Standard Model Physics

- Extra contribution to anomalous magnetic moment

$$a_\mu = a_{\mathrm{QED}} + a_{\mathrm{weak}} + a_{\mathrm{hadron}} + a_{\mathrm{BSM}}$$

- Naïve scaling

$$\Delta a_{\mathrm{l}}^{\mathrm{BSM}} \propto \frac{g_{\mathrm{BSM}}}{16\pi^2} \frac{(\text{lepton mass})^2}{(\text{new particle mass})^2}$$

- Comparison with electron g-2

$$\left(\frac{m_\mu}{m_{\mathrm{e}}}\right)^2 = \left(\frac{105\,\mathrm{MeV}}{0.5\,\mathrm{MeV}}\right)^2 \approx 43000$$

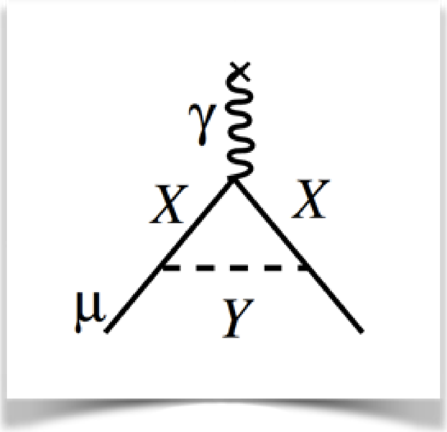

- Muon g-2 is ~43000 more sensitive to new physics compared to electron g-2

Lattice approach

- BMW20: First sub% calculation of HVP contribution on lattice
- Calculation of “1 particle Irreducible diagrams”

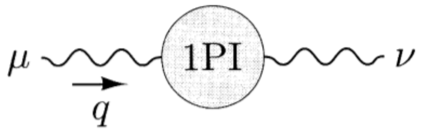

$$\equiv i\Pi^{\mu\nu}(q),$$

- Large systematics from **continuum limit**

➢ upper right panel: limit and uncertainty estimation

➢ lower right panel: limit for central window compared to other lattice and data-driven results

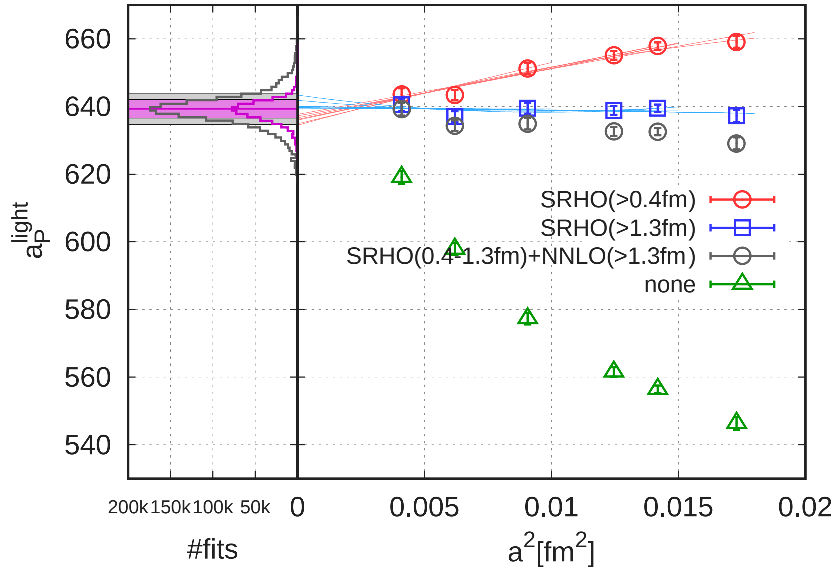

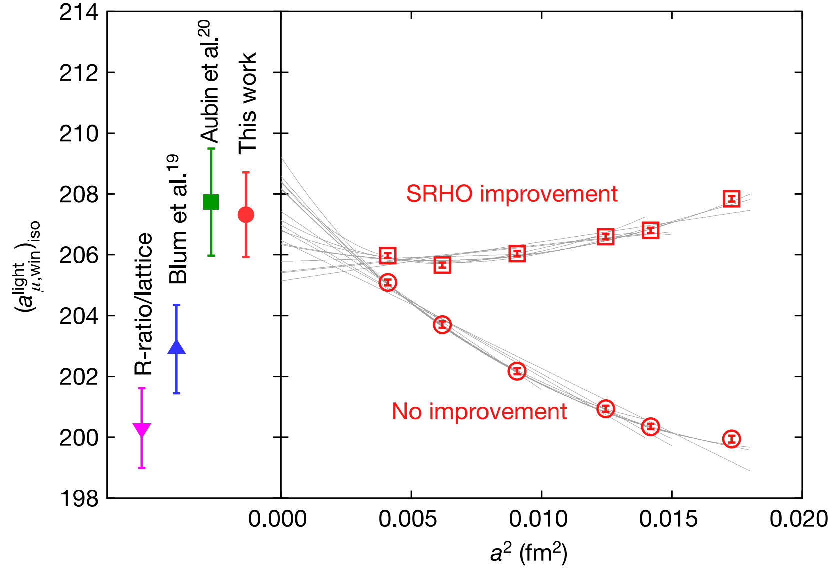

BMW20 [Borsanyi et al, arXiv:2002.12347, 2021 Nature]

Lattice approach

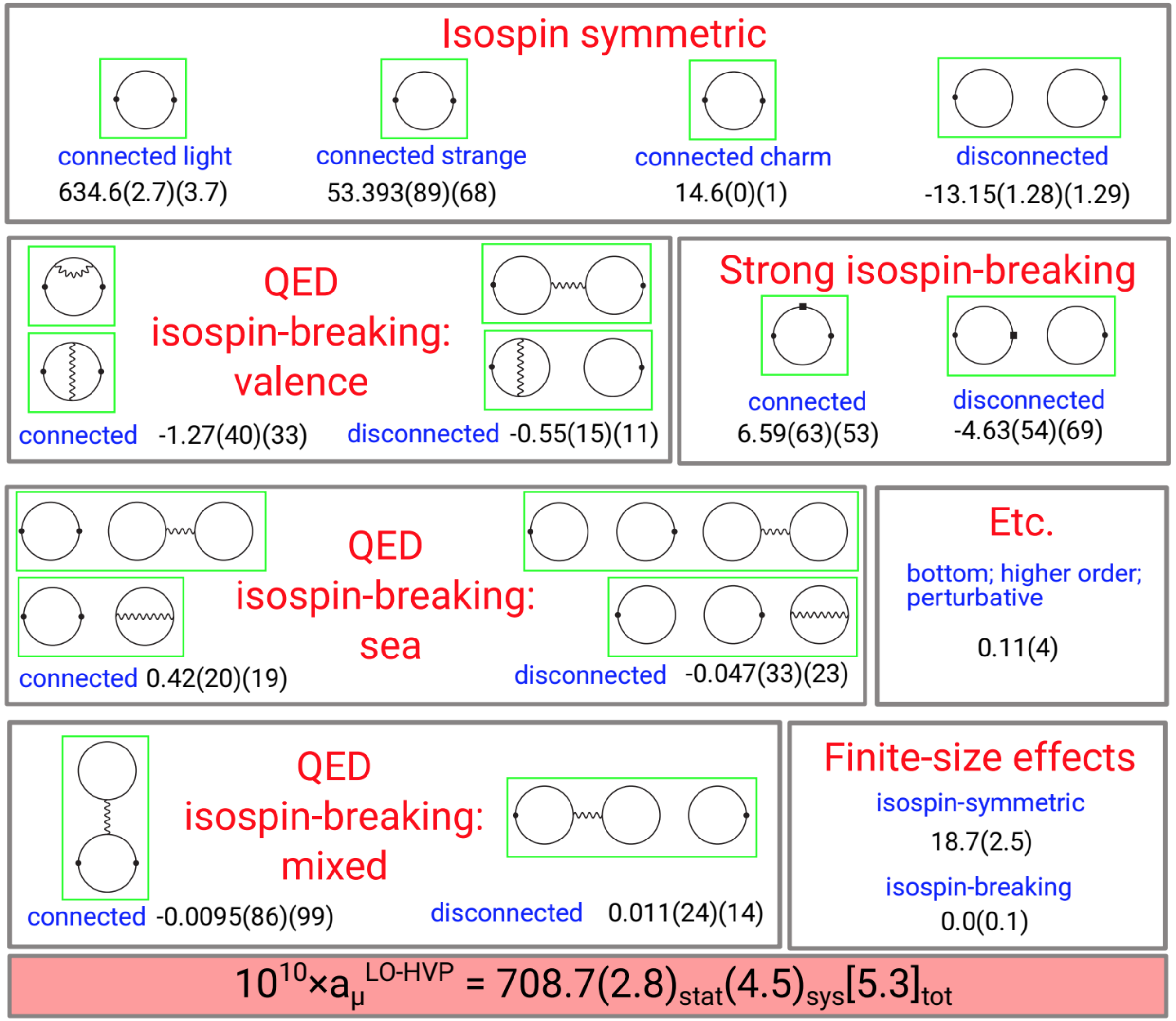

BMW20 [Borsanyi et al, arXiv:2002.12347, 2021 Nature]